DISSERTATIONES ASTRONOMIAE UNIVERSITATIS TARTUENSIS

6

MODELS OF REGULAR GALAXIES

by

PEETER TENJES

TARTU 1993

DISSERTATIONES ASTRONOMIAE UNIVERSITATIS TARTUENSIS
6

MODELS OF REGULAR GALAXIES

by
PEETER TENJES

Supervisors:	Prof. J. Einasto, Dr. Sci. M. Jõeveer, Cand. Sci.
Official opponents:	B. Sundelius, Ph. D. (Göteborg) A. Chernin, Dr. Sci (Moscow) E. Saar, Dr. Sci. (Tartu)

The Thesis will be defended on February 1993 at in the Council Hall of Tartu University, Ülikooli 18, EE2400 Tartu, Estonia.

Secretary of the Council U. Uus

The author was born in 1955 in Türi, Estonia. In 1978 he graduated from the University of Tartu as a theoretical physicist and started work at the Chair of General Physics of the same University. In 1980 he started work at Tartu Astrophysical Observatory in the work group of extragalactic studies.

Address of the author:
Institute of Astrophysics and Atmospheric Physics,
EE2444 Tõravere, Estonia

CONTENTS

CHAPTER 1 INTRODUCTION AND SUMMARY

1 The structure of galaxies

One of the outstanding problems in modern astronomy is the investigation of the distribution of mass in galaxies, the decomposing of the galaxy into subsystems of ordinary and dark matter, and a study of their relationship. The structure of visible populations and the distribution of dark matter with respect to the visible one allows us to choose between various galaxy formation scenarios and to clarify the nature of dark matter in more detail. Simple one-component models, based on the radial light profiles, have not so far provided a strong test of theories of galaxy formation, since several evolution scenarios can be proposed that yield equally good fits to these observations (Gott 1977). Better results can be obtained by multiple-component models which incorporate the presence of physically different populations in galaxies. A useful diagnostic of galactic structure and evolution, at least for spheroidal systems, is provided by the structure of isophotes and the metallicity gradients that are often observed in elliptical galaxies and spiral bulges (Kormendy & Djorgovski 1989). The importance of the measurement of colours in galaxies is that they supply information on the link between the chemical and dynamical evolution of galaxies and yield clues about how chemical evolution proceeded as stars formed in the history of a galaxy. Models of galaxy formation involving dissipative or dissipationless collapse or mergers (Larson 1990) predict relations between colour distribution and stellar density. Also, scenarios of galaxy formation, in which mergers play an important role, predict core–halo colour differences as opposed to smooth continous gradients.

During the collapse of the protogalaxy and the continuing star formation morphology of galaxies was established. The form of a galaxy depends on dynamical properties of the collapsing matter and on the star formation process. The star formation products in different eras differ from each other physically, having different spatial distribution, chemical composition, as well as different kinematic properties that maintain the spatial distributions. Therefore, while studying the structure of stellar populations in galaxies it is possible to obtain quantitative information to understand the formation and evolution processes. The most effective tool for the analysis of the structure of stellar systems is construction of models. An appropriate empirical model of the galaxy should represent distribution of various structural constituents (globular clusters, gas, etc.), kinematical data, changes in chemical composition etc.

Decomposition of a galaxy into subsystems on the basis of observations is complicated. Due to the large number of free parameters there may not be a unique solution to the problem. But when comparing the values of the parameters during the modelling also with the structure of other galaxies and with the models of chemical evolution (Tinsley 1980, Iraat 1990), it is possible to avoid obviously nonphysical solutions.

The modelling techniques of spiral galaxies have been well elaborated. The problem of the mass distribution in external galaxies was first formulated and solved by Öpik (1922) and Babcock (1938, 1939). Babcock's model for M31 consisted of a spherical nucleus surrounded by several coaxial ellipsoids of rotation, representing the remaining part of the galaxy. The density in every structural element was believed to be constant. Comparing surface brightnesses and mass densities, he derived increasing M/L ratios when moving away from the centre.

Naturally, the next step was to modify the model by introducing the dependence of the volume density on the galactocentric distance. The first models of this kind were constructed by Kuzmin (1943, 1952) and Schmidt (1957).

All the models referred above were based on the rotation curve, and they did not take into consideration the remaining data on the structure of galaxies. A new approach was developed by Sizikov (1969) and Einasto (1969, 1972). In these papers kinematic as well as photometric data were taken into account and it was shown that these data enable us to describe the galaxies as sums of subsystems. This allows us also to synthesize various observational data more effectively and to determine more realistic mass distribution models.

On the contrary, up to 80-ies, the modelling of elliptical galaxies has been given much less attention. The first models of ellipticals were based on photometric data (e.g. Fish 1964). The luminosity profile of the galaxy is represented by a simple analytical formula (the most popular are the empirical laws of de Vaucouleurs, King and Hubble). The galaxies were assumed to be dynamically homogeneous, oblate spheroids with the flattening supported by their rotation. Nevertheless, it was obtained as early as in 50-ies by Kuzmin (1953) that the existence of the third integral of motion influences the rotation velocities of a stellar system. Einasto (1972) proposed the algorithm for the mass modelling of a spheroidal system where the configuration of the galaxy is supported by the velocity dispersions, i.e. where the stellar orbits are not circular and the rotational velocities being much lower than circular velocities.

The rotation velocity measurements by Bertola & Capaccioli (1975) and Illingworth (1977) stimulated Binney (1978) to conclude that the dynamics of elliptical galaxies may be triaxial in shape. The problem became even more complicated when Davies et al. (1983) demonstrated that there is a clear dif-

ference between faint and bright ellipticals: faint elliptical galaxies rotate with higher speed, resembling in this sense bulges of spiral galaxies. These results show that the dynamics of ellipticals is at least as interesting as that of spiral galaxies. Variations of apparent ellipticities (di Tullio 1979), isophotal twists (Williams & Schwarzschild 1979), the discovery of counter rotating cores (Franx & Illingworth 1988) in ellipticals also show that the structure is complex. Now it seems to be well established that elliptical galaxies have in general triaxial symmetry (de Zeeuw & Franx 1991). In this case additional free parameters appear in model construction and with the exception of some special cases at present we must limit ourselves with one-component models. As an approximation, also spherical (Kuzmin et al. 1986) and biaxial (Binney et al. 1990) models of elliptical galaxies can be useful for certain purposes.

In the 1970's 21-cm line observations of HI in galaxies showed that the circular velocity outside the optical radius is more or less constant (Roberts & Whitehurst 1975, Krumm & Salpeter 1979). Similar results were obtained later for nearly 60 galaxies from optical [SII], [NII] and Hα lines (Rubin et al. 1980, 1982). This was an unexpected result because it was customary to think in terms of stars as the main contributors to the mass. Since most of the light comes from the region within optical radius, the circular velocity was expected to decline at large radii. Freeman (1970) has calculated the expected rotation curve for an exponential disk with constant M/L. This curve has a maximum at about 2.2 scale lengths, and then declines steadily and eventually becomes Keplerian. The discrepancy between observed and predicted rotation curves can be characterized by local M/L ratios calculated to be $\sim 5-10$ for the central regions and $> 100-500$ for the outer regions of galaxies (Sizikov 1969, Einasto 1972 etc.). This indicates that there must be additional matter beyond the optical radius. In other words, spiral galaxies are surrounded by dark coronas (Einasto et al. 1974, Ostriker et al. 1974).

From very different kinds of observations it results that the masses of galaxies are larger than it results from a simple assumption of constant mass-to-luminosity ratio. Large masses in the outer parts of galaxies result also from the thermal emission of hot gas detected in X-rays (Fabbiano 1989). One more complementary method for evaluation of masses results from gravitational lensing effects indicating that $M/L \sim 100$ for cD galaxies (Blandford & Narayan 1992, Mellier et al. 1992). All these data lead us to a conclusion that a significant amount of dark matter may be associated with galaxies.

The spatial distribution of the dark matter can be studied by dynamics of test bodies which lie at considerable distance from the galactic centre. One way to determine its parameters is to probe the potential of the corona by measuring the rotation of disk galaxies as far out as possible. Then, using mass models, to subtract the contribution of the disk potential to the observed rotation curve. This can be done if we assume a mass-to-light ratio for the disk component

because the light distribution can then be transformed into a mass distribution. A similar problem arises in all cases when it is necessary to decompose the dark and the visible matters. The dark matter reveals only through its gravitational potential. Unfortunately, both the visible and the dark matter contibute to the potential. As the scale and structure parameters of the distribution of visible matter can be obtained from the surface photometry, a free parameter remains – the mass-to-light ratio of the visible matter or the dark-to-visible matter ratio. To derive the amount and distribution of the dark matter often the dark-to-visible matter ratio is assumed to be minimal (the 'maximum' disk hypothesis) or some constant mass-to-light ratio is assumed to the visible matter. However, in order to increase the accuracy of our final results it is desirable to determine all parameters of galactic populations directly from observations.

In order to help to orient in observations by the IAU Working Groups on galaxy photometry and kinematics a subgroup was organized, which recommended to prepare a list of elite galaxies with principal references. This was realized (Tenjes et al. 1982) and from this list a sample of galaxies suitable for modelling was selected. This sample includes galaxies of various morphological types and of different luminosities. We have used the same modelling technique for all galaxies of the sample. We hope that in this way we can obtain an adequate picture of the visible structure of galaxies and the distribution of dark matter.

2 Summary

The aim of the present Dissertation is to investigate the structure of a sample of nearby well-observed galaxies by determining numerical values of parameters of their main populations. The galaxies were assumed to be in a steady state, therefore, we choosed for modelling only regular galaxies with no global activity. All components represent physical subsystems composed of stars with similar age, chemical composition, and velocity distribution, i.e. physically homogeneous. Equidensity surfaces of the galactic populations are approximated by similar concentric ellipsoids or as sums of such ellipsoids.

This work was initialised at the end of 1978 when the preliminary versions of the models presented here were constructed (Tenjes & Haud 1978, Einasto et al. 1979, 1980a, 1980b, 1980c, 1981, Einasto & Tenjes 1981) However, the amount of observational data has considerably increased during the last decade, which made it necessary to revise the models. The first revision of models were published in 1988 (Tenjes 1988, see also Tenjes 1991) and the detailed results were available from 1991 as a series of papers published in *Astronomy and Astrophysics* (Tenjes & Haud 1991, Tenjes et al. 1991, 1992a, 1992b).

Several Chapters have been written as separate papers. As a result, a small degree of overlap between some chapters could not be avoided.

The structure of our neighbouring Andromeda galaxy M31 is studied in Chapter 2. Observational data on surface photometry in seven colours (from the U to the K bands), the rotation curve, the stellar velocity dispersions, the distribution of globular clusters, as well as the distribution of the young stellar component and gas have been collected. These data were used to decompose the galaxy into a central nucleus, a metal-rich core and bulge, a metal-poor halo, an old stellar disk, a young gaseous-stellar population and a massive dark corona. Sensivity of the population parameters to various observational data is analysed. The density distribution parameters, colour indices and mass-to-light ratios of these populations are derived. The mean M/L ratio of optically visible parts of the galaxy is found to be $M/L_B = 4.8 \pm 1.5\,M_\odot/L_\odot$, and the ratio of the total mass to the visible one $M_T/M_{vis} = 43$. The local M/L ratio at the edge of surface photometry data resulting from a best-fit model is 2500.

In Chapter 3 the structure of the young stellar population of the galaxy M31 is studied. The averaged radial surface density distribution of the extreme flat component is derived, taking into account the distribution of stellar associations, open clusters and young field stars. This distribution is compared with the distribution of neutral ($HI+H_2$) hydrogen. The density of the young stellar component is found to be proportional to the gas surface density in the power of 1.30 ± 0.22, or to the space density in the power of 1.17 ± 0.25. The characteristic time of star formation is $t_o = 4.6 \pm 1.5 \times 10^9$yrs, the star formation rate at present $\dot{M} = 0.81 \pm 0.36\,M_\odot$/yr.

The structure of the giant elliptical galaxy M87 is studied in Chapter 4. All available observational data on surface photometry in the UBVRI bands, stellar velocity dispersions, distribution of globular clusters and their velocity dispersions, as well as the distribution of X-rays have been collected. These data were used to decompose the galaxy into a central nucleus, a metal-rich bulge, a metal-poor halo and a massive dark corona. The structural parameters, colour indices and mass-to-light ratios of these populations are derived. The gravitational potential and mass distribution functions of M87 and subsystems are found. The mass-to-luminosity ratio of optically visible parts of the galaxy is $M/L_B = 4.9 \pm 2.0\,M_\odot/L_\odot$, the ratio of the total mass to the visible mass $M_T/M_{vis} = 130$ inside the radius of 90'.

The structure of the spiral galaxy M81 is studied in Chapter 5. The modelling method was similar to that used in Chapter 2 and 4. On the basis of observations the galaxy was decomposed into a nucleus, a metal-rich core, a bulge, a metal-poor halo, a disk, a young population and a dark corona. For the nucleus only an upper limit for the radius and the mass were obtained. The parameters of the corona were calculated from the distribution and kinematics

of satellite galaxies. The density distribution parameters, colour indices and mass-to-light ratios of all populations are derived. The mean M/L ratio of optically visible parts of the galaxy is found to be $M/L_B = 5.5 \pm 1.9\,M_\odot/L_\odot$.

In Chapter 6 we give the best-fit parameters for the sample of 11 galaxies. Observational data needed for modelling is described. The modelling method is the same as it was for the galaxies studied in previous Chapters. These results can be used to analyse the physical properties of galactic populations.

In Chapter 7 the physical properties of galactic populations are studied. As the spheroids and disks have different star formation histories we analyse their mass-to-light ratios separately. The relation between the mass-to-light ratios for old subsystems and their colour indices was constructed. We conclude that both old and young stars are present in the bulges of late-type spiral galaxies. Their *effective* age is 1.5–4 Gyr. For early-type bulges and ellipticals it seems that the differences in their M/L ratios must be ascribed to different initial chemical composition. Similar relation was constructed also for disk models. For a given (B–V) larger scatter of mass-to-light ratios exists. Probably this is the result of infall or capture events unrelated to the bulk of the galaxy formation process.

Because our sample of galaxies includes representatives of all main morphological types with wide range of luminosities, we calculated the mean mass-to-light ratio in our local Universe. By using the luminosity function of the 'standard' Virgo cluster of galaxies the mean luminosity weighed mass-to-ratio of the visible matter was found to be $M/L_B = 4.1 \pm 1.4\ M_\odot/L_\odot$. When using the luminosity function of the field galaxies corresponding value is $M/L_B = 3.7 \pm 1.3\ M_\odot/L_\odot$.

In Chapter 8 we present a method to use observational data to constrain the intrinsic axial ratios, viewing angles, and kinematic misalignment (i.e. the angle between the angular momentum and the shortest axis) of elliptical galaxies. The method requires the knowledge of the photometric and kinematic properties of the stellar and, where available, of the gaseous component. By applying the analysis on three ellipticals we find that in two of the cases the kinematic misalignment is small or absent.

References

Babcock, H.W.: 1938. *Publ. Astron. Soc. Pacific* **50**, 174

Babcock, H.W.: 1939. *Lick Obs. Bull.* **19**, 41

Bertola, F., Capaccioli, M.: 1975. *Astrophys. J.* **200**, 439

Binney, J.: 1978. *Phil. Trans. Roy. Soc. London* **A296**, 329

Binney, J.J., Davies, R.L., Illingworth, G.D.: 1990. *Astrophys. J.* **361**, 78

Blandford, R.D , Narayan, R.: 1992. *Annual Review Astron. Astrophys.* **30**, 311

Davies, R.L., Efstathiou, G., Fall, S.M., Illingworth, G , Schechter, P.L.: 1983. *Astrophys. J.* **266**, 41

de Zeeuw, P.T., Franx, M.: 1991. *Annual Review Astron. Astrophys.* **29**, 239

di Tullio, G.A.: 1979. *Astron. Astrophys. Suppl.* **37**, 591

Einasto, J.: 1969. *Astrofizika* **5**, 137

Einasto, J.: 1972. *Tartu Astophys. Obs. Teated* Nr. 40, 3 = Einasto, J.: 1974. In: *Proc. First European Astron. Meet. vol. 2, Stars and the Milky Way System.* L.N.Mavridis (ed.), Berlin, Heidelberg, New-York: Springer, p. 291

Einasto, J., Kaasik, A., Saar, E.: 1974. *Nature* **250**, 309

Einasto, J., Tenjes, P., Traat, P.: 1979. *Astron. Circ.* Nr. 1032, pp. 5–7.

Einasto, J., Tenjes, P., Traat, P.: 1980a. *Astron. Circ.* Nr. 1089, 1–3.

Einasto, J., Tenjes, P., Barabanov, A.V., Zasov, A.V.: 1980b. *Astrophys. Space. Sci.* **67**, pp. 31–44.

Einasto, J., Tenjes, P., Traat, P.: 1980c. *Astron. Circ.* Nr. 1132, pp. 5–6.

Einasto, J., Tenjes, P., Traat, P.: 1981. *Astron. Circ.* Nr. 1179, pp. 1–2.

Einasto, J., Tenjes, P.: 1981. *Astron. Circ.* Nr. 1179, pp. 2–4.

Fabbiano, G.: 1989. *Annual Review Astron. Astrophys.* **27**, 87

Fish, R.A.: 1964. *Astrophys. J.* **139**, 284

Franx, M., Illingworth, G.: 1988. *Astrophys. J.* **327**, L55

Freeman, K.C.: 1970. *Astrophys. J.* **160**, 811

Gott, J.R.: 1977. *Annual Review Astron. Astrophys.* **15**, 235

Illingworth, G.: 1977. *Astrophys. J.* **218**, L43

Kormendy, J., Djorgovski, S.: 1989. *Annual Review Astron. Astrophys.* **27**, 235

Krumm, N., Salpeter, E.E.: 1979. *Astron. J.* **84**, 1138

Kuzmin, G.: 1943. *Tähetorni kalender 1943. aastaks*, 85

Kuzmin, G.: 1952. *Tartu Aston. Obs. Publ.* **32**, 211

Kuzmin, G.: 1953. *Trans. Acad. Sci. Est.SSR* **2**, 368

Kuzmin, G.G., Veltmann, U.-I.K., Tenjes, P.L.: 1986. *Tartu Astrophys. Obs. Publ.* **51**, pp. 232–242.

Larson, R.B.: 1990. *Publ. Astron. Soc. Pacific* **102**, 709

Mellier, Y., Fort, B., Kneib, J.-P.: 1992. *Astrophys. J.* in press

Öpik, E.: 1922. *Astrophys. J.* **55**, 406

Ostriker, J.P., Peebles, P.J.E., Yahil, A.: 1974. *Astrophys. J.* **193**, L1

Roberts, M.S., Whitehurst, R.N.: 1975. *Astrophys. J.* **201**, 327

Rubin, V.C., Ford, W.K., Thonnard, N.: 1980. *Astrophys. J.* **238**, 471

Rubin, V.C., Ford, W.K., Thonnard, N., Burstein, D.: 1982. *Astrophys. J.* **261**, 439

Sandage, A., Binggeli, B., Tammann, G.A.: 1985. *Astron. J.* **90**, 1759

Schmidt, M.: 1957. *Bull. Astron. Inst. Netherl.* **14**, 17

Sizikov, V.S.: 1969. *Astrofizika* **5**, 317

Tenjes, P.: 1988. In: *The formation and evolution of galaxies and their constituents. I.*, M.Jõeveer (ed.). Tallinn: Valgus, pp. 74–97.

Tenjes, P.: 1991. In: *Galaxy Environments and the Large Scale Structure of the Universe, Proc. Intern. Workshop at Trieste, Oct. 23–25, 1991.* SISSA-ISAS. pp. 335–340.

Tenjes, P.: 1992. *Baltic Astronomy* **1**, 7–16.

Tenjes, P., Haud,U.: 1978. In: *All Union conference of young astrophysicists, devoted to V.A. Ambartsumjan's 70-th birthday*, Yerevan: Acad.Sci. Armenian SSR, pp. 16.

Tenjes, P., Haud, U.: 1991. *Astron. & Astrophys.* **251**, 11–14.

Tenjes, P., Kalamees, P., Einasto, J., Jõeveer, M., Brosche, P., Lentes, F.-Th.: 1982. *A List of Elite-Galaxies*, Tartu Astron. Obs. Teated Nr. 68, Tallinn: Valgus, pp. i–vii, 1–56

Tenjes, P., Einasto, J., Haud, U.: 1991. *Astron. & Astrophys.* **248**, pp. 395–403.

Tenjes, P., Haud, U., Einasto, J.: 1992a. *Astron. & Atrophys.* (submitted).

Tenjes, P., Busarello, G., Longo, G., Zaggia, S.: 1992b. *Astron. & Astrophys.* (submitted).

Tenjes, P., Busarello, G., Longo, G.: 1992c. "Triaxial elliptical galaxies with

dust lanes: an atlas of velocity fields." *Memorie dell'Accademia di Scienze Fisiche e Matematiche.* Napoli: Liguori Editori, pp. i–xi, 1–89.

Tinsley, B.: 1980. *Fund. Cosm. Phys.* **5**, 287

Traat, P.: 1990. In *Chemical and Dynamical Evolution of Galaxies*, F.Ferrini, J.Franco, F.Matteucci (eds.), Pisa: ETS Editrice, p 650

Williams, T.B., Schwarzschild, M.: 1979. *Astrophys. J.* **227**, 56

CHAPTER 2 THE ANDROMEDA GALAXY M31*

1 Introduction

In the present paper we have investigated the structure of M31 by determining numerical values of parameters of its main populations. We tried to estimate the accuracy of these parameters and their sensivity to observational data.

The first models by Babcock (1938, 1939), Kuzmin (1943, 1952) and Schmidt (1957) were constructed to solve the problem of mass distribution in M31. All these models were based on the rotation curve, and they did not consider the remaining data on the structure of the Andromeda nebula. The main purpose of the present work is different – to obtain as much information as possible on the structure of populations in M31. This approach was initialized by Sizikov (1969) and Einasto (1969, 1972). In these papers the kinematic as well as photometric data and chemical composition were taken into account and it was shown that these data enable us to describe our neighboring galaxy as a sum of subsystems. For our Galaxy this approach dates from early 1940s (q.v. review by Sandage 1986). This work was continued and the preliminary version of the model presented here was constructed about ten years ago (Einasto et al. 1979, 1980). However, the amount of observational data during last decade has considerably increased, which made it neccessary to review the model.

Our present model differs from previous ones in the following:

1. The largest set of various observational data was taken into account.
2. The galaxy was decomposed into several subsystems with different physical characteristics and the parameters of these subsystems were derived. In this sense our model may be called as a model of the stellar population of the Andromeda galaxy.
3. As a result of the superposition of several subsystems the model has a variable M/L ratio and chemical composition.

Models with variable M/L ratios and chemical compositions give better understanding of the distribution of mass in galaxies and the possible presence of the dark matter (DM) population. The distribution of DM with respect to

* This Chapter bases on the paper by Tenjes, P., Haud, U., Einasto, J., "Galactic models with massive coronae. IV. The Andromeda galaxy M31." *Astronomy and Astrophysics* in press

the visible matter allows us to clarify the nature of DM in more detail.

In Sect. 2 the observational data used in modelling process is described. In Sect 3 we describe the subsystems in M31: the nucleus, the metal-rich core, the bulge, the metal-poor halo, the old disk, the extreme flat subsystem, and the invisible massive corona. Section 4, Appendixes A and B are devoted to the modelling process. In Sect. 5 we give the parameters and mass distribution functions of our final model and in Sect 6 discussion of the model is presented. Most simple 3-component model will be described in Appendix C.

Throughout this paper all luminosities and colour indices have been corrected for absorption in our Galaxy according to Burstein & Heiles (1984). The distance to M31 has been taken as 690 kpc, the position angle of the major axis PA = 37.7°, the angle of inclination to the line of sight $i = 12.5°$ (eg. Walterbos & Kennicutt 1988).

2 Analysis of observational data

In this Section we describe observational data which were used as initial data in model calculations.

By now a detailed *surface photometry* of M31 is available in seven colours. An analysis of the photometry by Redman & Shirley (1937), Fricke (1954), de Vaucouleurs (1958), Lyngå (1959), Sharov & Lyutyj (1980), Hoessel & Melnick (1980) and Hiromoto et al. (1983) is done by Walterbos & Kennicutt (1988). The photometry by Johnson (1961) and Kinman (1965) was discussed by Light et al. (1974). Therefore in Table 1 we describe only additional data. Table 1 presents references, the faintest observed isophotes (magarcsec^{-2}), corresponding distances along the major axis (arcmin), colour systems used and some remarks on the observations in the direction of the minor axis.

In the cases when the observers have presented the profiles along the axis which forms an angle ψ with the major axis (the EW-profiles, e.g.), we reduced the distances given by the observer to the distances along the major axis according to the formula

$$a = r\sqrt{\frac{1-e^2\cos\psi^2}{1-e^2}},$$

where r is the distance along the measured axis and e is the isophote eccentricity related to the axial ratio by the formula $e = \sqrt{1-\epsilon^2}$. For reduction we used mean axial ratios (open circles in Fig. 2b).

Table 1. Photometrical data

Reference	Faintest isophote	Radius (')	Colour system	Minor axis?
Alloin et al. 1976	17.6	.35	BV	
Battaner et al. 1986	19.6	50.	HJK	
Davis et al. 1982	23.0	44.	UBV	
Hodge, Kennicutt 1982	25.5	93.	B	Yes
Iijima et al. 1976	17.8	12.	K	
Kent 1983, 1987	24.2	94.	R	Yes
Martinez Roger et al. 1986	16.1	3.2	HJK	
Mould et al. 1989	12.5	0.12	JK	Yes
Nieto et al. 1986	(18.6)	0.5	U	Yes
Sandage et al 1969	19.3	2.0	UBVRK	Yes
Sharov, Lyutyj 1981		120	UBV	
Spillar et al. 1990	(12.3)	0.08	K	

In this way all the data on the surface photometry were used. The surface brightness profiles in the UBVRHJK colours along the major and minor axes were derived by averaging the results of different authors. This was done in two steps. First, all results were taken with equal weights. In the second approximation every measurement was prescribed a formal error, equal to the sum of the measurement error, given by the author, and the change of the first profile (equal weights) in the distance interval, corresponding to the radius of the diaphragm used. Thereafter individual results were averaged with weights inversely proportional to the squares of these formal errors. The error bars on figures indicate the resulting formal errors of mean values. Derived profiles form the initial data of our model. Here we present only the model profile in B (Fig. 1), (B–V) and (U–B) colour indices (Fig. 2a), for which most detailed information is available, and the axial ratios (Fig. 2b).

An analysis of the *rotation velocities* published before 1980 has been done by Haud (1981). In this work the gas rotation and expansion velocities as functions of galactocentric distance were derived. In the inner 1 kpc new observations by Boulesteix et al. (1987) and Ciardullo et al. (1988) were added. In the distance interval 4–27 kpc additional observations by Kent (1989b) and Braun (1991) were also taken into account. Unfortunately, it is not possible to use the thoroughgoing study of HI by Brinks & Shane (1984) as they do not construct an explicit rotation curve. For R <4 kpc the rotation velocities obtained by Braun (1991) differ noticeably from others. Partly it results from larger inclination angle of the galactic plane to the line of sight in this region, partly from the reduction method used. Because they are also in poor agreement with other dynamical information – the stellar velocity dispersion data in corresponding region – we did not used them in this work. The averaged

rotation curve is given in Fig. 3 by open circles.

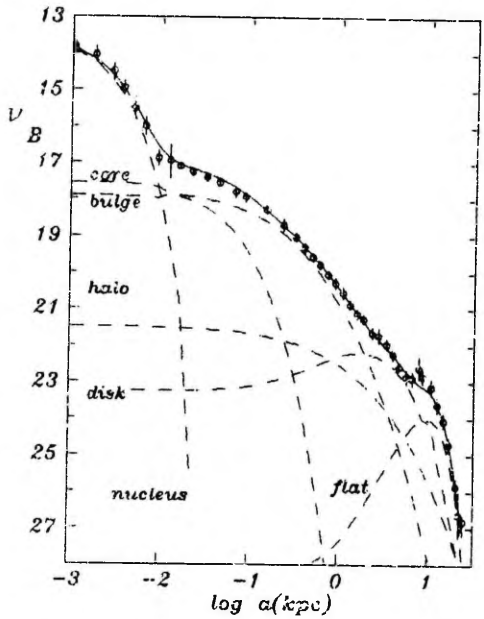

Figure 1 The averaged surface brightness profile of M31 in the B-colour. Open circles – observations, solid line – model, dashed lines – models for components.

Velocity dispersions have been measured by many observers. A collection of all available data is given in the catalogues by Whitmore et al. (1985) and Davoust et al. (1985) where the weighted mean values of 166 kms^{-1} and 162 kms^{-1}, respectivly have been derived for the central dispersion. We used observations by Simien et al. (1979), McElroy (1983), Dressler (1984), Kormendy (1988). Dressler & Richstone (1988), Delisle & Hardy (1992) as they are not confined only to the centre. By averaging dispersions at various distance intervals with the weights depending on seeing conditions and the velocity resolution, the dispersion curve presented in Fig. 4 by open circles was derived. The mean velocity dispersions of the globular clusters have been derived by van den Bergh (1969), Huchra et al. (1982, 1991) and Kent et al. (1989). The kinematics of the planetary nebulae is from Nolthenius & Ford (1987).

The observations on the distribution of individual objects (globular clusters, young stars, gas etc.) which we used for modelling will be referred to and analyzed in Sect. 3.

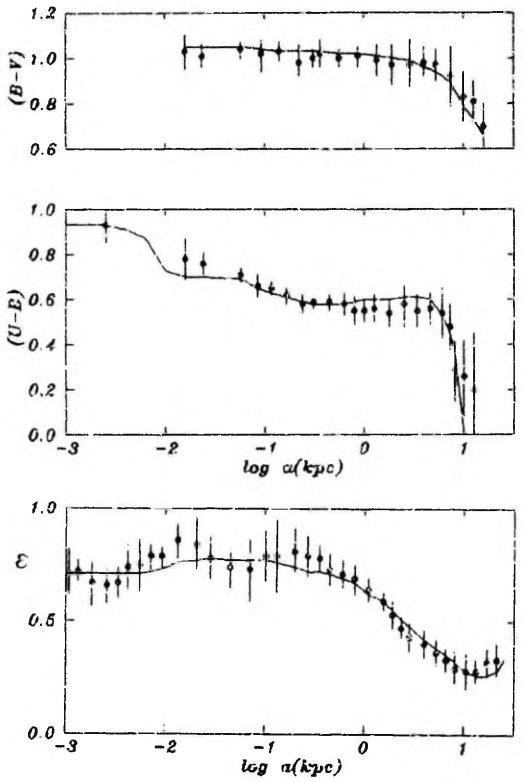

Figure 2 (a) The averaged profiles of the colour indices (B – V) and (U – B) of M31. Open circles – observations, solid line – model. **(b)** The axial ratios of isophotes of M31 as a function of the galactocentric distance. Open circles – observations, solid line – model.

3 Subsystems in M31

Although the general review of the subsystems in galaxies can be found in textbooks by Mihalas & Binney (1981) and Gilmore et al. (1990) we describe them briefly in this Section with the special emphasize to the Andromeda galaxy (cf. van den Bergh (1991)).

The nucleus

Photometry of inner regions of M31 obtained in excellent seeing conditions

was done by Light et al. (1974) and Nieto et al. (1986). Even a preliminary examination of the light distribution reveals a central peak in the brightness profile (Fig. 1), so it is natural to define the nucleus as the first component. An additional argument supporting the nucleus as a separate dynamical unit can be derived from velocity dispersions and rotation velocities (Kormendy 1988, Dressler & Richstone 1988). Unfortunately, colour indices in the nucleus have not been directly measured. The only result available is by Spinrad & Liebert (1975), who report the difference in the colour (U–V) between the nucleus and a region 4" off the centre to be $\Delta(U-V) = 0.13^m$.

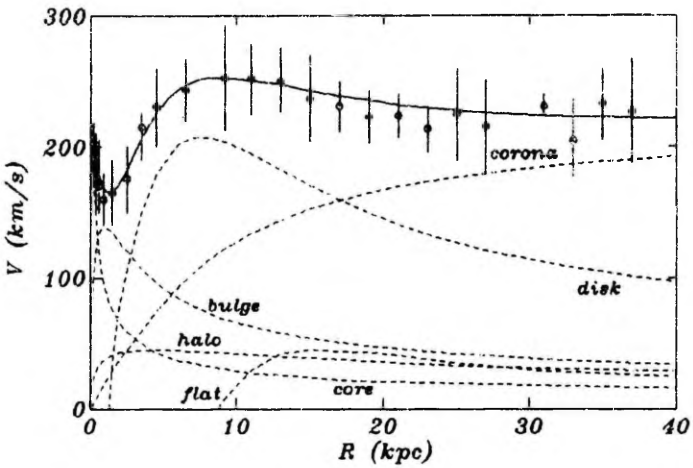

Figure 3 The rotation curve of M31. Open circles – observations, thick line – our best-fit model, dashed lines – models for components.

The core and the bulge

The bulge is usually defined as a spheroidal component with a normal metal content. In studying the chemical composition of the M31 spheroid, most informative for us is the colour index (U–B), as more sensitive to the metallicity variations. It is seen from Fig. 2a that at the distance interval 0.02–0.1 kpc there is a difference by 0.12^m in the (U–B) index, indicating that the inner part of the spheroid is more metal-rich. This has been confirmed by population synthesis models by Joly (1974): inwards $\sim$ 0.2 kpc the mass-to-light ratio increases. A similar phenomenon – a sudden increase of metallicity in the cores of spheroids – has been detected in several nearby galaxies (Cohen 1979, Delisle & Hardy 1992). For this reason we can separate a metal-rich core from

the bulge. A two-component structure of the bulge was used also by Rohlfs & Kreitschmann (1988) for our Galaxy (models 5 and 6). However, the problem of discriminating between the core and the bulge is a complicated one and will be discussed in Sect. 4.

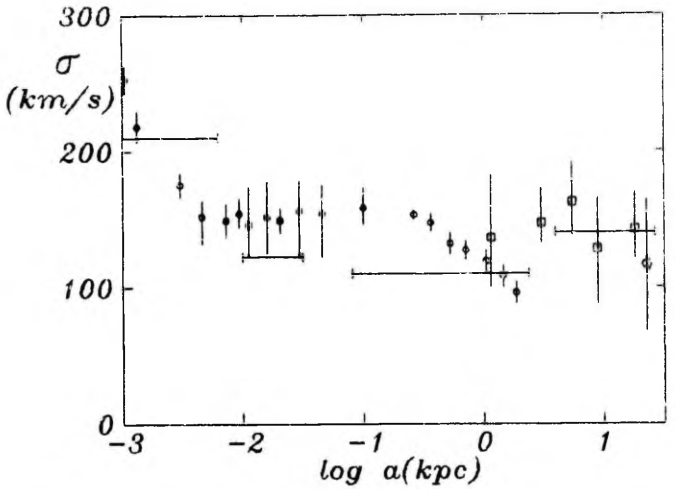

Figure 4 The averaged velocity dispersion profile of M31. Circles — stellar dispersions, squares — globular clusters, diamond — planetary nebulae. Horizontal bars denote the mean dispersions calculated from our best fit model at the corresponding distance intervals.

The halo

By 'halo' we mean a spheroidal metal-poor population II subsystem, typical representatives of which are old stars (like RR-Lyrae variables) and globular clusters. In our Galaxy (Haud & Einasto 1989) the distribution of globular clusters and RR-Lyrae stars is very similar. By analogy we can expect that the spatial distribution of globular clusters is representative enough for the halo subsystem in M31.

The observations of globular clusters have been made by Vetesnik (1962), van den Bergh (1969), Sargent et al. (1977), Battistini et al. (1980), Buonanno et al. (1982), Wirth et al. (1985), Sharov & Lyuty (1983) and Crampton et al. (1985). From these data a list of 608 observed globular cluster candidates

was compiled. At the first step we included all objects mentioned at least in one of the papers. From this compilation we excluded the objects, which on basis of analysis by Crampton et al. (1985), Huchra (1988) and Racine (1991) were referred to as misidentifications. The remaining number of clusters was 489 and their number surface density distribution is given in Fig. 5.

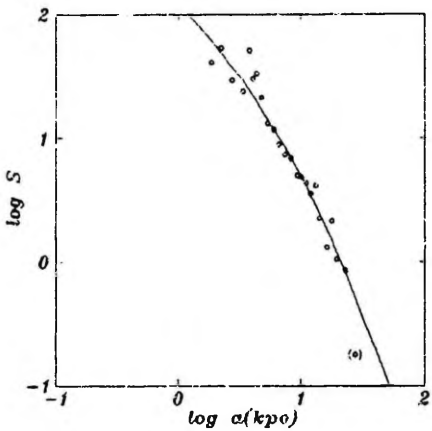

Figure 5 The distribution of globular clusters of M31. The observations have been averaged and presented by open circles. The continuous line gives the model distribution.

The observed cluster distribution is well approximated by our density distribution law (Eq. A1) with the parameters $N = 4.9 \pm 1.7$ and $a_0 = 4.8 \pm 0.4$ kpc. The distribution of globular clusters is not spherical in M31. From our compilation it results that the cluster system is flattened with the apparent axial ratio $E = 0.50 \pm 0.05$ corresponding to the true axial ratio $\epsilon = 0.46 \pm 0.07$. This coincides within the errors with the flattening derived by Elson & Walterbos (1988). The mean colour indices of M31 cluster population are $(B - V) = 0.75 \pm 0.17$, $(U - B) = 0.21 \pm 0.15$.

Measurements of individual globular clusters in our Galaxy by Illingworth (1976) give a mean M/L ratio 2.1 ± 0.6 $M_\odot/L_\odot$. This value can be taken as a reasonable approximation also in case of the Andromeda Galaxy (Cohen & Freeman 1991).

Therefore, the analysis of the subsystem of globular clusters enables us to derive rather precisely most of the halo parameters. We shall use these values in our least-square fit as fixed parameters.

The extreme flat subsystem

The flat subsystem consists of young objects (open clusters, OB-associations, O-B stars etc.) and of interstellar medium (atomic and molecular gas and dust). This is the youngest population. An analysis of these objects and gas has been done by Tenjes & Haud (1991) (Chapter 3 in present Thesis). In Fig. 6 the distribution of the surface density of stellar component and gas is given.

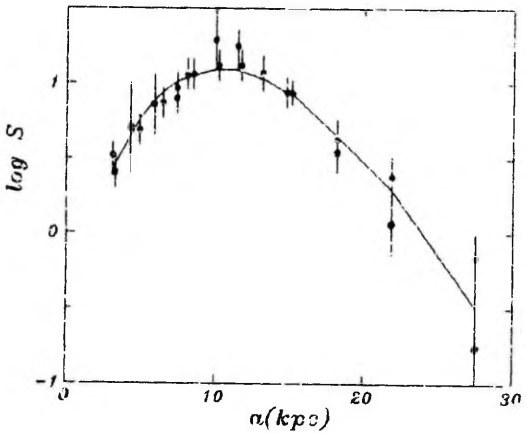

Figure 6 The distribution of young population I objects. Open circles – stellar component, filled circles – gas component, solid curve – model distribution.

The distribution of stars and gas in this population is well represented by our density distribution law (Eq. A1) with the parameter $a_o = 11.1 \pm 0.9$ kpc, $N = 0.30 \pm 0.07$, $\kappa = 0.56 \pm 0.1$. For the flattening of the subsystem we take as in our Galaxy $\epsilon = 0.02$.

The total mass of both atomic and molecular gas in M31 is $M_{gas} = M_{HI} + M_{H_2} = 4.6 \pm 0.5 \cdot 10^9\,M_\odot$ (Cram et al. 1980; Koper et al. 1991). To this value the mass fraction in the young stars ($M_S = 0.6 \pm 0.3 \cdot 10^8\,M_\odot$) can be added (Tenjes & Haud 1991). Therefore the total mass $M = 5.2 \pm 0.8 \cdot 10^9\,M_\odot$ results for the flat population of M31.

As in case of the halo subsystem we shall use these values in the least-square fit as fixed parameters for the flat subsystem.

The disk

It is convenient to define the disk to consist from stars with normal metallicity but with quite different ages (the mean age is about $7 \cdot 10^9$ yrs). As for the flat subsystem, we allow a toroidal structure for the disk, i.e. the central density

minimum. Otherwise it is difficult to model a minimum of the rotation velocity at 1 kpc (Einasto et al. 1980; Rohlfs & Kreitschmann 1981). Information on the gravitational field in the galactic plane can be derived also from the distribution and kinematics of the HI-layer. However, because these data are somewhat indirect, we shall use them only at the final stage of our study (Sect. 6).

The massive corona

A considerable amount of mass in the outer parts of M31 is indicated by the rotation law of the galaxy (Fig. 3) and by the velocity dispersion of most distant globular clusters (Fig. 4). The phenomena is similar to that found in other spiral galaxies: the rotation velocities of outer parts of these galaxies remain constant, contrary to that resulting from photometrical models (Sancisi & van Albada 1987). It is possible to avoid these discrepancies supposing that M31 is surrounded by a massive invisible corona, which influences the dynamics of the outer parts of the galaxy. Large masses in the outer parts of galaxies result also from the thermal emission of hot gas detected in X-rays (Fabbiano 1989) and for giant cD-galaxies from the gravitational lensing effects (Mellier et al. 1992).

4 Best-approximation process

The population structure of M31 has been studied by means of modelling described in Appendix A. For all models the best-approximation parameter set has been found using the least-squares algorithm. The algorithm minimizes the sum of squares of relative deviations of the model from all observations.

General parameters of the approximation process

The set of initial data consists of:

1. photometrical data (surface photometry in UBVRK colours along the major and minor axes, in JH colours along the major axis);
2. the distribution of the extreme flat population objects (young stars and gas);
3. the spatial distribution of globular clusters;
4. the rotational curve in the plane of the galaxy;
5. the mean line-of-sight stellar velocity dispersion for the nucleus, the core and the bulge;

6. the kinematics of globular clusters, planetary nebulae and satellite galaxies of M31.

The number of combined observational data points was 390. Photometrical profiles were taken with equal weights, and the rotation curve had the same weight as the surface photometry. The velocity dispersions and satellite kinematics were used only for mass determination.

In principle, the number of the degrees of freedom in the fitting process is 57 (6 visible populations with 9 parameters each (ϵ, a_o, M, κ, N, and 4 mass-to-light ratios in UBVR) and an invisible corona with 3 parameters (ϵ, a_o, M)). This number is reduced to 32, because some parameters were not changed. The parameter κ, indicating the depth of the central density depression, was fixed as zero for all components except the disk and the flat component. Next, the corona was assumed to be spherical (the axial ratio $\epsilon = 1$). Further, the nucleus is a well separated and dynamically independent subsystem, i.e. the parameters of the nucleus are independent of others and can be separately determined. In Sect. 3 we derived for the halo from the distribution of the globular clusters the density distribution parameters ϵ, a_o, N, the colour indices (B–V), (U–B), (V–R) and the mass-to-light ratio M/L_B. In Sect. 3 from the distribution of the young stellar component the parameters ϵ, a_o, N, κ and M for the flat population were derived. These parameters of the halo and the flat subsystems were also unchanged.

But even the final number of free parameters 32 at a first glance seems to be huge. Largely this number results because we use the photometrical information in several colours (four mass-to-light ratios for four subsystems gives 16 free parameters) and along the major and minor axis (5 free parameters). Let us assume for a moment that we use photometric information in ten colours, which means that additional 30 free parameters appear. Despite of this the complexity of the approximation process practically does not change, because these new mass-to-light ratios (as well as old) are nearly independent of the space of the remaining parameters. Actually, our model has the minimum number of parameters needed (every component must have at least a radius, a mass and a structural parameter).

Description of the fitting process

Formulae given in Appendix A are the relations connecting main observations with model parameters and they are used in estimating the values of these parameters in the procedure of the least square fitting. However, due to the complicated form of these relations and the composite structure of the galaxies, this fitting is not a straightforward procedure and it must be done in several steps. First of all, we must fix the number of populations to be used in the

model. The choice depends on the amount and quality of observational data available and on the goals of modelling.

The first step of model construction – the choice of populations – is directly related to the next stage, the construction of preliminary crude model for every population in the model. This can also be done by considering different observational and physical constraints on the model parameters and comparing different model distributions (see Figs. 1 and 2 in Einasto & Haud 1989) with the observational ones. As practically every galaxy has some specific observational data, the construction of preliminary population models differs considerably from galaxy to galaxy and can not be universally formalized. This stage enables us to eliminate obviously nonphysical solutions.

In the subsequent refinements of the model we use the standard set of observational data, available for most well-studied galaxies: rotation curve, mean velocity dispersions of the populations, photometric profiles and distributions of population tracers. This is done in a more objective way by using the least square fitting on a computer, but unfortunately this process is slightly subjective. In this respect we must consider two problems.

First of all, usually there are some model parameters, rather insensitive to the observations used in the least-square fitting. For example, the measured part of the rotation curve of the Andromeda Galaxy M31 is not long enough to determine completely the parameters of the dark corona and the corresponding parameter values depend more critically on other observational criteria (kinematics of the satellites and of the Local Group). If we ignore this aspect and allow the refinement of the parameters of the corona by the least squares program, we will probably get a mathematically good solution, but being astronomically unacceptable as conflicting with several observational constraints both for the corona and the disk component, because an acceptable approximation of the observed rotation curve can be obtained with several combinations of the parameter values for these two populations.

To overcome this problem, we must determine already in the stage of the construction of the preliminary crude population models, which parameters of every population are practically insensitive to the standard observations used in the least square fitting and try to fix their values as precisely as possible on the ground of independent data. In the following fitting procedure we must keep their values fixed at estimates obtained in the preliminary stage. Then the accuracy of the resulting model depends on the accuracy of the estimates of these fixed parameters and on the degree of the correlation of their values with the values of other parameters.

The second point for subjective decisions is related to the accuracy of observations. As we must deal with observations of unequal precision, we must include into the fitting process some kind of weights describing the expected

accuracy of observational results. However, as several systematic errors in observations are often unknown and the error estimates, given by the observers, follow different assumptions, the prescription of weights remains a somewhat tricky task. It was mentioned above that we assumed equal weights to photometrical and kinematical datasets. During the work we studied the influence of this assumption and it results that we may change the weight balance of these datasets by two or three times without any real changes in the final model. Only taking the weight of kinematical data an order of magnitude smaller than that of photometry, significant changes begin: such model has a larger and more diffuse core and a smaller bulge; the radius of the disk increases as well. The rotation curve of such a model is nearly flat without any characteristic features. But this version simply ignores the rotation law of the galaxy. The purpose of the present paper is to find a model which is in agreement with the largest available set of observations.

After allowing for described considerations, there remain mathematical problems of fitting the nonlinear functions in high-dimensional parameter space. Here we proceeded in a rather straightforward way. As mentioned in Paper I, to estimate the degree of consistence of the model with the observational data, we used the sum of squares of the relative deviations. As some model parameters enter into the main Eq. (A1) – (A9) always in certain combinations with others, we actually fitted the values of these parameter combinations $(1/ka_0,\ hM/(4\pi\epsilon a_1^3))$ and after that we computed the actual model parameters from these fitted combinations.

As for most parameters the main relations between observations and the model are nonlinear, but the dependence of the descriptive functions on $hM/(4\pi\epsilon a_0^3)$ and L can be represented in a linear form, we also divided every fitting step into two substeps: first we solved the approximately linearized problem for nonlinear fitting parameters and after every such solution we determined the best values of linear parameters for the obtained set of values of nonlinear parameters. As due to the complicated nature of the problem, not every new set of the values of the nonlinear parameters improved the sum of squares of the model deviations, we also computed for every set of parameter values the derivatives of the sum of squares of the deviations on every nonlinear parameter and in the case of unsuccessful fitting step we rejected the obtained new values and repeated the step with the parameter, corresponding to the smallest derivative, excluded from the fitting process. After some successful steps all free parameters were once again included into the fitting.

Table 2 characterizes the model sensitivity to the changes of nonlinear parameters. Quantities listed in the Table are defined as model deviations which are caused by changing particular parameters by 1 percent i.e. the partial derivations according to the parameters and they are in relative units.

Table 2. Changing effeciencies for nonlinear parameters

Population	ϵ	κ	c_o	N
Corona			47.	
Core	14.		0.29	6.9
Bulge	17.		80.	17.
Halo	0.46		0.001	35
Disk	0.39	5.	6.	1.5
Flat	3.8	1.7	750	34.

The described fitting algorithm converged satisfactorily. Actually, for populations, whoose parameters mainly depend on observational data, processable with the described fitting program, this fitting procedure was used for estimating the values of the parameters of these populations in determining the preliminary population models as well. At the beginning of the final fitting process these parameters were usually once again stated as free ones, but if first iterations demonstrated their independence of other components, corresponding values were fixed to speed up the remaining fitting process.

Coupling of parameters

As the galaxy is supposed to be a superposition of subsystems, in principle, all parameters are mutually related but the degree of dependence varies largely.

Spheroidal components

The core and the bulge subsystems are mixed in photometry, i.e. light profiles allow variation of their structural parameters in a quite large interval: if we limit ourselves to the light profile in B only the presence of the core is not even necessary. More strict limits to the parameters of these components result from kinematics. It is impossible to model the observed maximum of the rotation velocities at 0.2 kpc and the minimum with only one bulge component. The single bulge with the parameters determined from photometry gives the rotation maximum at 1-1.5 kpc – just where the observed minimum lies (cf. the 3-component model in Appendix C). To represent adequately the inner part of the rotation curve a two-component structure with different M/L ratios is needed.

Figure 7 demonstrates the sensivity of the rotation curve to the core radius. In these calculations the structure parameter N =1.5 and the mass of the core corresponds to the mean velocity dispersion of $\langle\sigma_{core}\rangle$ =125 km/s. The radii of the core are 0.05, 0.1, and 0.15 kpc, the masses of the core are 0.1, 0.2, and 0.3 (in units of 10^{10} $M_\odot$) for models (a), (b), and (c), respectively.

Figure 8 illustrates models with a different structure parameter N of the core (M = 0.2, a_o =0.1 kpc). In model (a) N =0.5 and in model (b) N =2.5. As the radius of the core is more than seven times smaller than the radius of the bulge, the latter is quite insensitive to the changes of the core parameters and also to the parameters of all other components.

Since a_o and N for the halo parameters were fixed on the basis of the distribution of globular clusters, all the remaining parameters for the core and the halo, and all parameters for the bulge can be determined with sufficient accuracy (15 parameters must be determined from 136 observational points from UBVR surface photometry in the region of interest).

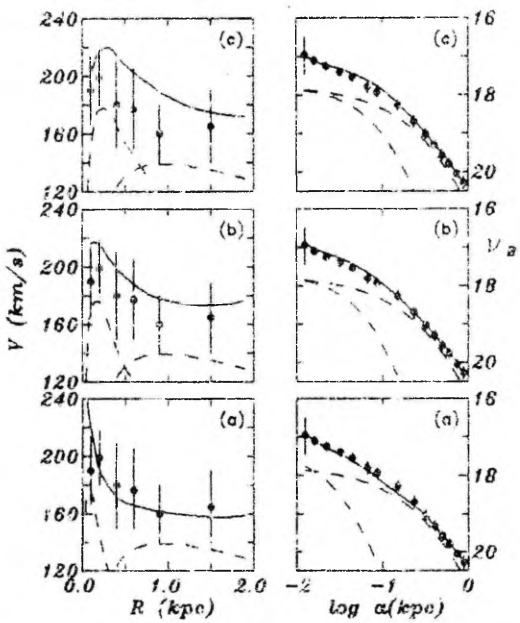

Figure 7 The inner part of the rotation curve and the surface brightness distribution in B (cf. Fig. 1) for three different models. The core radii are (a): 0.05 kpc, (b): 0.1 kpc, (c): 0.15 kpc.

Disk-like components and the massive corona

As it was noted in Sect. 4 the parameters ϵ, a_o, κ, N, and M for the flat subsystem were determined from the distribution of young objects and fixed thereafter. The contribution of this component to the rotation curve is small and therefore dynamical information does not influence the parameters of the flat system. The luminosities in BUVR colours can be determined from corresponding surface brightness profiles. It is seen from Fig. 2a steep decrease of

the colour indices beyond $R > 7$ kpc enabling to determine the luminosities of the component.

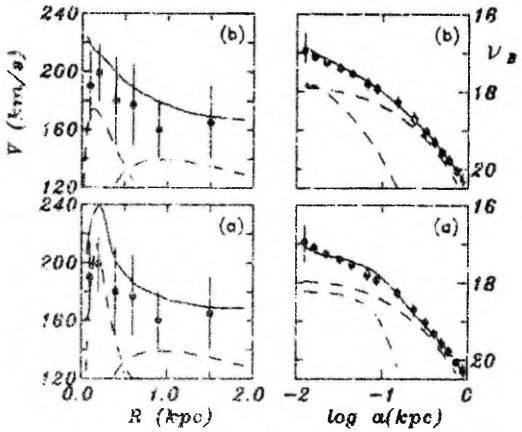

Figure 8 The inner part of the rotation curve and the surface brightness distribution in B for two core models. In model (a) $N = 0.5$, in model (b) $N = 2.5$.

The parameters of the disk depend both on the photometrical and on the kinematical data. Increasing eccentricity of the isophotes beyond $R > 1$ kpc (Fig. 2b) indicates to the region where the disk become dominating in the photometry. Therefore, the radii of two disk-like components are quite different and in photometry they are quite well separated. Additional limits result from kinematics. Figure 8 illustrates the sensitivity of the rotation curve and the major axis brightness profile to the disk parameters. Models (a) and (b) correspond to the models with fixed parameters of the central depression $\kappa = 0.2$ and $\kappa = 0.8$, respectively. The radii of the disk were $a_o = 5.5$ kpc and 3.1 kpc, the masses $M_+ = 6$ and 13., the mass-to-light ratios 13.5 and 14.3 in B. Figure 10 represents models with a fixed disk parameter N: in model (a) $N = 0.8$, $M_+ = 7.5$, $M/L = 17$, model (b) has $N = 2$, $M_+ = 9.5$, $M/L = 14$. The radius of the disk is practically independent of the parameter N. All other parameters except the fixed ones were determined from the best-fit process. The parameters of other components are from Table 3 as they remained practically unchanged. We would like to note that Fig. 9 – 10 illustrates the minimal disk model, i.e. when the model is the least sensitive to disk parameters (central density of the corona is the largest possible).

Discrimination between the disk and the corona is a complicated problem. Although the rotation curve of M31 extends up to 37 kpc from the centre it is not sufficient to determine all the parameters of the corona. In our model we assume the corona to be spherical ($\epsilon = 1$). From model construction it results that the least square algorithm allows the radius a_o for the corona in

the range from 60 to 140 and x in the range from 4.5 to 7. We have calculated two versions of the model, corresponding to the extreme cases. All models are in good agreement with the observed rotation law. Since the rotation velocities are known only up to 37 kpc, it is not possible to distinguish between the parameters a_o and x. The behaviour of the rotation law of the corona in its inner parts is quite similar when we fix x and allow a_o to vary or by fixing a_o and allowing x to vary. Differences appear only in the region of 80 – 200 kpc. For this reason in further calculations we will fix the parameter x =6 and vary the radius of the corona. In Fig. 11 model (a) corresponds to a_o = 60, model (b) to a_o = 140. The parameters of other components are listed in Table 3. The masses of the corona for the two versions of the model are 320 and 660, the disk masses are 5.1 and 8.5 (10^{10} $M_\odot$,) respectively. As we shall argue in Sect. 6 the first version of the model should be preferred.

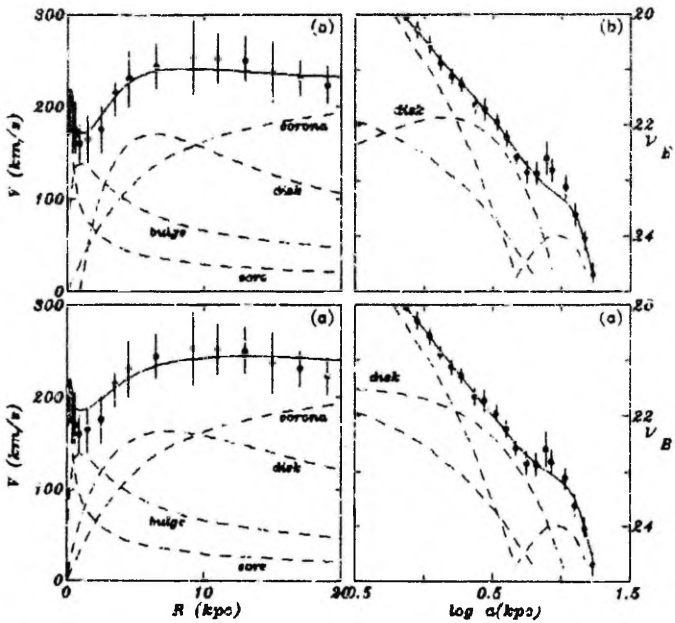

Figure 9 The rotation curve and brightness profile for different central depression of the disk. (a): κ =0.2, (b): κ =0.8.

5 Results

The seven component model fits all photometric profiles with a mean relative error 0.6% , and the rotational curve with the error 1.6% . Within our model there are no contradictions between the photometrical and kinematical data. The model is in good agreement with both sets of data. The parameters of this model (the axial ratio, ϵ, the harmonic mean radius, a_o, the total mass of the population, M, the structural parameters, κ and N, and the dimensionless normalizing constants, h and k, B-luminosities and colour indices) are given in Table 3. A colon designates fixed parameters. The model is represented by solid lines in Figs. 1–6.

The total luminosity of M31 is calculated to be $L_B = 1.62 \pm 0.21 \cdot 10^{10}\,L_\odot$, the optically visible mass $M_{vis} = 7.7 \pm 2.2 \cdot 10^{10}\,M_\odot$, the corresponding M/L ratio $4.8 \pm 1.5\,M_\odot/L_\odot$.

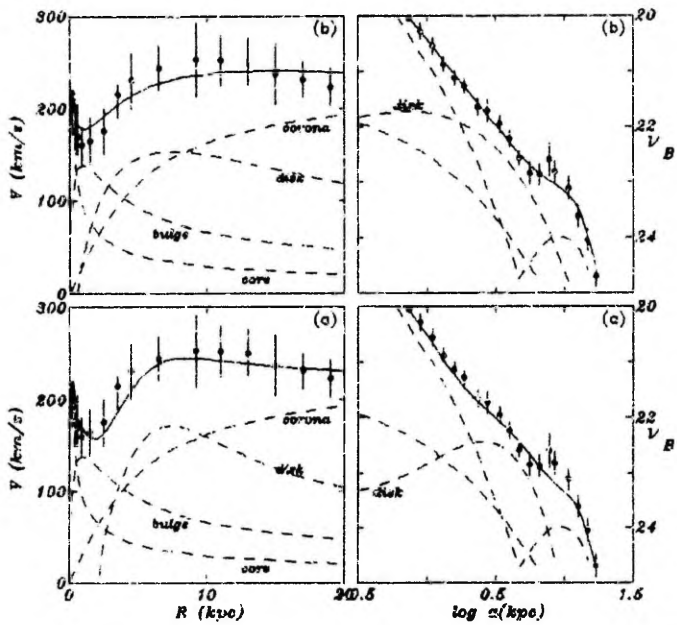

Figure 10 The rotation curve and brightness profile for different disk parameter N. (a): N =0.8, (b): N =2.

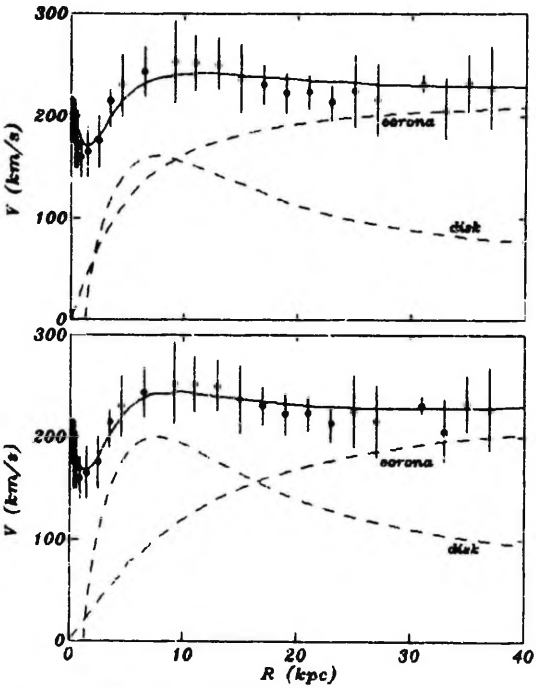

Figure 11 The rotation curve of M31 for different parameter x of the corona. (a): $a_o = 60$, (b): $a_o = 140$.

Table 3. Model parameters

Population	a_0 (kpc)	M (10^{10} $M_\odot$)	ϵ	N	κ	h	k
Nucleus	:0.0039	:0.031	:0.69	:1.2	:0.	6.007	0.334
Core	0.10	0.20	0.82	1.5	:0.	11.28	0.172
Bulge	0.75	1.0	0.67	2.4	:0.	93.32	0.0142
Halo	:4.8	0.8	:0.47	:4.9	:0.	25190.	5.91 10−6
Disk	4.1	5.1	0.10	1.3	0.63	7.393	0.270
Flat	:11.1	:0.52	:0.02	:0.30	:0.56	1.153	1.39
Corona	60.	320.	:1.			61.27	0.0631

Table 3. continued . . .

Population	M/L_B ($M_\odot/L_\odot$)	B-V	U-B	V-R
Nucleus	:32.		:0.88	
Core	13.	(1.03)	0.80	0.89
Bulge	2.6	0.97	0.54	0.75
Halo	:2.0	:0.79	:0.21	:0.68
Disk	15.	1.01	(0.90)	0.88
Flat	1.1	0.45	-0.38	0.54

1) Colour indices in parenthesis are uncertain.
2) The parameters a_o, ϵ for the disk and flat subsystems are for positive mass components.
3) The parameters marked with a colon were kept fixed during the fitting process.

The mass-to-light ratio of both disk-like components (disk + flat) together is $M/L_B = 7.1\,M_\odot/L_\odot$, of all spheroidal components (nucleus+core+bulge+halo) together $M/L_B = 2.5\,M_\odot/L_\odot$. High mass-to-light ratio for the nucleus $M/L = 32.$ is usually understood as the presence of a point mass in the centre of the galaxy (Richstone et al. 1990; Bradley et al. 1991). However, due to its small dimensions and mass, when compared to the whole galaxy, the detailed nuclear structure of M31 does not influence the general gravitational field of the galaxy.

Table 4 presents some descriptive functions calculated for our final model. $K_R \equiv \partial\Phi/\partial R$, where Φ is the gravitational potential, is the gradient of the gravitational potential in the radial direction (in the units of $km^2s^{-2}kpc^{-1}$) . $M(R)$ is the effective inner mass, defined as a point mass at the centre of the galaxy having the same gravitational attraction at R as the subsystem. The quantity f_B is the local M/L ratio in the B-colour derived by dividing the effective mass and the effective luminosity in a shell limited by the radiuses R and $R + \Delta R$. The radii are in kiloparsecs, the masses in the units of $10^{10}\,M_\odot$, the M/L ratios in solar units. Under the term 'spheroidal' in this Table we mean all spheroidal components together, i.e. the nucleus, the core, the bulge and the halo.

The calculated local mass-to-luminosity ratios are given in Fig. 12. A clear difference between the visible and dark matter begins at the distance $R =$ 14 kpc.

The mass-to-light ratio within the Holmberg radius is $17\,M_\odot/L_\odot$. The radius at which the masses of dark matter and visible matter become equal is 12 kpc. The effective inner and local M/L ratios for limiting radii of various

types of observations are given in Table 5.

The nearest distance limit is at $R = 26$ kpc – the outer radius of the surface photometry, so the integral and local M/L ratios at this radius are well established. And even this very conservative estimate for the M/L ratio of the dark matter is very large. Within the distance of outermost satellites the ratio of the visible mass to the total one is $M_{vis}/M_T = 0.023$.

Table 4. Calculated descriptive functions

R	K_R	$\log M(R)$									f_B
	(km^2/s^2kpc)	core	bulge	halo	spher.	disk	flat	visible	corona	total	
0.001	$2.94\ 10^7$	-6.13	-7.22	-7.90	-3.17			-3.17		-3.17	32.
0.002	3.65	-5.27	-6.36	-7.13	-2.47			-2.47		-2.47	32.
0.005	2.81	-4.13	-5.25	-6.13	-1.79			-1.79		-1.79	31.
0.01	1.27	-3.32	-4.43	-5.39	-1.54			-1.54		-1.54	26.
0.02	$3.75\ 10^6$	-2.56	-3.64	-4.70	-1.51			-1.47		-1.47	11.
0.04	1.23	-1.88	-2.90	-4.04	-1.34			-1.33		-1.33	8.6
0.06	$7.62\ 10^5$	-1.54	-2.48	-3.66	-1.20			-1.18		-1.18	8.3
0.08	5.75	-1.32	-2.20	-3.40	-1.07			-1.05		-1.05	7.7
0.1	4.69	-1.17	-1.98	-3.21	-0.96			-0.94		-0.94	7.1
0.2	2.34	-0.84	-1.37	-2.63	-0.65			-0.65	-3.72	-0.65	4.6
0.3	1.44	-0.74	-1.05	-2.31	-0.51			-0.52	-3.19	-0.52	3.3
0.4	$9.93\ 10^4$	-0.71	-0.85	-2.09	-0.42			-0.44	-2.82	-0.44	2.8
0.6	5.87	-0.70	-0.60	-1.81	-0.30			-0.33	-2.29	-0.33	2.6
0.8	4.09	-0.70	-0.44	-1.61	-0.21			-0.25	-1.92	-0.24	2.7
1.	3.12		-0.34	-1.47	-0.14			-0.18	-1.64	-0.16	3.0
2.	1.54		-0.11	-1.07	0.04	-0.77		0.12	-0.78	0.17	6.8
3.	1.21		-0.04	-0.86	0.11	-0.13		0.34	-0.31	0.43	13.
4.	1.07		-0.01	-0.74	0.15	0.20		0.51	0.00	0.63	18.
6.	$8.74\ 10^3$		0.01	-0.57	0.19	0.53		0.73	0.39	0.89	24.
8.	7.10		0.01	-0.47	0.20	0.68		0.85	0.62	1.05	19.
10.	5.83			-0.40	0.22	0.70	-1.11	0.90	0.79	1.15	13.
16.	3.58			-0.28	0.25	0.71	-0.34	0.92	1.11	1.32	20.
20.	2.78			-0.24	0.27	0.71	-0.29	0.93	1.24	1.41	180.
23.	2.36			-0.21	0.27	0.71	-0.29	0.93	1.31	1.46	800.
25.	2.15			-0.20	0.28	0.71	-0.29	0.93	1.36	1.50	2000.
30.	1.76			-0.18	0.29	0.71	-0.29	0.93	1.46	1.58	
40.	1.30			-0.14	0.30	0.71	-0.29	0.94	1.61	1.69	
60.	859.			-0.11	0.31	0.71	-0.29	0.94	1.81	1.86	

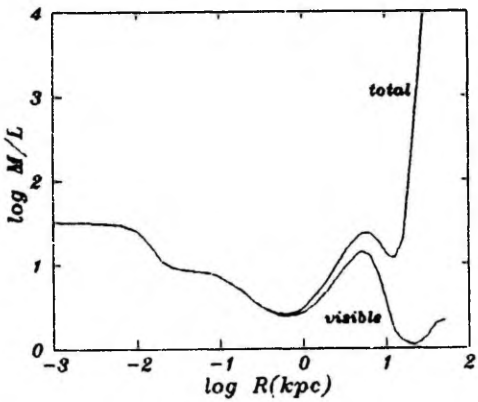

Figure 12 Local mass-to-luminosity ratios

Table 5. Mass-to-luminosity ratios for outer radii of various types of observations

Observations	Outer radius (kpc)	M/L_{int} ($M_\odot/L_\odot$)	M/L_{loc} ($M_\odot/L_\odot$)
Surface photometry	26	20	2500
Globular clusters	35	26	> 4000
Rotation curve	37	28	> 4000
Satellites	650*	190	

*The mean projected distance of the outermost satellites IC 1613, Pegasus, WLM.

6 Discussion

The model constructed in this paper for the galaxy M31 is based on a large body of observational data. Surface photometry along the major and minor axis in the UBVRJHK colours, rotation velocities, velocity dispersion data, distributions of neutral and molecular hydrogen, open clusters, stellar associations and globular clusters have been taken into account for decomposing the galaxy into subsystems and for the determination of population parameters.

Our result for the M/L ratio $M/L(R < 0.7$ kpc$) = 4$ nearly coincides with the value $6\,M_\odot/L_\odot$ by Simien et al. (1979). Kent (1989a) calculated the mass-to-light ratios in a three-component model for the spheroidal component $M/L = 6$ and for the disk component $M/L = 13$ in B (corrected for the absorption in our Galaxy). From a two-component model Braun (1991) obtained M/L =4.2 and 6 4 for the bulge and the disk, respectively. Taking into account

the differences in approximations the agreement between their results and ours is normal.

As it was mentioned earlier, two versions of the model were constructed, corresponding to different radii of the corona. Both models are in good agreement with the observed rotation curve. The masses of the corona for the models were 320 and 660, and the disk masses were 5.1 and 8.5, respectively, resulting in the mass-to-light ratios for the disk in the B-colour 15 and 25. The disk in the second version is essentially the 'maximum disk'. However, the M/L ratio is too large in this case, therefore the first version seems to be preferable as the final model. It is possible to discriminate between our two models on the ground of the HI distribution and kinematics. As it is known, the velocity dispersion σ_g and the characteristic thickness z_0 of the gas layer are connected with the density of the gravitating matter in the galactic plane ρ_0 as (Rohlfs 1977, p. 34) $\rho_0 = \sigma_g^2/(2\pi G z_0^2)$. For the distance $R = 8$ kpc, where the disk dominates in the light profile, the thickness of the gas layer was determined by Whitehurst et al. (1978) as $z_0 = 0.7$ kpc. The velocity dispersion at the same distance of the gas was found by Emerson (1976) to be $\sigma_g = 32$ km/s. From these data, the density of the gravitating matter at the galactic plane is $\rho_0 = 0.08\,\mathrm{M_\odot pc^{-3}}$. The values from our models are 0.085 and 0.13, respectively. Again it is evident that the data support the model with a smaller disk.

This result does not depend on the total mass of the corona used in the model since we deal with the balance of the disk and the corona masses in a region R <10 kpc. As a rule, the separation of the disk–corona masses in galaxies an unsolved problem yet. M31 is a lucky chance, because the volume density of the mass in the galactic plane can be calculated from HI observations. This density is more sensitive to the mass of the disk when compared with the corona as the disk and the corona in our model have different forms, enabling us to set constraints on the balance between them. Arguments supporting the spheroidal form of the dark matter distribution are given by Rohlfs (1982).

Using the positions and velocities of the Milky Way and Andromeda galaxies, Einasto & Lynden-Bell (1982) derived for the total mass of the Local Group $3-6\cdot10^{12}\,\mathrm{M_\odot}$. From the velocities of the satellites of our Galaxy Zaritsky et al. (1989) calculated the Galactic mass $M_G = 1.3\cdot10^{12}\,\mathrm{M_\odot}$ (the outermost satellites in this investigation have the distances 220–230 kpc). It is possible to use also an estimate of the ratio of masses of the Andromeda and Milky Way galaxies $M_A/M_G \simeq 2$ (Yahil et al. 1977). All these results are in mutual agreement, if the total mass of Andromeda is $M_A = 3\cdot10^{12}\,\mathrm{M_\odot}$.

Therefore, the 'maximum disk' is not the best approximation in the case of M31. It seems rather that every galaxy must be handled individually and the optimum disk must be chosen for every galaxy (for M81, e.g. just the 'maximum disk' is the best (Tenjes 1993).

Braun (1991) constructed a model of M31 without the massive corona. But the rotation curve he used in model construction extends only to R = 27 kpc. True enough, there is really a slightly decreasing rotation curve in the distance interval of 13 – 27 kpc. Accepting also high rotation velocities in the central region it is possible to construct a model without any dark matter. However, in this case we ignore 1) the rotation velocities in the region of 27 – 37 kpc, 2) the velocity dispersion of outermost globular clusters, 3) the kinematics of the Local Group galaxies. For this reason it seems to us that the models of M31 without the massive corona are not the best ones.

Appendix A: model construction

We assume M31 to consist of several physically homogeneous components with masses M, mass-to-light ratios f and fixed colour indices. The density distribution of each component is approximated as an inhomogeneous ellipsoid of rotation with a constant axial ratio $\epsilon = b/a$. All components, except the corona, form an optically visible part of the galaxy, and their volume densities are described by a modified exponential law

$$\rho(a) = \rho(0)\exp(-[a/(ka_0)]^{1/N}), \qquad (A1)$$

enabling to describe both the light profiles of disks and spheroidal components simply by varying the structure parameter N. The remaining component – the invisible massive corona – is represented by a modified isothermal law

$$\rho(a) = \begin{cases} \rho(0)([1+(\frac{a}{a_c})^2]^{-1} - [1+(\frac{a^0}{a_c})^2]^{-1}) & a \le a^0 \\ 0 & a > a^0, \end{cases} \qquad (A2)$$

resulting from the flatness of the rotation curves in outer parts of galaxies. In these formulae $\rho(0) = hM/(4\pi\epsilon {a_0}^3)$ is the central density, a is the distance along the major axis, $a_c = ka_0$ – the core radius, a_0 – the harmonic mean radius, a^0 – the outer cutoff radius for the corona, and h and k are normalizing parameters, depending on the parameter N (Appendix B).

For some subsystems (the disk and the flat components) it results from observations that a more suitable density distribution would be

$$\rho(a) = \rho_+(a) + \rho_-(a), \qquad (A3)$$

having a density depression in the central regions. If we demand that the density is zero at a = 0 and positive elsewhere, the following relations must held between the parameters of components ρ_+ and ρ_- : $a_{o-} = \kappa a_{o+}$, $M_- = -\kappa^2 M_+$, $\epsilon_- = \epsilon_+/\kappa$, where $\kappa < 1$ is a parameter which determines the relative

size of the hole in the centre of the disk. The structural parameters N_- and N_+ were assumed to be equal.

The density distributions for visible components were projected along the line of sight and their superposition gives us to the surface brightness distribution of the model

$$L(A) = 2\sum_i^n \frac{\epsilon_i}{E_i f_i} \int_A^\infty \frac{\rho_i(a) a da}{(a^2 - A^2)^{1/2}}. \qquad (A4)$$

A is the major semiaxis of the equidensity ellipse of the projected light distribution, n is the number of components and E_i are their apparent axial ratios.

The masses of the components can be determined from the rotation law

$$v_i^2(R) = 4\pi\epsilon_i G \int_0^R \frac{\rho_i(a) a^2 da}{(R^2 - e_i^2 a^2)^{1/2}}, \qquad (A5)$$

$$V^2(R) = \sum_i^n v_i^2(R). \qquad (A6)$$

where G is the gravitational constant and R is the distance in the eqatorial plane of the galaxy.

For 'hot' components the masses were determined from the tensor virial theorem

$$-M\mathbf{D} = \mathbf{W}$$

where $\mathbf{D}$ is the velocity dispersion tensor, and

$$\mathbf{W} = \int \rho \vec{r} \otimes \vec{g} dV$$

is the potential energy tensor. In case of n-component system the objects of a 'test' subsystem with the index k move under the gravitational potential of the whole galaxy and for this subsystem

$$-M_k \mathbf{D}_k = \int \rho_k \vec{r} \otimes \sum_{l=1}^n \vec{g}_l dV, \qquad (A7)$$

where $\vec{g}_l$ is the gravitational acceleration due to the subsystem with the index l. The mean line-of-sight velocity dispersion is in general

$$\langle \sigma^2 \rangle = \vec{e} \cdot \mathbf{D} \vec{e},$$

where $\vec{e} = (\cos\alpha, \cos\beta, \cos\gamma)$ is the line-of-sight unit vector. In componental form

$$\langle\sigma^2\rangle = d_{11}\cos^2\alpha + d_{22}\cos^2\beta + d^{33}\cos\gamma +$$

$$+2(d_{12}\cos\alpha\cos\beta + d_{13}\cos\alpha\cos\gamma + d_{23}\cos\beta\cos\gamma), \qquad (A8)$$

where d_{ij} are the elements of the tensor D. In case of our density distribution law Eq. (A1) from Eqs (A7) and (A8) one can derive a system of equations which connects the mean velocity dispersion of the k-th component along the line of sight with the masses of all components M_l (for detailed calculations see Einasto (1971))

$$\langle\sigma^2\rangle_k = \frac{G}{a_{0k}}\sum_{l=1}^{m} H_{kl}M_l. \qquad (A9)$$

In this formula m is the total number of components and H_{kl} are dimensionless coefficients depending on the mass distribution laws of the components k and l. It is evident that all subsystems contribute to the mean velocity dispersion of a particular component, but usually the influence of the component $k = l$ is more or less dominating. We note that in calculations we assume the velocity dispersion ellipsoid to be biaxial, i.e. $\sigma_R = \sigma_\theta \neq \sigma_Z$.

Appendix B: normalizing parameters

Let $\mu(a)$ be the mass of an ellipsoidal layer of unit thickness at the equator

$$\mu(a) = 4\pi\epsilon a^2\rho(a). \qquad (B1)$$

This function can be written in a dimensionless form

$$\mu(a) = \mu_o\mu^o(\alpha), \qquad (B2)$$

where $\alpha = a/a_o$ and μ_o, a_o are scale parameters having the dimensions of mass/lenght and lenght, respectively.

Moments of $\mu(a)$ are generally

$$\mathcal{M}_n\{\mu(a)\} \equiv \int_0^\infty \mu(a)a^n da = \mu_o a_o^{n+1}\int_0^\infty \mu^o(\alpha)\alpha^n d\alpha \qquad (B3)$$

(because $a^n da = a_o^{n+1}\alpha^n d\alpha$). Function $\mu^o(\alpha)$ is normalized so that

$$\mathcal{M}_{-1}\{\mu^o(\alpha)\} = \mathcal{M}_0\{\mu^o(\alpha)\} = 1. \qquad (B4)$$

In these cases (n=-1 and n=0) we get

$$\mathcal{M}_{-1}\{\mu(a)\} = \mu_o, \tag{B5}$$

$$\mathcal{M}_0\{\mu(a)\} = \mu_o a_o. \tag{B6}$$

On the other hand, from the definition of the function $\mu(a)$ it follows that

$$\mathcal{M}_0\{\mu(a)\} = M, \tag{B7}$$

thus

$$\mu_o = M/a_o \tag{B8}$$

and

$$\mathcal{M}_n\{\mu(a)\} = M a_o^n \int_0^\infty \mu^o(\alpha)\alpha^n d\alpha.$$

In the case of exponential density distribution (Eq. A1) using Eqs. (B1), (B2) and (B8)

$$\mu^o(\alpha) = h \exp[-(\frac{\alpha}{k})^{1/N}]\alpha^2.$$

Constants h and k can be calculated from Eq. (B4).

Appendix C: the 3-component model

As the nucleus, the halo and flat subsystems contribute little to the gravitational potential of the Andromeda Galaxy and if our purpose is to derive only general mass and light distribution form we may construct a model without these components. Morever, it would be interesting to construct a model with one spheroidal component, i.e. without the core. Therefore, in the present Appendix we construct a 3-component model consisting of the spheroidal component, the disk and the corona.

The process of the model construction was as described in Sect. 4. The initial data set consists of the surface brightness profile along the major and the minor axis in BUVR colours, the rotation curve and the velocity dispersion profile. The number of observational data points was 269, the number of free parameters 19 (the bulge: ϵ, a_o, M, N, L_B, L_U, L_V, and L_R; the disk: ϵ, κ, a_o, M, N, L_B, L_U, L_V and L_R; the corona: a_o.) The mass of the corona was fixed $M = 320 \cdot 10^{10}\,\mathrm{M}_\odot$ from the 7-component model.

The final parameters obtained from the best fit process are presented in Table C1. The comparison of the model with the observations can be seen in Figs. C1 and C4. The mean velocity dispersion of the bulge resulting from the model is $\langle \sigma_{bulge} \rangle = 140$ km/s.

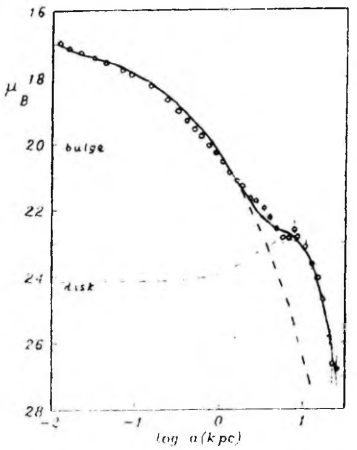

Figure C1 The surface brightness of the 3-component model of M31 in the B-colour. Open circles – observations, solid line – model, dashed lines – models for components.

Table C1. Model parameters

Population	a_0 (kpc)	M (10^{10} $M_\odot$)	ϵ	N	κ	h	k
Bulge	1.1	4.5	0.51	3.6	:0.	1229.	0.00047
Disk	8.3	7.0	0.10	0.7	0.73	2.240	0.848
Corona	80.	:320.	:1.			61.27	0.0631
Population	M/L_B ($M_\odot/L_\odot$)	B-V	U-B	V-R			
Bulge	5.8	0.91	0.62	0.67			
Disk	8.5	0.84	0.35	0.76			

The parameters a_o, ϵ for the disk are for positive mass components.

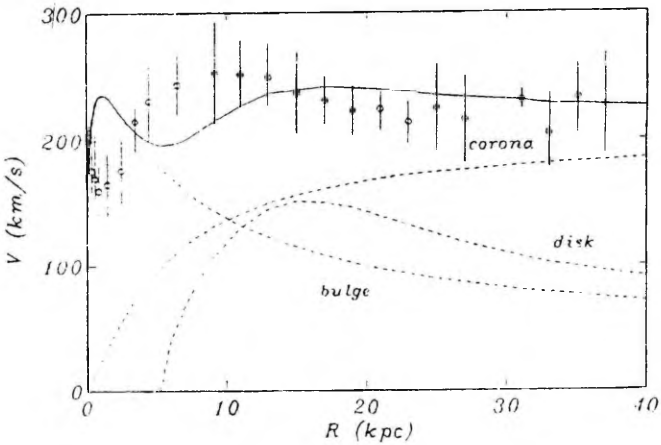

Figure C2 The rotation curve of the 3-component model of M31. Open circles – observations, solid line – our best-fit model, dashed lines – models for components.

References

Alloin D., Pelat D., Bijaoui A.: 1976. *Astron. Astrophys.* **50**, 127

Babcock H.W.: 1938. *Publ. Astron. Soc. Pacific* **50**, 174

Babcock H.W.: 1939. Lick Obs. Bull. 19, 41

Battaner E., Beckman J.E., Mediavilla E. et al.: 1986. *Astron. Astrphys.* **161**, 70

Battistini P., Bònoli F., Braccesi A. et al.: 1980. *Astron. Astrophys. Suppl.* **42**, 357

Boulesteix J., Georgelin Y.P., Lecoarer E., Marcelin M., Monnet G.: 1987. *Astron. Astrophys.* **178**, 91

Braun R.: 1991. *Astrophys. J.* **372**, 54

Bradley M., Curir A., de Felice F.: 1991. *Astrophys. J.* **381**, 72

Brinks E., Shane W.W.: 1984. *Astron. Astrophys. Suppl.* **55**, 179

Buonanno R., Corsi C., Battistini P., Bònoli F., Fusi Pecci F.: 1982. *Astron.*

Astrophys. Suppl. **47**, 451

Burstein D., Heiles C.: 1984. *Astrophys. J. Suppl.* **54**, **33**

Ciardullo R., Rubin V.C., Jacoby G.H., Ford H.C., Ford Jr. W.K.: 1988. *Astron. J.* **95**, 438

Cohen J.: 1979. *Astrophys. J.* **228**, 405

Cohen J.G., Freeman K.C.: 1991. *Astron. J.* **101**, 483

Cram T.R., Roberts M.S., Whitehurst R.N.: 1980. *Astron. Astrophys. Suppl.* 40, 215

Crampton D., Cowley A.P., Schade D., Chayer P.: 1985. *Astrophys. J.* **280**, 494

Davis J., Code A.D., Mathis J.S., Welch G.A.: 1982. *Astron. J.* **87**, 849

Davoust E., Paturel G., Vauglin I.: 1985. *Astron. Astrophys. Suppl.* **61**, 273

Delisle S., Hardy E.: 1992. *Astron. J.* **103**, 711

de Vaucouleurs G.: 1958. *Astrophys. J.* **128**, 465

Dressler A.: 1984. *Astrophys. J.* **286**, 97

Dressler A., Richstone, D.O.: 1988. *Astrophys. J.* **324**, 701

Einasto J.E.: 1969. *Astrofizika* **5**, 137

Einasto J.: 1971. *Structure and Evolution of Regular Galaxies*, Tartu (unpublished Ph. D. thesis, in russian)

Einasto J.: 1972. Tartu Astrofüüs. Obs. Teated Nr. 40, 3 = Einasto J.: 1974. In: *Proc. First European Astr. Meet. vol 2, Stars and the Milky Way System*, L.N.Mavridis (ed), Berlin, Heidelberg, New-York: Springer, p. 291

Einasto J., Haud U.: 1989. *Astron. Astrophys.* **223**, 89

Einasto J., Lynden-Bell D.: 1982. *Monthly Notices Roy. Astron. Soc.* **199**, 67

Einasto J., Tenjes P., Traat P.: 1979. Astron. Circ No. 1032, 1

Einasto J., Tenjes P., Barabanov A.V., Zasov A.V.: 1980. *Astrophys. Space Sci.* **67**, 31

Elson R.A.W., Walterbos R.A.M.: 1988. *Astrophys. J.* **333**, 594

Emerson D.T.: 1976. *Monthly Notices Roy. Astron. Soc.* **176**, 321

Fabbiano G.: 1989. *Annual Review Astron. Astrophys.* **27**, 87

Fricke W.: 1954. *Zeitschr. für Astroph.* **34**, 137

Gilmore G., King I., van der Kruit P.: 1990. *The Milky Way as a Galaxy*, Geneva Observatory: Sauverny-Versoix, Switzerland

Haud U.: 1981. *Astrophys. Space Sci.* **76**, 477

Haud U., Einasto J.: 1989. *Astron. Astrophys.* **223**, 59

Hiromoto N., Maihara T., Oda N., Okuda H.: 1983. *Publ. Astron. Soc. Japan* **35**, 413

Hodge P.W., Kennicutt R.C.: 1982. *Astron. J.* **87**, 264

Hoessel J.G., Melnick J.: 1980. *Astron. Astrophys.* **84**, 317

Huchra J.P.: 1988. In: *From Asteroids to Quasars: The W. Liller Symposium.* P.Lugger (ed.), Cambridge University Press

Huchra J., Stauffer J., van Speybroeck L.: 1982. *Astrophys. J.* **259**, L57

Huchra J., Brodie J.P., Kent S.M.: 1991. *Astrophys. J.* **370**, 495

Iijima T., Ito K., Matsumoto T., Uyama K.: 1976. *Publ. Astron. Soc. Japan* **28**, 27

Illingworth G.: 1976. *Astrophys. J.* **204**, 73

Johnson H.M.: 1961. *Astrophys. J.* **133**, 309

Joly M.: 1974. *Astron. Astrophys.* **33**, 177

Kent S.M.: 1983. *Astrophys. J.* **266**, 562

Kent S.M.: 1987. *Astron. J.* **94**, 306

Kent S.M.: 1989a. *Astron. J.* **97**, 1614

Kent S.M.: 1989b. *Publ. Astron. Soc. Pacific* **101**, 489

Kent S.M., Huchra J.P., Stauffer J.: 1989. *Astron. J.* **98**, 2080

Kinman T.D.: 1965. *Astrophys. J.* **142**, 1376

Koper E., Dame T.M., Israel F.P., Thaddeus P.: 1991. *Astrophys. J.* **383**, L11

Kormendy J.: 1988. *Astrophys. J.* **325**, 128

Kuzmin G.: 1943. *Tähetorni kalender 1943. aastaks*, 85

Kuzmin G.G.: 1952. *Tartu Astron. Obs. Publ.* **32**, 211

Light, E.S., Danielson, R.E., Schwarzschild, M.: 1974. *Astrophys. J.* **194**, 257

Lyngå G.: 1959. *Medd. Lunds Astron. Obs. Ser. II*, Nr. 137, 3

Martinez Roger C., Phillips J.P., Sanchez Margo C.: 1986. *Astron. Astrophys.* **161**, 237

McElroy D.B.: 1983. *Astrophys. J.* **270**, 485

Mellier Y., Fort B., Kneib J.P.: 1992. *Astrophys. J.* (in press)

Mihalas D., Binney J.: 1981. *Galactic astronomy: structure and kinematics, 2nd ed.*, Freeman: San Francisco

Mould J., Graham J., Matthews K., Soifer B.T., Phinney E.S.: 1989. *Astrophys. J.* **339**, L21

Nieto J.-L., Macchetto F.D., Perryman M.A.C., di Serego Aligheri S., Lelièvre G.: 1986. *Astron. Astrophys.* **165**, 189

Nolthenius R., Ford H.C.: 1987. *Astrophys. J.* **317**, 62

Racine R.: 1991. *Astron. J.* **101**, 865

Redman R.O., Shirley E.G.: 1937. *Monthly Notices Roy. Astron. Soc.* **97**, 416

Richstone D., Bower G., Dressler A.: 1990. *Astrophys. J.* **353**, 118

Rohlfs K.: 1977. *Lectures on Density Wave Theory. Lecture Notes in Physics, 69.* Springer-Verlag, Berlin, Heidelberg

Rohlfs K.: 1982. *Astron. Astrophys.* **105**, 296

Rohlfs K., Kreitschmann J.: 1981. *Astrophys. Space Sci.* **79**, 289

Rohlfs K., Kreitschmann J.: 1988. *Astron. Astrophys.* **201**, 51

Sancisi R., van Albada T.S.: 1987. In: *Proc. IAU Symp. 117, Dark Matter in the Universe*, J.Kormendy, G.R.Knapp (eds.), Reidel, Dordrecht: Kluwer, p. 67

Sandage A.: 1986. *Annual Review Astron. Astrophys.* **24**, 421

Sandage A.R., Becklin E.E., Neugebauer G.: 1969. *Astrophys. J.* **157**, 55

Sargent W.L.W., Kowal C.T., Hartwik F.D.A., van den Bergh S.: 1977. *Astron. J.* **82**, 947

Schmidt M.: 1957. *Bull. Astron. Inst. Netherl.* **14**, 17

Sharov A.S., Lyutyj V.M.: 1980. *Astron. Zh.* **57**, 449

Sharov A.S., Lyutyj V.M.: 1981. *Pisma v Astron. Zh.* **7**, 394

Sharov A.S., Lyutyj V.M.: 1983. *Astrophys. Space Sci.* **90**, 371

Simien F., Pellet A., Monnet G.: 1979. *Astron. Astrophys.* **72**, 12

Sizikov V.S.: 1969. *Astrofizika* **5**, 317

Spillar E.J., Canterna R., Carels K.H., Benson J.A., Dyck H.M.: 1990. *Astrophys. J.* **349**, L13

Spinrad H., Liebert J.W.: 1975. *Astrophys. J.* **200**, 582

Tenjes P.: 1993. in preparison

Tenjes P., Haud U.: 1991. *Astron. Astrophys.* **251**, 11

Tinsley B.: 1980. *Fund. Cosm. Phys.* **5**, 287

Traat P.: 1991. In: *Chemical and dynamical evolution of galaxies*, F.Ferrini, J.Franco, F.Matteucci (eds.), Pisa: ETS Editrice

van den Bergh S.: 1969. *Astrophys. J. Suppl.* **19**, 145

van den Bergh S.: 1991. *Publ. Astron. Soc. Pacific* **103**, 1053

Vetesnik M.: 1962. *Bull. Astron. Inst. Czechoslovakia* **13**, 180

Walterbos R.A.M., Kennicutt Jr. R.C.: 1988. *Astron. Astrophys.* **198**, 61

Whitehurst R.N., Roberts M.S., Cram T.S.: 1978. In: *Structure and Properties of Nearby Galaxies, IAU Symp. 77*, E.M.Berkhuijsen, R.Wielebinski (eds.),Dordrecht: Reidel, p. 175

Whitmore B.C., McElroy D.B., Tonry J.L.: 1985. *Astrophys. J. Suppl.* **59**, 1

Wirth A., Smarr L.L., Bruno T.L.: 1985. *Astrophys. J.* **290**, 140

Yahil P.J., Tammann G.A., Sandage A.: 1977. *Astrophys. J.* **217**, 903

Zaritsky D., Olszewski E.W., Schommer R.A., Peterson R.C., Aaronson M.: 1989. *Astrophys. J.* **345**, 759

CHAPTER 3 STAR FORMATION IN M31*

1 Introduction

The relation between the star formation rate and the local density of the interstellar gas was proposed by Schmidt (1959) in the form $d\rho_s/dt = \gamma\rho_g^n$, where ρ_s and ρ_g are the volume densities of stars and gas, and γ and n are parameters. For solar vicinity he found $n = 2$. Later the same expression was used for surface densities and for n the values between 1.4 – 2.9 were derived for several nearby galaxies (q.v. Einasto 1972, Berkhuijsen 1977). In most cases the surface density distributions of HII regions and the HI emission were compared for this purpose. The advantages of this approach are evident: HII regions are luminous in the H_α line and therefore easier to observe. As a result, the corresponding data samples are usually more complete than those of individual stars.

However, dimensions and brightnesses of HII regions depend on several factors besides the properties of the central star, e.g. the density of the surrounding gas. We must take into account that the atomic and molecular gas is not smoothly distributed but consists of individual clouds of various sizes. In connection with this, the influence of the gas densities is twofold.

1. Formation of a HII region depends on the probability of the spatial coincidence of giant gas clouds and bright young stars after the star formation. As the lifetime of HII regions may depend on the surrounding gas density as well (Nakai & Sofue 1984), the distribution of HII regions does not necessarily correspond to that of young stars.
2. The radius of a HII region depends on the density of the surrounding gas (the area of the region is proportional to the density in power $-2/3$). Unfortunately, little is known about the variation of mean densities in gas clouds.

Therefore, the distribution of HII regions depends on the gas density in a complicated way, which is difficult to quantify. In addition, the interstellar dust may influence the brightness and the dimensions of HII regions (Lequeux

* This Chapter bases on the paper by Tenjes, P. & Haud, U., "The Schmidt star formation law in the Andromeda galaxy." *Astronomy and Astrophysics* **251**, 11–14, 1991

et al. 1981). From the observations by Sharov (1968) and Hodge (1980) it follows that in M31 the dust regions may be found at distances of $0 - 70'$ from the centre. Evidently, inside this interval the dust may considerably alter the distribution of HII regions when compared to that of young stars. For these reasons it seems better to use for the determination of star formation rates direct observations of the objects of the young stellar component: OB-associations, open clusters and young field stars (young luminous stars, not belonging to OB-associations or open clusters). The vicinity of M31 makes it an ideal candidate for such studies.

2 An analysis of observational data

Stellar associations have been observed by van den Bergh (1964), who identified 188 associations, Richter (1971) and Efremov et al. (1987), who added 7 and 15 associations, respectively. Due to the larger mean diameter of associations in M31 in comparison with those in our Galaxy, these objects were identified as star complexes by Efremov et al. (1987). We deprojected the distribution of associations to 'face on' and calculated the number surface densities and the total area of associations in concentric rings. The position angle of the major axis was taken to be $PA = 37.7°$ and the inclination angle $i = 12.5°$. The distribution of the surface density of association areas with the galactocentric distance is shown in Fig. 1 by crosses. The number surface density distribution of 403 *open clusters*, identified by Hodge (1979), is represented by squares. Altogether about a thousand *young field stars* were studied by van den Bergh (1958), Reddish (1962), Richter (1976), Berkhuijsen & Humphreys (1989). From the paper by Berkhuijsen & Humphreys we chose a sample of stars with colour indices $(U - B) \leq -0.9$ because the slope of the luminosity function of this sample is close to the slope of the luminosity function found in several nearby galaxies, as noted by the authors. From the data by Richter the background density of 6.4 stars per square degree was subtracted. The averaged distribution of stars is represented in Fig. 1 by triangles.

All three distributions were normalized to the same area under the distribution curve. As the possible systematic errors in the distributions of three types of extreme population I objects are independent, we may increase the weight of our results by averaging these distributions. The result is given in Fig. 1 by dots.

The distribution of neutral hydrogen has been studied by many observers through four decades. From aperture synthesis observations most valuable for us are those made by Emerson (1974), Unwin (1980) and Brinks & Shane (1984) and from single dish observations those by Roberts & Whitehurst (1975) and Cram et al. (1980). For inner regions, where a high spatial resolution is needed,

we preferred the aperture synthesis observations. In outer regions of the galaxy synthesis observations have some drawbacks: a relatively poor sensitivity and the loss of extended structures. For these reasons in outer regions we favoured single dish observations.

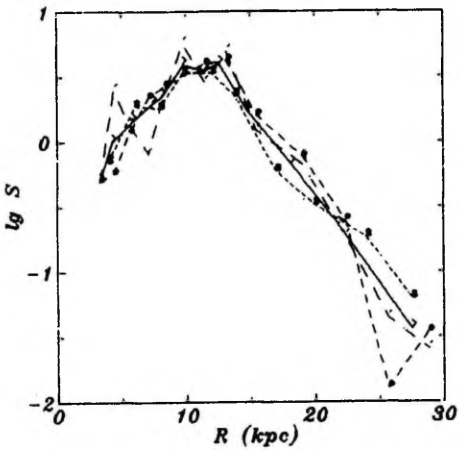

Figure 1. The averaged surface density distributions of young stellar constituents of M31. The densities are in arbitrary units. Crosses represent stellar associations, squares – open clusters, triangles – individual stars, dots – the mean distribution.

In the Schmidt law we must consider the total density of hydrogen, both the atomic and molecular one. The H_2 distribution was derived using the CO observations by Dame et al. (1990) and the CO to H_2 conversion factor $5 \cdot 10^{20}$ $mol/cm^2[K\ km/s]^{-1}$ (Koper et al. 1990), which is twice the value accepted for our Galaxy. The sum of mean HI and H_2 surface density distributions is represented in Fig. 2 by a dashed line.

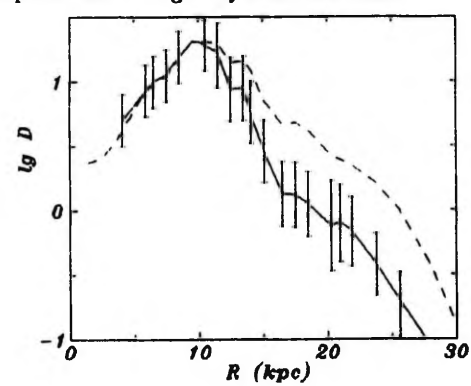

Figure 2 The averaged surface density distribution of neutral (atomic + molecular) hydrogen. The dashed line shows surface densities, the solid line – space densities.

3 Results

A comparison of the surface densities of the young stellar component with the densities of gas demonstrates an obvious correlation (Fig. 3). Using logarithmic scales the relation is approximately linear in accordance with the results of Schmidt (1959). The best fit line has a slope $n = 1.30 \pm 0.22$.

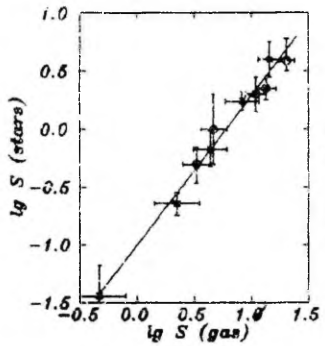

Figure 3 The correlation between the mean surface density of the young stellar component and the gas density. Open rings correspond to the inner regions of the galaxy R $\leq$ 10kpc, crosses – to the outer regions R > 10kpc.

The Schmidt law was originally formulated for spatial densities. To convert our result to spatial densities, we must take into account the young stellar disk and gas layer thickness variations in M31. For the stellar component the observations of late-type edge-on galaxies indicate that the thickness of the disk is independent of R (van der Kruit & Searle 1981, 1982) and, therefore, spatial densities are simply proportional to surface densities. For gas, the conversion of gas surface densities to spatial densities is also simple if we use for the thickness of the layer the model derived by Emerson (1976) and supposing the usual $\mathrm{sech}^2(z/z_0)$ - law for the density distribution in the z-direction. The derived spatial densities for gas are given in Fig. 2 by a solid line. Using these results, we derive for the parameter n a value $n = 0.95 \pm 0.20$ (Fig. 4).

If we handle separately the inner (R $\leq$ 10kpc) and outer (R > 10kpc) regions of the Andromeda galaxy we can see from Fig. 4 somewhat surprisingly that while the parameter n is the same ($n = 1.0$) in both regions, the parameter γ differs by a factor of 2.6. As it was stressed by the referee, the stellar disk with a constant thickness, as proposed by van der Kruit & Searle (1982) is at variance with the Schmidt law at R > 10 kpc if the thickness of the gas disk is variable. We also investigated the correlation between the densities of the gas and the stars for the case that the thickness of the stellar disk changes in a similar way as the thickness of the gas layer. As it is seen from Fig. 5, in

this case no difference of the parameter γ between the inner and outer regions of the galaxy can be noticed. The parameter $n = 1.17 \pm 0.23$ is somewhat larger than the one resulting from a constant disk thickness hypothesis, but it is also evident that within the errors the assumption $n = 1$ is a reasonable approximation for the evolution models of the stellar systems.

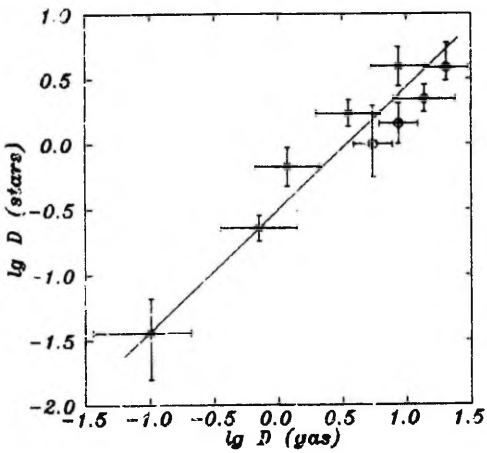

Figure 4 The correlation between the spatial densities of the young stellar component (constant disk thickness) and the gas. Coded as in previous figure.

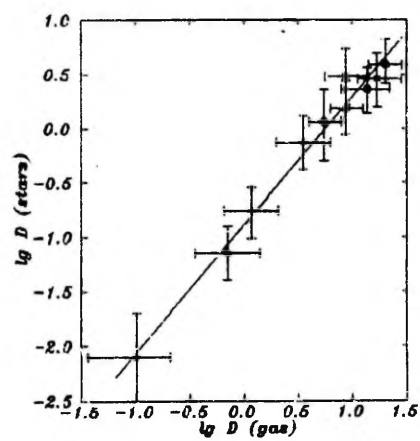

Figure 5 The correlation between the spatial densities of the young stellar component (variable disk thickness) and the gas. Coded as in previous figure.

Knowing the gas mass $M_{gas} = 4.6 \cdot 10^9\,M_\odot$ and the total visible mass of the galaxy $M = 77 \cdot 10^9\,M_\odot$ (Tenjes et al. 1992, Chapter 2 in present Thesis)

we can calculate the characteristic time of star formation in the Andromeda galaxy. If $n = 1$, the Schmidt law in an integral form is $M_g = M \exp(-t/t_o)$, where t is the star formation age of the galaxy and t_o is the characteristic time of star formation. If the age of the galaxy is taken to be $20 \cdot 10^9$ yrs (the age of the oldest globular clusters, Carney (1992)), for t_o we derive the value $t_o = 4.6 \pm 1.5 \cdot 10^9$ yrs. The star formation rate at present is $\dot{M} = 0.81 \pm 0.36\, M_\odot/yr$.

4 Discussion

Our results for the correlation between the spatial densities of the young stellar component and gas strongly support the star formation law parameter $n = 1$ and exponential gas depletion in galactic evolution models. Earlier Berkhuijsen (1977) found from HII regions and the spatial densities of HI the value $n = 1.5$. Nakai & Sofue (1982) compared the spatial densities of OB associations and open clusters with that of HI and derived $n = 1.3 - 1.9$.

In principle, the correlation between the surface densities of young stellar and gas components lack any physical meaning. Only if the thicknesses of both components have similar behaviour, the correlation between the spatial densities, as proposed by Schmidt (1959), is reduced to a similar relation between the surface densities. The observations of the Andromeda nebula (Emerson 1976) and several other galaxies (van der Kruit & Allen 1978) indicate that the thickness of the HI layer changes considerably in the intermediate and outer regions of galaxies. Therefore, from the correlations presented in Figs. 4 and 5 it follows that the young stellar component of M31 may have a nearly constant thickness only up to the distance R $\sim$ 12kpc (corresponding to the surface brightness $\mu_B \simeq 23.5$). Beyond this we may expect a substantial thickening of the young stellar population disk in a way as it was derived from the observations of neutral hydrogen. Unfortunately, such a phenomenon would be difficult to observe.

References

Berkhuijsen, E.M.: 1977. *Astron. Astrophys.* **57**, 9

Berkhuijsen, E.M , Humphreys, R M.: 1989. *Astron. Astrophys.* **214**, 68

Brinks, E., Shane, W.W.: 1984. *Astron. Astrophys.* **55**, 179

Carney, B.W.: 1992. In: *The Stellar Populations of Galaxies. IAU Symp. No. 149*, B.Barbuy, A.Renzini (eds.), Dordrecht: Kluwer, p. 15

Cram, T.R., Roberts, M.S., Whitehurst, R.N.: 1980. *Astron. Astrophys.* **40**, 215

Dame, T.M., Koper, E., Israel, F.P., Thaddeus, P.: 1990. Leiden Observ. Prepr. 1990–149

Einasto, J.: 1972. *Astrophys. Lett.* **11**, 195

Efremov, Y.N., Ivanov, G.R., Nikolov, N.S.: 1987. *Astrophys. Space Sci.* **135**, 119

Emerson, D.T.: 1974. *Monthly Notices Roy. Astron. Soc.* **169**, 607

Emerson, D.T.: 1976. *Monthly Notices Roy. Astron. Soc.* **176**, 321

Hodge, P.W.: 1979. *Astron. J.* **84**, 744

Hodge, P.W.: 1980. *Astron. J.* **85**, 376

Hodge, P.W., Mateo, M., Lee, M.G., Geisler, D.: 1987. *Publ. Astron. Soc. Pacific* **99**, 173

Koper, E., Dame, T.M., Israel, F.P., Thaddeus, P.: 1990. Leiden Observ. Prepr. 1990–149

Lequeux, J., Maucherat-Joubert, M., Deharveng, J-M., Kunth, D.: 1981. *Astron. Astrophys.* **103**, 305

Nakai, N., Sofue, Y.: 1982. *Publ. Astron. Soc. Japan* **34**, 199

Nakai, N., Sofue, Y.: 1984. *Publ. Astron. Soc. Japan* **36**, 313

Reddish, V.C.: 1962. *Zeitschr. für Astroph.* **56**, 194

Richter, G.A.: 1971. *Astron. Nachr.* **292**, 275

Richter, G.A.: 1976. *Astron. Nachr.* **297**, 269

Roberts, M.S., Whitehurst, R.N.: 1975. *Astrophys. J.* **201**, 327

Schmidt, M.: 1959. *Astrophys. J.* **129**, 243

Sharov, A.S.: 1968. *Astron. Zh.* **45**, 980

Tenjes, P., Haud, U., Einasto, J.: 1992. *Astron. and Astrophys.* in press (Chapter 2 in present Thesis)

Unwin, S.C.: 1980. *Monthly Notices Roy. Astron. Soc.* **192**, 243

van den Bergh, S.: 1958. *Publ. Astron. Soc. Pacific* **70**, 109

van den Bergh, S.: 1964. *Astrophys. J. Suppl.* **9**, 65

van der Kruit, P.C., Searle, L.: 1981. *Astron. Astrophys.* **95**, 105

van der Kruit, P.C., Searle, L.: 1982. *Astron. Astrophys.* **110**, 61

van der Kruit, P.C., Allen, R.J.: 1978. *Annual. Rev. Astron. Astrophys.* **16**, 103

CHAPTER 4 THE ELLIPTICAL GALAXY M87*

1 Introduction

The first attempts to decompose elliptical galaxies into several actually existing components was made by Bertola & Capaccioli (1970) and Einasto (1972a). They tried to derive the parameters of the components from photometrical and spectrophotometrical data. However, at that time the amount of observations was insufficient for this purpose, so the decomposition was poorly determined. By now the amount and precision of all kinds of observations has remarkably increased, and we believe that our decomposition is more unambiguous and the parameters of the components are reliable enough.

One of the most favorable ellipticals for population studies is the galaxy M87. It has been observed from the infrared K-band to X-rays and is nearby enough for detailed observations of globular clusters. The galaxy M87 is also of interest as one of the luminosity distribution standards recommended by the IAU (de Vaucouleurs 1979). We hope to be able to answer three questions:

1. What are the stellar populations in M87 and what values do their parameters take?
2. Can the observed central rise in the M87 brightness profile be explained by normal stellar constituents?
3. Do the observations require a massive corona?

Throughout this paper all luminosities have been corrected for absorption in our Galaxy according to Burstein and Heiles (1984). The distance to M87 has been taken 20 Mpc corresponding to $H_o = 50 kms^{-1} kpc-1$. For different values of the Hubble constant the distances, luminosities and mass-to-light ratios must be multiplied by a factor h_{50}^{-1}, h_{50}^{-2}, h_{50} respectively, where $h_{50} = H_o/50$.

---

* This Chapter bases on the paper by Tenjes, P., Einasto, J., Haud, U., "Galactic models with massive coronae. III. Giant elliptical galaxy M87." *Astronomy and Astrophysics* **248**, 395–403, 1991

2 Analysis of observational data

An acceptable model of an elliptical galaxy should represent the observed brightness profile along minor and major axes, which yield the axial ratios, and the changes in colour indices and kinematical data with radius (the velocity dispersion profile). In the case of M87 we must fit our model also to the distribution and mean velocity dispersion of globular clusters and X-ray radiation. Here we give some comments on the data used.

By now the *photometry* of M87 is available in seven colours. The status of the surface photometry made up to 1978 has been described by Carter & Dixon (1978). Here we shall summarize only later work. Table 1 presents references, the faintest observed isophotes (mag/arcsec^2), corresponding distances along the major axis (arcmin), colour systems used and some remarks on the observations in the direction of the minor axis.

Table 1. Photometrical data

Reference	Faintest isophote	Radius (')	Colour system	Minor axis?
Bagnuolo, Chambers 1987	(17.4)	0.05	V	
Boroson et al. 1983	23.9	2.6	BVRI	
Boughn. Saulson 1983	23.3	9.5	K	
Caon et al. 1990	27.6	16.	B	Yes
Davis et al. 1985	23.4	2.2	BUR	
Ichikawa et al. 1986	27.5	7.5	B	
Jedrzejewski 1987	22.5	1.4	BR	Yes
Kormendy 1985	(18.8)	(0.1)	V	
Michard 1985	27.6	12.1	B	Yes
Oleak 1980	27.6	24.	B	Yes
Peletier et al. 1990	17.8	1.	KJB	
Peterson et al. 1979	27.3	9.	B	
Strom et al. 1981	26.6	11.	UR	Yes
Surma et al. 1990	25.5	10.	R	
de Vaucouleurs, Nieto 1978	29.7	32.	B	
de Vaucouleurs, Nieto 1979	22.3	1.2	B	Yes
Watanabe 1983	25.9	10.	V	Yes
Young et al. 1978	22.4	1.3	BVR	Yes

In some papers the surface brightness is given as a function of the equivalent radius $r^* = \sqrt{ab}$, where a and b are the distances along the semimajor and semiminor axes, respectively. If the axial ratios are also given, the reduction of the profile to the major axis is simple, otherwise we used for reduction the profile of mean axial ratios (open circles in Fig. 2b). In the U- and R-colour

profiles by Strom et al. (1981) systematic differences of 0.30^m and 0.35^m can be found if compared with measurements of other observers. We decided to decrease the surface brightnesses of Strom et al. by the values mentioned above.

In the cases when observers have presented the profiles along the axis which forms an angle ψ with the major axis, we reduced the distances given by the observer to the distances along the major axis according to the formula

$$a = r\sqrt{\frac{1 - e^2\cos\psi^2}{1 - e^2}},$$

where r is the distance along the measured axis and e is the isophote eccentricity related to the axial ratio by the formula $e = \sqrt{1 - \varepsilon^2}$. The position angle of the major axis is taken to be PA = 156°.

In this way all the data on the surface photometry were used and the surface brightness profiles in the BVURI colours along the major and in BVUR colours along minor axes were derived. These profiles form the initial data of our model. Here we present only the model profile in B (Fig. 1), (B–V), (U–B) colour indices (Fig. 2a) and axial ratios (Fig. 2b).

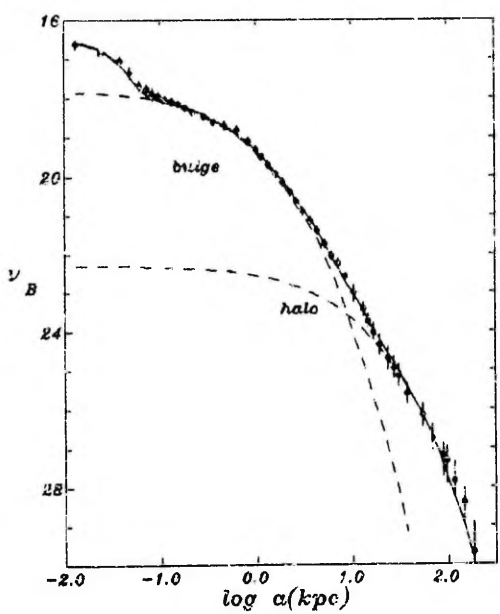

Figure 1. The averaged surface brightness profile of M87 in the B-colour. Open rings – observations, solid line – model, dashed lines – models for components.

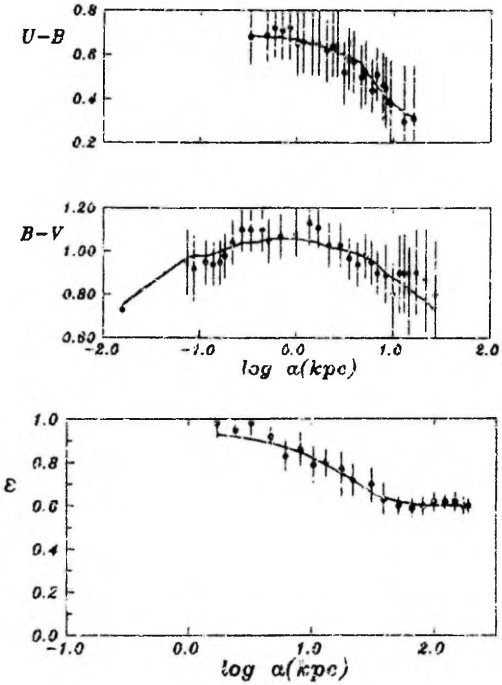

Figure 2 (**a**) The averaged profiles of the colour indices (B−V) and (U − B) of M87. Open rings – observations, solid line – model. (**b**) The axial ratios of isophotes of M87 as a function of the galactocentric distance. Open rings – observations, solid line – model.

Velocity dispersions have been obtained by many observers. A collection of all available data is given in a catalog by Whitmore et al. (1985) where the weighted mean value of 335 km/s is derived for the central dispersion. However, observations by Sargent et al. (1973), Dressler (1980), Jenkins (1980), Davies & Birkinshaw (1988), Dressler & Richstone (1990) have been most useful for us as they are not confined only to the centre. Unfortunately, we cannot use the data by Jenkins (1980) as his results describe the gas, but we have no information on the distribution of the gas. From datasets referred to above, the mean dispersions at various distance intervals were calculated, and represented in Fig. 3.

Another source of information is *X-ray observations* by Fabricant et al. (1980), Fabricant & Gorenstein (1983). The X-rays from the direction of M87 originate in two sources: the hard component with a nonthermal spectrum and a temperature of 10^8 K is radiated by the nucleus of M87 and/or by the whole Virgo cluster; the soft component with a thermal spectrum and a temperature of 10^7 K comes from the outer regions of the galaxy M87. We agree

with Fabricant & Gorenstein (1983) that the hot gas must be in hydrostatic equilibrium and responsible for the emission of the soft component. Therefore, it is possible to estimate the mass of the gas producing the emission and the depth of the potential well needed to bind this gas. The X-ray data will be used to determine the parameters of the corona after some processing (for details see Sect. 4).

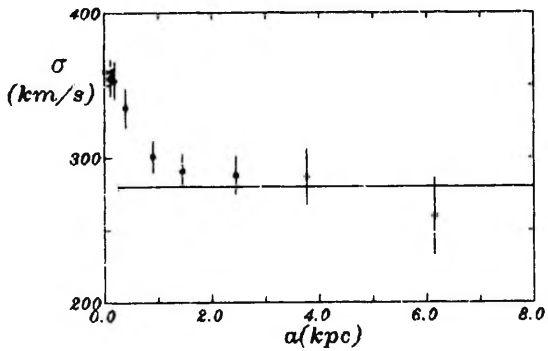

Figure 3 The averaged velocity dispersion profile of M87. Horizontal bars denote the mean dispersions calculated from our best fit model at the corresponding distance intervals.

In addition, we have data on the distribution of *globular clusters* (Strom et al. 1981, Harris 1986, Grillmair et al. 1986, Lauer & Kormendy 1986, Cohen 1988) and their mean velocity dispersions (Huchra & Brodie 1987, Mould et al. 1987, Mould et al. 1990). The investigations of the distribution of globular clusters were made in most cases with different filters and therefore with different depths of survey. For this reason the distributions of clusters were shifted arbitrarily in the vertical direction to get the best fit with others. This procedure does not influence our final results. The resulting averaged surface number density distribution is given in Fig. 4.

3 Model construction

A detailed description of the modelling technique has been given in Einasto (1972a) and more recently in Tenjes et al. (1992) (Chapter 2, Appendixes A and B), so here we shall review only basic features.

We assume an elliptical galaxy to consist of several physically homogeneous components with masses M, mass-to-light ratios M/L and fixed colour indices. The density distribution of each component is approximated as an inhomogeneous ellipsoid of rotation with a constant axial ratio $\epsilon = b/a$. All components, but corona, form an optically visible part of the galaxy, and their volume densities are described by the modified exponential law (Einasto 1969,

Sersic 1968)

$$\rho(a) = \rho(0)\exp(-[a/(ka_0)]^{1/N}).$$

The remaining component – the invisible massive corona – is represented by the modified isothermal law

$$\rho(a) = \begin{cases} \rho(0)([1+(\frac{a}{a_c})^2]^{-1} - [1+(\frac{a^0}{a_c})^2]^{-1}) & a \le a^0 \\ 0 & a > a^0. \end{cases}$$

In these formulae $\rho(0) = hM/(4\pi\epsilon{a_0}^3)$ is the central density, a is the distance along the major axis, $a_c = ka_0$ – the core radius, a_0 – the harmonic mean radius, a^0 – the outer cutoff radius, and h and k are the normalizing parameters depending on the parameter N.

The masses of the components can be determined from the virial theorem for multicomponent systems. From this theorem we derive a system of equations which connects the mean velocity dispersion along the line of sight of the i-th component with the masses of all components M_k

$$\langle\sigma^2\rangle_i = G/a_{0i}\sum_{k=1}^{m} H_{ik}M_k. \qquad (1)$$

In this formula m is the total number of components, G is the gravitational constant, H_{ik} are dimensionless coefficients depending on mass distribution laws of the components i and k. It is evident that all components contribute to the mean velocity dispersion of a particular component, but usually the influence of the component $i = k$ is more or less dominating. We note that in calculations we assume the velocity dispersion ellipsoid to be biaxial, i.e. $\sigma_R = \sigma_\theta \neq \sigma_Z$.

4 Subsystems in M87

The $r^{1/4}$-law of de Vaucouleurs represents quite well the luminosity profiles of elliptical galaxies (the standard elliptical NGC 3379 is a fine example (de Vaucouleurs & Capaccioli 1979)). In the case of M87 the agreement with the observed profile is good in the range of 8" –270" from the centre. The King and Hubble laws have been used for the same purposes. It is difficult to overestimate the role of these approximations, because all acceptable galactic formation scenarios must lead to galaxies with these density laws. But the formulae mentioned above do not explain the variations of isophote ellipticities and chemical compositions with the galactocentric radius. These variations are often remarkable and they may indicate specific conditions at the formation stage of galaxies (Eggen et al. 1962). It seems natural for the authors

of this paper *to represent these changes as transitions from one subsystem to another while subsystems are dealt as chemically homogeneous structures with different ages, ellipticities, and kinematic parameters.*

Surely, decomposition of a galaxy into subsystems on the basis of observations is complicated and often uncertain. This uncertainty can be diminished if we can use large samples of observational data and therefore we confine ourselves to well-observed galaxies, e.g. M87. A methodological point must be stressed here – we do not add artifical components to improve the fit with observations. All components of the model are really existing subsystems with different physical properties.

The nucleus

Even a preliminary examination of the light distribution of M87 reveals a central peak in the brightness profile (Fig. 1), so it is natural to define it as the first component the nucleus. The photometry of central parts obtained in good observational conditions (Young et al. 1978, de Vaucouleurs & Nieto 1979, Kormendy 1985, Bagnuolo & Chambers 1987) gives the structural parameters for the nucleus $a_0 = 0.033 \pm 0.003$ kpc, $N = 0.34 \pm 0.05$ and $\epsilon = 1$. But we must keep in mind that these values may be determined by seeing conditions only: Dressler (1980) referred to unpublished speckle observations by A. Boksenberg and W. Sargent, who report the radius of the nucleus to be $\sim 0.02'' \simeq 2$pc. The gas spectrophotometry with NTT by Jarvis (1989) indicates, that the structure of the nucleus may be even more complicated. However, despite some uncertainties in determining the radius, total luminosity of the nucleus does not strongly depend on real dimensions of the nucleus – we just calculate the light excess above the underlying extrapolated bulge luminosity and derive $L_B = 5.8 \pm 0.7 \cdot 10^7 L_\odot$ in B.

It is useful to study also colour indices. Observations by Young et al. (1978) indicate the decrease of (B – V) from 1.02 to 0.88 when moving inward from $a = 1.5"$ to $0.5"$, Bagnuolo & Chambers (1987) give at the very centre (B – V) = 0.73. Therefore, the integrated colour index (B – V) of the nucleus is by $\sim 0.3^m$ bluer than that of the bulge. This may be said also for (V – R) : the nucleus is by 0.26^m bluer.

The nucleus-dominated region is well determined by the luminosity spike in the brightness profile and by rather strong gradients in colour indices. The nucleus is also a dynamically independent component. Due to its small dimensions, the basic results of the present paper are practically independent of the detailed nuclear mass model. However, because of the popular problem of a possible presence of black holes in the centres of galaxies, we shall discuss the dynamical model of the nucleus in more detail. First, we must know the mean

velocity dispersion of the nucleus. Both, the nucleus and the underlying bulge, contribute to the dispersion measured at the centre. If the mean systematic velocities of both subsystems along the line of sight are the same, the measured dispersion is related with the dispersion of bulge and nucleus according to the formula

$$\sigma^2 = \frac{1}{L^*}(\sigma_1^2 L_1^* + \sigma_2^2 L_2^*). \qquad (2)$$

Here asterisk denotes the luminosities in B colour inside the spectrograph slit width, indices 1 and 2 denote the nucleus and bulge respectively. Knowing the bulge dispersion at the centre and the measured dispersion, the velocity dispersion of the nucleus averaged over the spectrograph slit can be calculated. All luminosities needed in Eq. 2 are derived from the light distribution model. If the dispersion of the underlying bulge is 330 ± 30 km/s (extrapolated from the region outside the nucleus with the help of a one-component model) and the dispersion measured at the very centre is 360 km/s (Dressler & Richstone 1990) we find the pure nuclear dispersion to be $(\sigma_{nucl}) = 370 \pm 20$ km/s. Therefore, the nuclear mass can be calculated from Eq. (1). We shall discuss two possibilities, based on different assumptions.

1. The radius of the nucleus is $a_0 = 0.033$ kpc. From the BVR photometrical profiles we can calculate colour indices of the nucleus. Supposing the nucleus to resemble a dense star cluster with a normal stellar content it is possible to estimate the M/L ratio of the nucleus from its colour indices and chemical evolution models of stellar systems. From the models by Traat (1988) the M/L ratio corresponding to $(B-V) = 0.73$ and $(V-R) = 0.56$ is $2.0 \pm 0.8\,M_\odot/L_\odot$. Therefore, the mass of the nucleus is $\sim 1.2 \pm 0.5 \cdot 10^8\,M_\odot$. Unfortunately, this result is in strong contradiction with the velocity dispersion data. To get the dispersion measured at the centre a nuclear mass $\simeq 9.8 \cdot 10^{10}\,M_\odot$ is required and therefore $M/L_B \simeq 160\,M_\odot/L_\odot$ results. The simplest way to solve this discrepancy is to suppose the presence of an additional point mass (black hole) at the centre of the galaxy. We can find the value of this additional mass from a modified virial theorem (Einasto 1972b, Eq. 1) as $M_{BH} = 3.5 \cdot 10^9\,M_\odot$. Thus our first model for the central parts of M87, fitting all observations, includes the nucleus with a normal stellar content, mass $1.2 \cdot 10^8\,M_\odot$, the M/L ratio $2\,M_\odot/L_\odot$, and the central black hole with a mass $3.5 \cdot 10^9\,M_\odot$. The parameters of the solution are given in Table 2 (model A).

   Recently Dressler & Richstone (1990) developed models with an anisotropic velocity dispersion ellipsoid. By using the Schwarzschild linear programming method the variants with and without a black hole were calculated. The crucial point in this type of models is the degree of the anisotropy of the dispersion that can be accepted. In all models presented by Dressler and Richstone the tangential dispersion exceeds

the radial one at $R > 20''$. N-body calculations with various initial conditions by Merrit (1980), Schwarzschild (1982), van Albada (1982), Norman et al. (1985), and theoretical studies of the influence of irregular forces in stellar systems by Kuzmin (1961) indicate that the velocity ellipsoid becomes more and more radially elongated, when moving away from the centre. For this reason anisotropic models cannot be considered completely satisfactory at present.

2. The visible radius is determined by seeing conditions and the real radius is $a_0 \simeq 1.5$ pc. The nuclear luminosities in BVR coincide with those in model A, and the main difference arises from mass determination. Since the radius of the nucleus is now about 20 times smaller, the mass calculated from velocity dispersions is $M_{nucl} = 4.6 \cdot 10^3\,M_\odot$ and $M/L_B = 7.5\,M_\odot/L_\odot$. So, in this model we do not see any urgent need to introduce an additional component (a black hole). This version we denote as model B. It is difficult to calculate the errors for the masses and the mass-to-light ratio of this model, because the estimate of the radius of the nucleus is very crude. As of reasonable quess, we may take the relative errors to be at least 50 percent.

The halo

As Einasto (1972a) we mean by 'halo' a spheroidal metal-poor population II subsystem, typical representatives of which are old stars (like RR-Lyrae variables) and globular clusters. Because of a quite large distance to M87, globular clusters are the best test-particles for the halo. In our Galaxy (Haud & Einasto 1989, Fig. 3) the distribution of globular clusters and RR-Lyrae stars is very close. By analogy, we can expect that globular clusters represent the whole halo subsystem in M87.

The galaxy M87 has an enormously large cluster population: the number of counted clusters is 4500, their total number is estimated to approach 20 000 (Harris 1986). Fig. 4 shows a good agreement between the observed cluster distribution and our best-fit model with the parameters $N = 2.7 \pm 0.6$ and $a_0 = 32 \pm 3$ kpc.

As in our Galaxy, the distribution of globular clusters is not spherical in M87 either. According to Cohen (1988) the mean ellipticity of the cluster subsystem is nearly equal to isophote ellipticities in outer parts of the galaxy, i.e. $\epsilon_{halo} \simeq 0.6$. From Fig. 2b we see that the halo starts to dominate in luminosity beyond a distance $a \simeq 30$ kpc. A change in ellipticity, indicating a transition from one subsystem to another, is seen at distances larger than 8 kpc. Relying on these facts, we derive from surface photometry the luminosities of the halo in several colours (Table 2). The mean relative error is 12 percent.

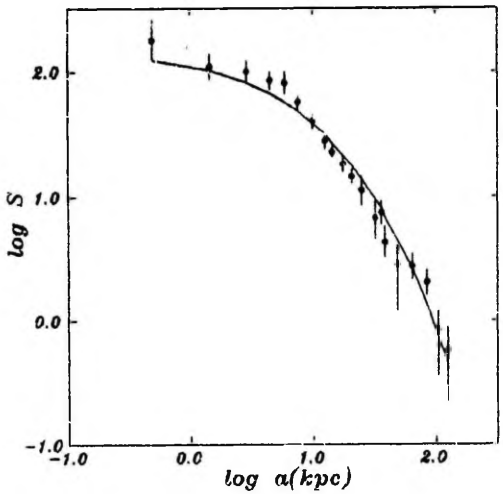

Figure 4. The distribution of globular clusters of M87. The observations referred to in Sect. 2 have been averaged and presented by open circles. The continuous line gives the model distribution.

Estimation of the halo mass by the virial theorem using the velocity dispersion of globular clusters leads us to unrealistic results. The system of clusters is not self-gravitating and the mass derived in this way belongs rather to the whole galaxy than to the halo subsystem.

For this reason we must use the mean M/L ratio for globular clusters or the M/L ratio from evolution models of stellar systems, and to calculate the mass from the photometrical model. Measurements for individual globular clusters by Illingworth (1976) give a mean M/L ratio $2.1 \pm 0.6\,M_\odot/L_\odot$, from the evolution models by Traat (1988) $M/L_B \simeq 2.5 \pm 0.8\,M_\odot/L_\odot$. These values are in good mutual agreement: the integrated M/L ratio of the halo must exceed that of globular clusters, because evaporation of stars with smaller masses decreases the M/L ratio of clusters compared with the halo as a whole. Therefore, we can take $(M/L_B)_{halo} = 2.5\,M_\odot/L_\odot$. In this case the halo mass is $M_{halo} = 1.5 \pm 0.7 \cdot 10^{11}\,M_\odot$. Taking 20 000 for the total number of clusters (Harris 1986) and $2 \cdot 10^5\,M_\odot$ for the mean mass of a cluster (Mihalas & Binney 1981, p. 122) it results that the total mass of globular clusters is only 45 times less than the mass of the halo compared with the usual mass ratio of 100. This supports the enormously large value of the specific frequency S (defined as the number of the globular clusters per $M_V = -15$) for M87 when compared with the mean for elliptical galaxies (Harris & van den Bergh 1981). However, in the present case a contradiction with the observations of the velocity dispersion still remains. This question will be discussed in Sect. 4.4.

The bulge

The main spheroidal component – the bulge – is an old subsystem with a normal metal content. It is clearly distinguished from the halo, as the colour indices are rather constant in the bulge region up to the distance $a \sim 8$ kpc (Fig. 2a). Beyond that distance a transition begins from the bulge to halo which is indicated by decreasing metallicities.

The kinematics of the bulge and halo are different, at least in spiral galaxies. The bulges of spirals are rotating with the speed nearly equal to their velocity dispersions (Kormendy & Illingworth 1982). This does not hold for halos. The rotation velocity of the halo in our Galaxy is believed to be < 60 km/s (Frenk & White 1980) which is about a factor of two smaller than the velocity dispersion of the halo subsystem.

In the bulge region the largest number of photometrical observations have been made and the light distribution is best known. So the determination of the density distribution parameters of the bulge is relatively simple. The derived values are $a_o = 2.7 \pm 0.3$ kpc, $N = 2.9 \pm 0.2$ and $L_B = 4.6 \pm 0.5 \cdot 10^{10}\,L_\odot$. When compared with the corresponding values for the halo we see that the colour index (U – B) for the bulge is by 0.4^m redder. Secondly, ellipticities are obviously different. In the case of M87 the isophotes of the bulge are apparently circular, while the axial ratio of the halo is quite small, $\epsilon = 0.6$. These two differences are the main ones, resulting directly from observations. In Figs. 1 and 2 a rather good agreement between our model and the numerous photometrical data is shown.

For mass calculation we use the measurements of velocity dispersions, described in Sect. 2 and Fig. 4 up to a distance $\sim$ 6kpc. To use Eq. (1) we must know the mean velocity dispersion of the subsystem. By using the derived light distribution model, a value of $\langle\sigma\rangle = 280 \pm 40$ km/s is obtained for mass-weighted mean dispersion. This yields $3.7 \pm 1.1 \cdot 10^{11}\,M_\odot$ for the bulge mass and together with the data from the photometrical model, the M/L ratio 8.0 ± 2.4.

The massive corona

The velocity dispersion determined from observations of globular clusters gives for the old metal-poor halo subsystem an extremely large M/L ratio $170\,M_\odot/L_\odot$. Obviously, that is not realistic for a metal-poor population II subsystem. The discrepancy is similar to that found in the case of many spiral galaxies: the rotation velocities of outer parts of these galaxies remain constant, contrary to those resulting from photometrical models (Sancisi & van Albada

1987). Therefore, it is possible to avoid the discrepancy supposing that M87 is surrounded by a massive invisible component, which influences the dynamics of the outer parts of the galaxy.

An additional argument comes from X-ray observations. It is well known that in the case of many clusters of galaxies the mass needed to bind the hot gas, responsible for X-ray luminosity, exceeds substantially the visible mass of all member galaxies of the cluster. The same is known for M87 and for many other galaxies (eg. Fabian et al. 1986). Fabricant & Gorenstein (1983) measured the distribution of the X-ray brightness of M87 and calculated the amount of mass needed to stabilize the gas responsible for the X-ray emission. This mass exceeds considerably that given by any realistic model of visible parts of the galaxy. Again this calls for introduction of the fourth component – a massive and invisible in optical wavelengths corona.

To determine the parameters of the corona it is not advisable to use the dwarf galaxies surrounding M87, as was done for the model of our Galaxy (Haud & Einasto 1989), because 1) at the distance of 20 Mpc only the most luminous galaxies can be observed; 2) some satellites may have been disrupted by dynamical influence of the neighbouring Virgo cluster galaxies. For these reasons the distribution of M87 dwarf satellite galaxies does not necessarly correspond to the true mass distribution of the corona. In principle, it is possible to use for galactic mass estimation also the tidal truncation of close companion galaxies, but the practical use of this method is complicated (Prugniel et al 1987).

Therefore, we must use X-ray data. We know the surface density distribution of the emitting gas. The gas lies in a potential well caused by the visible matter of M87 and by the invisible corona. The parameters of the corona can be estimated after subtraction from the total potential the potential caused by visible matter. As found by Fabricant & Gorenstein (1983), a model, where the gas temperature is constant or has a power-law dependence on galactocentric distance, gives a good fit with X-ray spectral observations. From this the linear dependence of the inner mass $M(R)$ on R up to the last measured point at $R_L = 525$ kpc results. This is a limiting condition for the core radius a_c and the parameter k of the corona. Unfortunately, we cannot find the outer cutoff radius a^0 from X-ray observations. Only the lower limit can be estimated as $a^0 > 1$ Mpc.

It is possible to use also the models for X-ray distribution or dispersion of globular clusters for mass estimation. Both variants give results which are in good mutual agreement. From the velocity dispersion $\sigma = 390 \pm 40$ km/s we obtain the mass for the corona $M_{cor} = 1.2 \pm 0.2 \cdot 10^{14}\,M_\odot$. This gives for the mass within R_L the value $M(R \leq R_L) = 7.0 \pm 1.4 \cdot 10^{13}\,M_\odot$ in good agreement with the models by Fabricant & Gorenstein (1983).

4 Best-approximation model

The best-approximation parameter set has been found on the basis of all observational data listed in Sect. 2, using the least-squares method. The set of initial data consists of:

1. photometrical data (surface photometry in BVUR colours along the major and minor axes, in I colours along the major axes);
2. the distribution of globular clusters;
3. the X-ray brightness and temperature distributions;
4. the mean velocity dispersions for the nucleus and the bulge.

The algorithm, that finds the best-fit parameters, tries to minimize the sum of squares of relative deviations of all observations. The photometrical profiles were taken with equal weights. The X-ray and the velocity dispersion data were used only for the determination of the masses of components and wwere independent of photometrical data.

The final model fits all profiles with a mean relative error 0.5 percent. The distribution of globular clusters was fitted by the halo model with a mean relative error 1.2 percent. The set of best-approximation parameters (the axial ratio, ϵ, the harmonic mean radius (in kpc), a_o, the total mass and luminosity of the population (in $10^{10}\,M_\odot$), M, the structural parameter, N, the dimensionless normalizing constants, h and k, and colour indices) is given in Table 2. The final model is represented by solid lines in Figs. 1, 2, and 4.

Table 2. Model parameters

Population	a_0	M	ϵ	N	h	k
Nucleus: A	0.033	0.012*	1.	0.36	1.264	1.316
Nucleus: B	0.0015	0.037	1.	0.36	1.264	1.316
Bulge	2.7	37.	0.93	2.9	262.1	0.00377
Halo	32.	15.	0.6	2.7	162.6	0.00702
Corona	200.	12000.	1.	1.	61.27	0.0631

Population	L_B	M/L_B	(B − V)	(U − B)	(V − R)	(R − I)
Nucleus: A	0.0058	2.0	0.73		0.56	
Nucleus: B	0.0058	6.4	0.73		0.56	
Bulge	4.6	8.0	1.01	0.66	0.79	1.59
Halo	6.1	2.5	0.60	0.23	(0.8)	(1.5)

* The model includes an additional black hole with a mass of $3.5 10^9\,M_\odot$.

Remarks: 1) Colour indices in parenthesis are uncertain.

The total luminosity of M87 in B is calculated to be $L_B = 10.7 \pm 1.2 \cdot 10^{10}\,L_\odot$, the optically visible mass $M_{vis} = 5.2 \pm 1.7 \cdot 10^{11}\,M_\odot$, the corresponding M/L ratio $4.9 \pm 2.6\,M_\odot/L_\odot$.

Table 3 presents some descriptive functions calculated for our final model. K_R is the gradient of the gravitational potential in the radial direction (in the units of $km^2s^{-2}kpc^{-1}$) $K_R \equiv \partial\Phi/\partial R$, where Φ is the gravitational potential. The function $M(R)$ is the inner mass, in the case of a multi-component model defined as a point mass at the centre of the galaxy having the same gravitational attraction at R as the subsystem. The quantity f_B is the local M/L ratio in B-colour derived by dividing the mass and the luminosity in a shell limited by the radiuses R and $R + \Delta R$. The radii are in kiloparsecs, the masses in the units of $10^{10}\,M_\odot$, the M/L ratios in solar units.

5 Discussion

The model constructed in this paper for the galaxy M87 is based on a large body of observational data. Surface photometry along the major and minor axis in the UBVRI colours, X-ray observations, velocity dispersion data, distribution and kinematics of globular clusters have been taken into account for the determination of population parameters.

We presented two versions for the model of the nuclear region. One of them has a radius of 0.032 kpc, derived directly from the photometry of the central part of the galaxy without any correction for seeing effects and it contains a point mass at the centre with the mass of $M_{BH} = 3.5 \cdot 10^9\,M_\odot$. In recent years the problems connected with the presence of massive black holes in the centres of galaxies have become more and more actual. Detailed data on the kinematics for central parts of several nearby galaxies (M31, M32, M81, M104) are available at present, supporting the possibility that massive black holes may be more common in galaxies than usually supposed. However, in the present work the model without a central point mass is found as well. The only hypothesis we must make is the quite small dimensions of the nucleus. This model has a radius of only ~ 1.5pc and a normal stellar content. Unfortunately, observational data do not allow to choose between these two models at present. It is interesting to note that the nuclear radius of M87 in our model B is close to the nuclear radius of the Andromeda Galaxy (M31). The central density of the nucleus is $\rho_0 = 1.2 \cdot 10^7\,M_\odot/pc^3$, i.e. about 30 times larger than that of M31.

By the end of 1990 about 40 elliptical galaxies with detected globular clusters have been found. Our population model gives a simple explanation to the fact that the surface density distribution of the globular cluster subsystem

has a slope that differs from that of the light distribution of galaxies (Strom et al. 1981, Forte et al. 1981). In the region compared the luminosity distribution is formed both by the bulge and the halo, and accordingly, the total light distribution and globular cluster distribution cannot coincide. It seems to be an additional argument for the separation of bulges and halos.

Table 3. Calculated descriptive functions

R	K_R	log $M(R)$				f_B
		bulge	halo	corona	total	
0.02	$4.00\ 10^6$	-3.37	-6.68	-6.93	-3.37	7.3
0.04	1.05	-2.60	-5.83	-6.03	-2.60	7.5
0.06	$5.22\ 10^5$	-2.16	-5.33	-5.50	-2.16	7.9
0.1	2.59	-1.63	-4.72	-4.83	-1.63	7.9
0.15	1.84	-1.23	-4.23	-4.30	-1.23	7.9
0.2	1.60	-0.95	-3.90	-3.93	-0.95	8.0
0.3	1.46	-0.58	-3.63	-3.40	-0.58	8.0
0.4	1.38	-0.32	-3.10	-3.03	-0.32	8.0
0.6	1.28	0.01	-2.66	-2.50	0.01	8.0
1.	1.10	0.39	-2.11	-1.83	0.39	8.1
1.5	$9.13\ 10^4$	0.66	-1.69	-1.30	0.66	8.2
2.	7.68	0.83	-1.40	-0.93	0.84	8.4
3.	5.74	1.05	-1.01	-0.40	1.06	9.2
4.	4.53	1.17	-0.75	-0.03	1.19	10.3
6.	3.23	1.32	-0.40	0.49	1.37	14.7
8.	2.58	1.40	-0.18	0.85	1.51	22.
10.	2.22	1.45	-0.01	1.12	1.58	32.
20.	1.55	1.54	0.46	1.92	2.09	96.
30.	1.26	1.56	0.68	2.32	2.41	150.
40.	1.06	1.56	0.82	2.57	2.63	195.
60.	$8.03\ 10^3$	1.56	0.97	2.88	2.91	290.
80.	6.43		1.05	3.08	3.09	410.
100.	5.34		1.10	3.21	3.23	570.
120.	4.65		1.13	3.32	3.33	900.
150.	3.75		1.16	3.44	3.45	1600.
200.	2.88		1.18	3.58	3.59	4100.

The calculated local mass-to-luminosity ratios are given in Figure 5. We can see a clear difference between the visible and dark matter even at the distance $R_{25} = 36$ kpc.

The mass-to-light ratio within the Holmberg radius is $85\,M_\odot/L_\odot$. The radius at which the masses of dark matter and visible matter become equal is 12 kpc. The integral and local M/L ratios for limiting radii (in kpc) of various

kinds of observations are given in Table 4.

Table 4. Mass-to-luminosity ratios for outer radii of various kind of observations

Observations	Outer radius	M/L_{int}	M/L_{loc}
Globular clusters	100.	120.	510.
Surface photometry	190.	220.	3500.
X-ray temperature	150.	180.	1440.
X-ray brightness	525.	600.	–

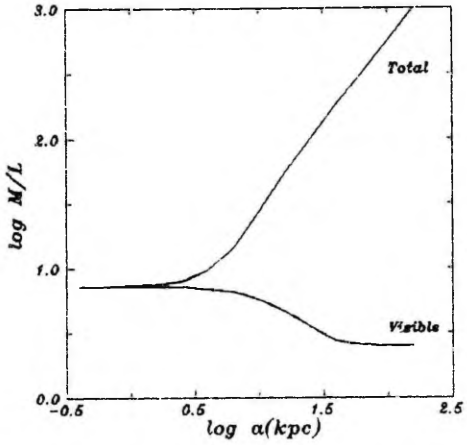

Figure 5 Local mass-to-light ratios.

The nearest limit is at $R = 100$ kpc – the outer radius of the globular cluster system, the velocity dispersion of which can be found directly from observations. For this population good photometry exists as well, so the integral M/L ratio inside this radius is well established. And even this very conservative estimate is quite large. Within the outermost point of X-ray data the ratio of the visible mass to the total one is $M_{vis}/M_T = 1/130$, i.e. less than 1%.

References

Bagnuolo Jr.,W.G., Chambers, R.W.: 1987. *Nature* **326**, 691

Bertola, F., Capaccioli, M.: 1970. *Mem. Soc. Astron. Italiana* **41**, 57

Boroson, T.A., Thompson, I.B., Shectman, S.A.: 1983. *Astron. J.* **88**, 1707

Boughn, S.P., Saulson, P.R.: 1983. *Astrophys. J. Letters* **265**, L55

Burstein, D., Heiles, C.: 1984. *Astrophys. J. Suppl.* **54**, 33

Caon, N., Capaccioli, M., Rampazzo, R.: 1990. *Astron. Astrophys. Suppl.*, in press

Carter, D., Dixon, K.L.: 1978. *Astron. J.* **83**, 574

Cohen, J.G.: 1988. *Astron. J.* **95**, 682

Davies, R.L., Birkinshaw, M.: 1988. *Astrophys. J. Suppl.* **68**, 409

Davis, L.E., Crawson, M., Davies, R.L., Illingworth, G.: 1985. *Astron. J.* **90**, 169

de Vaucouleurs, G.: 1979. in *Photometry, Kinematics and Dynamics of Galaxies*, ed. D.S.Evans. Austin: Univ. of Texas Press, p. 1

de Vaucouleurs, G., Capaccioli, M.: 1979. *Astrophys. J. Suppl.* **40**, 699

de Vaucouleurs, G., Nieto, J.-L.: 1978. *Astrophys. J.* **220**, 449

de Vaucouleurs, G , Nieto, J.-L.: 1979. *Astrophys. J.* **230**, 697

di Tullio, G.A.: 1979. *Astron. Astrophys. Suppl.* **37**, 591

Dressler, A.: 1980. *Astrophys. J. Letters* **240**, L11

Dressler, A., Richstone, D.O.: 1990. *Astrophys. J.* **348**, 120

Einasto, J.: 1969. *Astrofizika* **5**, 137

Einasto, J.: 1971. *Structure and Evolution of Regular Galaxies*, Tartu (unpublished Ph. D. thesis, in russian)

Einasto, J.: 1972a. *Tartu Astrofüüs. Obs. Teated* Nr. 40, 3 = Einasto, J.: 1974. in *Stars and the Milky Way System*. Proc. First European Astr. Meeting, Athens Sept 4–9, 1972, vol 2, ed. L.N. Mavridis, Springer, Berlin, Heidelberg, New-York, p. 291

Einasto, J.: 1972b. in *External Galaxies and Quasi-Stellar Objects*, ed. D.S. Evans, D. Reidel Publ. Co., Dordrecht, p. 37

Eggen, O.J., Lynden-Bell, D., Sandage, A.: 1962. *Astrophys. J.* **136**, 748

Fabian, A.C., Thomas, P.A., Fall, S.M., White III, R.E.: 1986. *Monthly Notices Roy. Astron. Soc.* **221**, 1049

Fabricant, D., Lecar, M., Gorenstein, P.: 1980. *Astrophys. J.* **241**, 552

Fabricant, D., Gorenstein, P.: 1983. *Astrophys. J.* **267**, 535

Forte, J.C., Strom, S.E., Strom, K.M.: 1981. *Astrophys. J. Letters* **245**, L9

Frenk, C.S., White, S.D.M.: 1980. *Monthly Notices Roy. Astron. Soc.* **193**, 295

Grillmair, C., Pritchet, C., van den Bergh, S.: 1986. *Astron. J.* **91**, 1328

Harris, W.E.: 1986. *Astron. J.* **91**, 822

Harris, W.E., van den Bergh, S.: 1981. *Astron. J.* **86**, 1627

Haud, U., Einasto, J.: 1989. *Astron. Astrophys.* **223**, 95.

Huchra, J., Brodie, J.: 1987. *Astron. J.* **93**, 779

Ichicawa, S.-I., Wakamatsu, K.-I., Okamura, S.: 1986. *Astrophys. J. Suppl.* **60**, 475

Illingworth, G.: 1976. *Astrophys. J.* **204**, 73

Jarvis, B.: 1989. *The Messenger* Nr. 58, 10

Jedrzejevski, R.I.: 1987. *Monthly Notices Roy. Astron. Soc.* **226**, 747

Jenkins, C.R.: 1980. *Monthly Notices Roy. Astron. Soc.* **192**, 41p

Kormendy, J.: 1985. *Astrophys. J. Letters* **292**, L9

Kormendy, J., Illingworth, G.: 1982. *Astrophys. J.* **256**, 460

Kuzmin, G.G.: 1961. Tartu Astr. Obs. Publ. **33**, 351

Lauer, T., Kormendy, J.: 1986. *Astrophys. J. Letters* **303**, L1

Merritt, D.: 1980. *Astrophys. J. Suppl.* **43**, 435

Michard, R.: 1985. *Astron. Astrophys. Suppl.* **59**, 205

Mihalas, D., Binney, J.: 1981. *Galactic Astronomy: structure and kinematics*, 2nd ed., Freeman, San Francisco, 13+597pp.

Mould, J.R., Oke, J.B., Nemec, J.M.: 1987. *Astron. J.* **93**, 53

Mould, J.R., Oke, J.B., de Zeeuw, P.T., Nemec, J.M.: 1990. *Astron. J.* **99**, 1823

Norman C.A., May, A., van Albada, T.S.: 1985. *Astrophys. J.* **296**, 20

Oleak, H.: 1980. personal communication

Peletier, R.F., Valentijn, E.A., Jameson, R.F.: 1990. *Astron. Astrophys.* **233**, 62

Peterson, B.M., Strom, S.E., Strom, K.M.: 1979. *Astron. J.* **84**, 335

Prugniel, P., Nieto, J-L., Simien, F.: 1987. *Astron. Astrophys.* **173**, 49

Sancisi, R., van Albada, T.S.: 1987. in *Dark Matter in the Universe,* ed. J.Kormendy, G.R.Knapp. D. Reidel Publ. Co. Dordrecht: Kluwer, p. 67

Sargent, W.L.W., Young, P.L., Boksenberg, A., Shotridge, K., Lynds, C.R., Hartwick, F.D.A.: 1978. *Astrophys. J.* **221**, 731

Schwarzschild, M.: 1982. *Astrophys. J.* **263**, 599

Sersic, J.L.: 1968. *Atlas de Galaxies Australes*, Observatorio Astronomico, Cordoba, Argentina

Strom, S.E., Forte, J.C., Harris, W.E., Strom, K.M., Wells, D.C., Smith, M.G: 1981. *Astrophys. J.* **245**, 416

Surma, P., Seifert, W., Bender, R.: 1990. *Astron. Astrophys.* **238**, 67

Tenjes, P., Haud, U., Einasto, J.: 1992. *Astron. Astrophys.* in press (Chapter 2 in present Thesis)

Traat, P.: 1988. in *The Formation and Evolution of Galaxies and heir Constituenses. I.,* ed. M. Jõeveer, Tallinn, p. 23

van Albada, T.S.: 1982. *Monthly Notices Roy. Astron. Soc.* **201**, 939

van Albada, T.S., Sancisi, R.: 1986. *Phil. Trans. Roy. Soc. London* **A320**, 447

Watanabe, M.: 1983. *Ann. Tokyo Astron. Obs.* **19**, 121

Whitmore, B.C., McElroy, D.B., Tonry, J.L.: 1985. *Astrophys. J. Suppl.* **59**, 1

Young, P., Westphal, J.A., Kristian, J., Wilson, C.P., Landauer, F.P.: 1978. *Astrophys. J.* **221**, 721

CHAPTER 5 THE GALAXY M81*

1 Introduction

Due to its relatively large size in the sky the spiral galaxy M81 (type SA(s)ab) is suitable for detailed studies of stellar content and for discrimination of stellar ensembles by their age, kinematics and spatial distribution. M81 is an example of galaxies with a falling rotational curve. In connection with this we have to answer a question, is there any dark matter associated with M81? The problem may be complicated because the radial velocities of four neighbouring galaxies M81, M82, NGC 3077, and NGC 2976 differ so largely that it is difficult to explain with conventional masses of galaxies. This is further confirmed by the measurements of the velocity dispersions of the satellite galaxies of M81, resulting a value of $\langle\sigma\rangle = 140$ km/s (Karachentsev 1986).

The preliminary version of the model presented here was constructed more than ten years ago (Einasto et al. 1980a, 1980b). However, the amount of observational data during last decade has considerably increased, which made it necessary to review the model.

Throughout this paper all luminosities and colour indices have been corrected for absorption in our Galaxy according to Burstein & Heiles (1984). The distance to M81 has been taken as 3.3 Mpc (Freedman 1988), the position angle of the major axis PA = 152°, the angle of inclination to the line of sight $i = 31°$ (Rots 1975, Gottesman & Weliachew 1975).

2 Observations and data reduction

By now a detailed *surface photometry* of M81 is available in BVRI colours. Beside the papers referred in Tenjes et al. (1982) we can use the photometry by Elmegreen & Elmegreen (1984) (B, I-colours), Keel (1989) (B-colour), Kent (1987) (R-colour), Kormendy (1985) (V-colour)and Georgiev & Getov (1991) (B, V-colours). Unfortunately, the information on the light distribution in the U-band is contradictory and scanty. At the same time the colour index U–B is more informative than, e.g. the index B–V, if we study the chemical composition of galaxies. For this reason it was needed to made additional surface photometry enabling to obtain (U–B) colour profile.

---

* This Chapter bases in part on the paper by Tenjes, P., "Surface photometry of galaxies. I. NGC 3379 and M81." *Baltic Astronomy* **1**, 7–16

The plate material consist of five $5^\circ \times 5^\circ$ photographs of different exposures in the B- and U-colours taken in March and August, 1983 with the Latvian 80/120/240 Schmidt telescope in Baldone. The plate scale is 85"/mm. For calibration at the edges of every plate two sets of calibration spectrograms with different exposure times were made. Both sets provide 8 calibration bands, each with intensity ratios of about 1.4 between neighbouring bands.

The plates were digitized with a microdensitometer PDS 1010A at the Tõravere Observatory, and the density distributions $D(x, y)$ of the object galaxy and the surrounding area were obtained as 500×500 pixels. The scanning was made with a square 20 μm diaphragm and with 20 μm stepping intervals for the plates of short exposures (less than 10 min) and with a 50 μm diaphragm and 50 μm stepping intervals for all other plates. The long-exposure plates were scanned also with a step of 100 μm to measure more blank sky areas.

Digital frames were processed using the Tartu Image Data Analysis System, a set of software procedures that have been designed mainly for the surface photometry of galaxies. This system was initialised and developed by a working group from Tõravere Observatory, which includes the author of this Dissertation.

At first, the initial data array needs to be filtered. For this purpose an adaptive filter is better than common median-filters, gaussian smoothing or simple averaging procedures. This filter is designed to increase the signal-to-noise ratio of digitised images and reduce the redundancy in digital information. But its most important feature for the present application is that it smoothes the data in the noisy outskirsts of galaxies without smearing out the inner regions and the stellar images, i.e. the dimensions of the smoothing window depend on the density gradients. In our case the largest smoothing window used was 13×13 pixels.

The next step is to convert the densities of the photographic emulsion into the flux intensities. Both spectrogram sets are used to increase the dynamical range and to reduce the errors on the characteristic curve. Every point in the characteristic curve was obtained as a mean of about 200 pixels. For the density-intensity relation the analytical function proposed by de Vaucouleurs (1968) $\log I = a \log \omega + b$, is used. In this formula $\omega = 10^{D-D_o} - 1$, where D_o is the fog intensity, a and b are free parameters. Afterwards, the density distributions $D(x, y)$ are converted into the intensity distributions $I_{G+S}(x, y)$, here G means the galaxy and S means the sky.

The third step is determination of the sky background. This is the most crucial step in surface photometry (Carter & Dixon 1978, Capaccioli & de Vaucouleurs 1983). For this purpose a mask frame is constructed at first, to exclude certain regions. The mask frame includes *(a)* all pixels, which deviate from the mean value of the whole frame by more than 0.5σ, where σ is the

standard deviation; *(b)* all pixels in the box (or boxes), the dimensions of which are given interactively. Part *(a)* of the mask excludes all sufficiently bright stars and the plate defects, our criterion of 0.5σ is rather strong. Part *(b)* exludes the faint outer parts of the galaxy and some bad areas, if needed. Usually the mask frame includes about 5–10 percent of all pixels. The program calculates then the sky background as a two-dimensional polynomial in x and y with the help of a least-square algorithm. At the first iteration all pixels which have not been excluded by the mask frame are taken into account. Following Jones et al. (1969), in subsequent iterations the points, which deviate from the average by more than 2.5σ (in the second iteration) and by 1.0σ (in all other iterations), are also excluded. The process stops when no significant change is found between two subsequent solutions. This process is then repeated, varying the order of the polynomial. Inspecting the final background isophotes and the moments of the distribution of our approximation, the final order of the background polynomial is chosen. The background local sky level $I_S(x,y)$ under the object galaxy is interpolated and subtracted from $I_{G+S}(x,y)$, leaving only $I_G(x,y)$, the intensity distribution of the galaxy. Because of the large dimensions of the galaxy in the plate (10 mm) and long exposure times, we assume that small-scale time fluctuations and small-scale spatial variations of the airglow are smeared out during the exposures. Therefore, we can hope that our two-dimensional polynomial represents adequately the background intensity of the sky.

In practice, $I_G(x,y)$ is expressed in units of the local sky intensity as $I_{rel}(x,y) = [I_{G+S}(x,y) - I_S(x,y)]/I_S(x,y)$, where I_{rel} is the relative intensity. By carefully modelling the nonuniform sky background and normalising $I_G(x,y)$ by $I_S(x,y)$, we can correct, at least to the first-order approximastion, the intensity distribution of the galaxy for the nonuniformity of the actual night-sky brightness and for the nonuniformity of the background density due to vignetting and/or photographic processing. To increase the dynamical range of the brightness profiles and to reduce accidental errors, the relative intensity distributions obtained from different plates are combined to yield the final intensity distribution.

Finally, the zero point of the relative intensity, i.e., the sky brightness, μ_{sky} in mag/arcsec^2, is determined on the basis of photoelectic measurements by Sandage et al. (1969).

Isophotes at equally spaced values of surface brightness are extracted from photographic images through a 4-point linear interpolation algorithm. Firstly, cluster analysis is used to separate the stars, defects and the galaxies. The remaining isophotes are approximated by ellipses. We assume that the galaxy is symmetric with respect to its center. A least square fitting algorithm finds five parameters: the semimajor and -minor axis lengths a and b, the center coordinates (x_o, y_o) in the reference frame of the digital map and the azimuth

of the major axis θ.

The obtained light profile for M81 are presented in Table 1. Brightness is given in mag/arcsec^2 and the radii are in arcsec.

μ_B	a	b	μ_U	a	b	μ_B	a	b	μ_U	a	b
18.63	12.4	8.7	19.37	11.1	8.14	18.85	15.6	10.3	19.45	13.2	9.13
19.15	20.6	14.0	19.50	15.9	10.1	19.40	27.8	19.3	19.58	18.4	11.8
19.48	31.2	21.8	19.68	19.6	12.7	19.83	41.6	28.6	19.75	22.4	15.2
20.20	55.2	32.5	19.85	24.3	18.7	20.45	64.5	41.4	19.95	27.9	22.3
20.60	71.8	45.1	20.55	41.6	33.2	20.75	77.9	50.9	20.65	47.1	35.0
20.85	81.8	56.8	20.73	51.5	36.5	21.05	103.	72.0	20.83	55.5	38.2
21.15	111.	76.2	20.90	61.5	40.1	21.35	128.	79.6	21.00	66.0	43.6
21.50	153.	87.6	21.10	73.2	46.8	21.65	173.	91.8	21.18	75.6	50.3
21.85	202.	109.	21.28	82.4	52.9	22.03	253.	134.	21.35	84.6	59.2
22.15	303.	129.	21.43	86.6	62.8	22.30	326.	145.	21.50	91.8	66.0
22.48	337.	185.	21.58	113.	71.3	22.60	343.	200.	21.65	118.	81.6
22.73	356.	209.	21.75	142.	87.6	22.90	371.	230.	21.85	159.	99.5
23.23	397.	259.	21.98	232.	101.	23.35	423.	277.	22.10	275.	104.
23.50	456.	278.	22.35	304.	186.	23.73	471.	298.	22.48	326.	187.
23.95	493.	317.	22.65	353.	200.	24.20	508.	414.	22.85	388.	250.
24.35	575.	421.	22.98	400.	249.	24.48	593.	430.	23.40	504.	314.

3 An analysis of observational data

The surface brightness profiles in the UBVRI colours along the major and minor axes were derived by averaging the results of different authors (Sect. 2) and they form one part of the initial data set of our model. Here we present only the light profile in V (Fig. 1), (B-V) and (U-B) colour indices, for which most detailed information is available (Fig. 2), and the axial ratios ϵ (Fig. 3).

The *rotation curve* we used for the modelling bases on gas velocities. For the inner 1.6 kpc of the galaxy the [NII], [SII] and Hα radial velocities were obtained and rotation curve was constructed by Goad (1976). The radial velocities of CO measured by Sage & Westphal (1991) give useful information on the rotation law at the distances of R = 1.3 – 3 kpc from the centre. High-resolution HI observations at 25″ resolution by Rots & Shane (1975), Rots (1975) and 2′ resolution by Gottesmann & Weliachew (1975) cover the region of R = 3.5 – 20 kpc. The averaged rotation velocities from the papers referred above are given in Fig. 4 by open circles. The outer parts of M81 were mapped in HI with a resolution of 9–10′ (∼ 9kpc) by Roberts & Rots (1973) and by Rohlfs & Kreitschmann (1980) and are marked by small filled dots and open

diamonds, respectively.

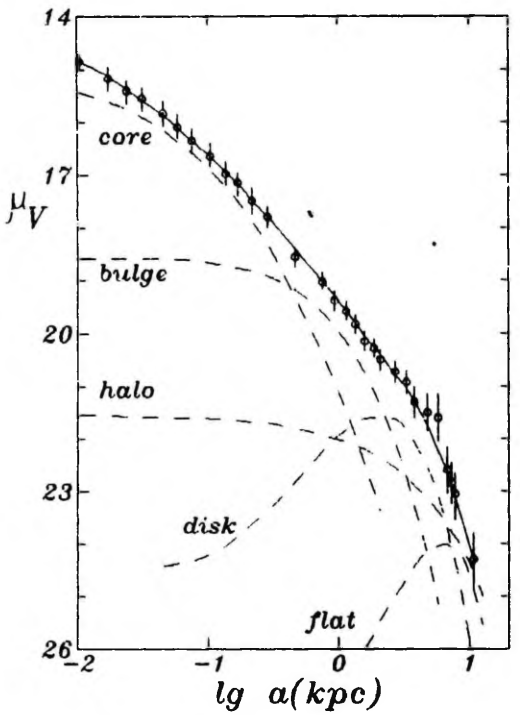

Figure 1 The averaged surface brightness profile of M81 in the V-colour. Open circles – observations, solid line - model, dashed lines – models for components.

Velocity dispersion profile in good seeing conditions (FWHM = 0.6") for the cental region (R $\sim$ 0.014 kpc) was obtained by Keel (1989). In the intermediate distance interval (R = 0.04 – 1.5 kpc) dispersions have been measured by Illingworth (1980) and by Delisle & Hardy (1992). By averaging dispersions at various distance intervals with the weights depending on seeing conditions and the velocity resolution, the dispersion curve presented in Fig. 5 was derived.

The observations on the distribution of individual objects which we used for modelling will be referred to and analysed in Sect. 4.

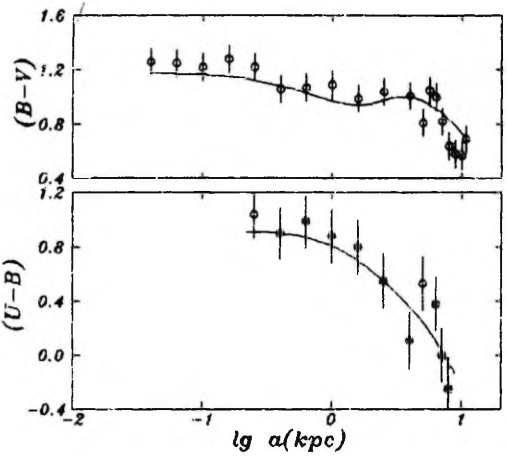

Figure 2 The averaged profiles of the colour indices (B – V) and (U – B) of M81. Open circles – observations, solid line – model.

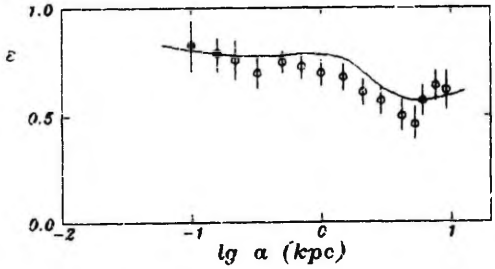

Figure 3 The axial ratios of isophotes of M81 as a function of the galactocentric distance. Open circles – observations, solid line – model.

4 Subsystems in M81

The nucleus

Photometry of inner regions of M81 obtained in excellent seeing conditions was done by Illingworth (1980), Kormendy (1985) and Keel (1989). The existence of a nucleus was suspected by Bendinelli et al. (1986), based on deconvolutions of the Illingworth's photometry. Radio observations reveal the central radio

source with the diameter $< 0.1'' = 1.6$ pc (de Bruyn et al. 1976). An additional argument supporting the nucleus as a separate dynamical unit is from velocity dispersions and rotation velocities (Keel 1989) of the central region. Unfortunately, no colour indices in the nucleus have been measured.

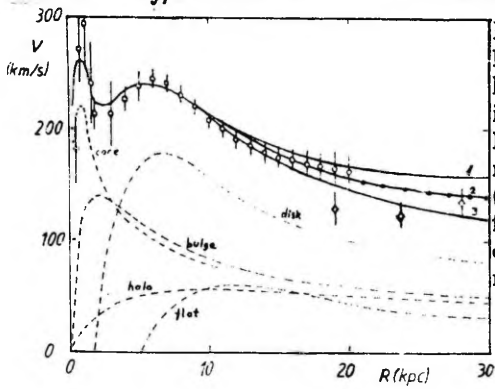

Figure 4 The rotation curve of M81. Open circles – high resolution observations of HI, of ionized gas and of CO, filled dots – Roberts & Rots (1973), open diamonds – Rohlfs & Kreitschmann (1980). Thick line – our best-fit model, dashed lines – models of the visible matter and of the massive corona.

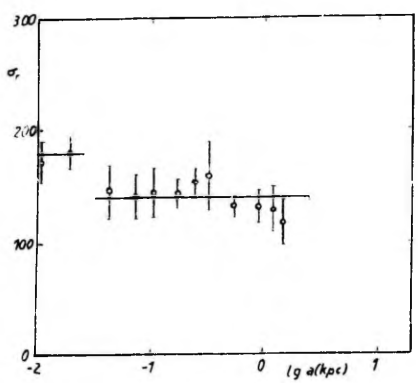

Figure 5 The averaged velocity dispersion profile of M81. Horizontal bars denote the mean dispersions calculated from our best fit model at the corresponding distance intervals.

The core and the bulge

The bulge is usually defined as a spheroidal component with normal metal content. In studying the chemical composition more informative for us is the colour index (U–B), being more sensitive to the metallicity variations. It is seen from Fig. 2 that the inner part of the spheroid is more metal-rich. This has been confirmed further by spectral observations (Cohen 1979). A similar

phenomenon - a sudden increase of metallicity in the cores of spheroids – has been detected in several nearby galaxies (Cohen 1979, Delisle & Hardy 1992). For this reason we can separate a metal-rich core from the bulge. A two-component structure of the bulge was used also by Rohlfs & Kreitschmann (1988) for our Galaxy (models 5 and 6) and emphasised by us in case of M31 (Chapter 2). However, the problem of discriminating between the core and the bulge is a complicated one and will be discussed in Sect. 5.

The halo

In our contects this is a synonyme of the term 'globular cluster system', designating the whole ensemble of old stars (age > 10 Gyr). At a distance of M81 the most complete dataset results from the analysis of globular clusters. The observations with the 6m telescope made by Georgiev et al. (1991) enabled to identify 60 probable candidates for globular clusters around M81. Their number surface density distribution is given in Fig. 6. The total expected number of clusters is estimated to be 100–150. The observed cluster distribution is well approximated by our density distribution law (Chapter 2, Eq. A1) with the parameters $N = 2.0 \pm 0.6$ and $a_0 = 8.0 \pm 1.2$ kpc.

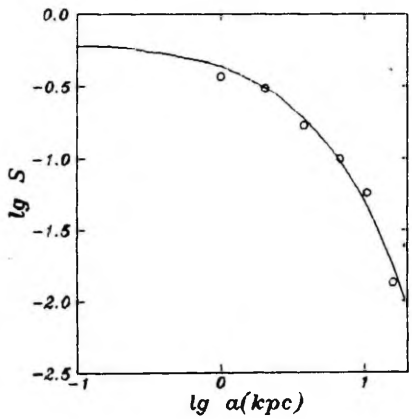

Figure 6 The distribution of globular clusters of M81. The observations have been averaged and presented by open circles. The continuous line gives the model distribution.

Measurements of individual globular clusters in our Galaxy by Illingworth (1976) give a mean M/L ratio 2.1 ± 0.6 $M_\odot/L_\odot$. This value we take as a reasonable approximation for M81. The luminosity of the halo remains as a free parameter in the final least-square fit.

Therefore, the analysis of the subsystem of globular clusters enables us to derive several halo parameters. We shall use these values in our least-square fit as fixed parameters.

The extreme flat subsystem

The presence of spiral arms results from oscillations of the luminosity superposed upon the disk. These oscillations are quite evident in the U-band and subsequently decrease toward longer wavelenghts.

The flat subsystem consists of young objects (open clusters, OB-associations, O-B stars etc.) and of interstellar medium (atomic and molecular gas and dust). In Fig. 7 the averaged distribution of the surface density of spiral arms stellar component (Schweizer 1976, Ivanov 1992) and gas (Rots 1975, Gottesmann & Weliachew (1975), Brouillet et al. 1988) is given.

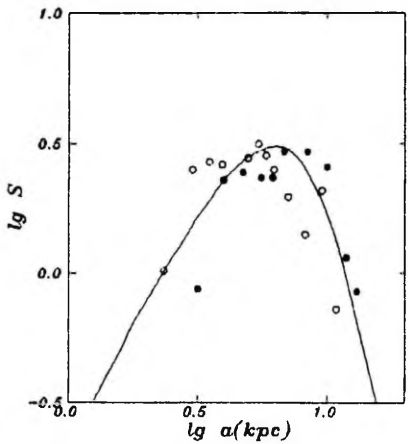

Figure 7 The distribution of young population I objects. Open circles – stellar component, filled circles – gas component, solid curve – model distribution.

The distribution of stars and gas in this population is well represented by our density distribution law (Chapter 2, Eq. A1) with the parameter $a_o = 6.4 \pm 0.8$ kpc, $N = 0.50 \pm 0.13$, $\kappa = 0.83$. For the flattening of the subsystem we take as in our Galaxy $\epsilon = 0.02$.

The total mass of both atomic and molecular gas in M81 is $M_{gas} = M_{HI} + M_{H_2} = 5.1 \pm 1.4 \cdot 10^9\,M_\odot$. To this value the mass fraction in the young stars ($M_S = 1.2 \pm 0.3 \cdot 10^9\,M_\odot$) can be added. Therefore the total mass $M = 6.3 \pm 1.7 \cdot 10^9\,M_\odot$ results for the flat population of M81.

As in case of the halo subsystem we shall use these values in the least-

square fit as fixed parameters for the flat subsystem.

The disk

It is convenient to define the disk to consist from stars with normal metallicity but with quite different ages. As for the flat subsystem, we allow a toroidal structure for the disk, i.e. the central density minimum. Otherwise it is difficult to model a minimum of the rotation velocity at 2.5 kpc (Einasto et al. 1980). The light listribution of the disk was obtained by Schweizer (1976) as a smooth background remaining after the subtraction of the spiral arms.

The massive corona

Despite of the fact that M81 has a falling rotational curve it is difficult to explain the high velocity dispersion of M81 satellite galaxies with the masses ascribed to the visible matter only. M81 is known to be the central galaxy of a group and it was derived by Vennik (1986) that the group member galaxies distribution is described by density distribution model for the corona with the parameters $a^o/a_o = 5.7$ and $a_o = 140$ kpc. The total mass of the matter needed to stabilise the group is $6 \cdot 10^{12}\,M_\odot$ resulting the mass-to-light ratio of $130\,M_\odot/L_\odot$. This value is quite high and establishes a problem is there any dark matter associated with M81. Morever, from the analysis of very different kind of observations reffered to in Chapter 1 it result that presence of some additional mass in the outskirsts of galaxies seems to be a common phenomena and detailed analysis is needed for M81.

5 Description of the fitting process

The population structure of M81 has been studied by means of modelling described in Chapter 2.

For all models the best-approximation parameter set has been found using the least-square algorithm, minimizing the sum of squares of relative deviations of the model from all observations.

The set of initial data consists of:

1. photometrical data (surface photometry in BVURI colours along the major and minor axes);
2. the distribution of the globular clusters;
3. the distribution of the extreme flat population objects;

4. the rotational curve in the plane of the galaxy;

5. the mean velocity dispersion for the nucleus, the core and the bulge;

6. the kinematics of the satellite galaxies of M81.

The number of combined observational points was 253. Photometrical profiles were taken with equal weights, and the rotation curve had the same weight as the surface photometry. The distribution of extreme flat population objects and globular clusters were used only for determination of the structure parameters (a_o, ϵ and N) of young and halo populations, respectively. The rotation curve had the equal weights with the surface photometry. The velocity dispersions and satellite kinematics were used only for mass determination.

In principle, the number of the degrees of freedom in the fitting process is 57 (6 visible populations with 9 parameters each (ϵ, a_o, M, κ, N, and 4 mass-to-light ratios in UBVR) and an invisible corona with 3 parameters (ϵ, a_o, M)). This number is reduced to 32, because some parameters were not changed. The parameter κ, indicating the depth of the central density depression, was fixed as zero for all components except the disk and the flat component. Next, the corona was assumed to be spherical (the axial ratio $\epsilon = 1$). Further, due to its little dimensions and mass the nucleus can be handled as dynamically independent subsystem, i.e. the parameters of the nucleus are independent of others and can be separately determined. In Sect. 4 we derived for the halo from the distribution of the globular clusters the density distribution parameters ϵ, a_o, N, and M/L_B. From the observed photometrical profiles we are not able to determine the colour indices for the halo as the profiles in the outer regions are noisy. For this reason in our further analysis we excluded the mass-to-light ratios in UVR-bands for the halo. In Sect. 4 from the distribution of the young stellar component the parameters ϵ, a_o, N, κ and M for the flat population were derived. These parameters of the halo and the flat subsystems were also unchanged.

Formulae given in Chapter 2, Appendix A are the relations connecting main observations with model parameters and they are used in estimating the values of these parameters in the procedure of the least square fitting. As in case of the Andromeda galaxy, this fitting must be done in several steps. First of all, we must fix the number of populations to be used in the model. For this we used the available data on the structure of M81 and referred to above as well as the data on the general structure of other spiral galaxies (e.g. Mihalas & Binney 1981, Gilmore et al. 1990).

As the galaxy is supposed to be a superposition of subsystems, in principle, all parameters are mutually related but the degree of dependence varies largely.

The core and the bulge subsystems are mixed in photometry, i.e. light

profiles allow variation of their structural parameters in a quite large interval: if we limit ourselves to the light profile in B only the presence of the core is not even necessary. More strict limits to the parameters of these components result from kinematics. It is impossible to model the observed features on the rotation curve with only one bulge component. Figure 8 represents the best-fit model with only one bulge component. To represent adequately the inner part of the rotation curve a two-component structure with different M/L ratios is needed.

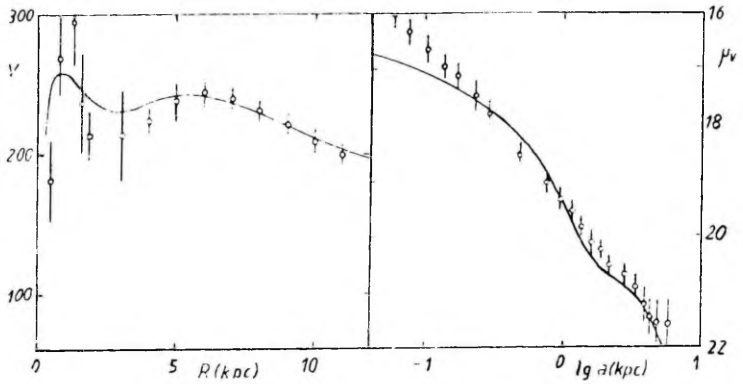

Figure 8 The inner part of the rotation curve and the surface brightness distribution in B for the best-fit model with only one bulge model.

Figure 9 demonstrates the sensivity of the rotation curve to the core radius. In these calculations the structure parameter $N = 2$ and the mass of the core corresponds to the mean velocity dispersion of $\langle\sigma\rangle_{core} = 138$ km/s. The radii of the core are 0.15 and 0.4 kpc, the masses of the core are 0.4 and 1 (in units of $10^{10}\,M_\odot$) for models (a) and (b), respectively.

Since a_o and N for the halo parameters were fixed on the basis of the distribution of globular clusters, all the remaining parameters for the core and the halo, and all parameters for the bulge can be determined with sufficient accuracy.

As it was noted earlier in Sect 4 the parameters ϵ, a_o, κ, N, and M for the flat subsystem were determined from the distribution of young objects and

fixed thereafter. The contribution of this component to the rotation curve is small and therefore dynamical information does not influence the parameters of the flat system. The luminosities in BUVR colours can be determined from corresponding surface brightness profiles.

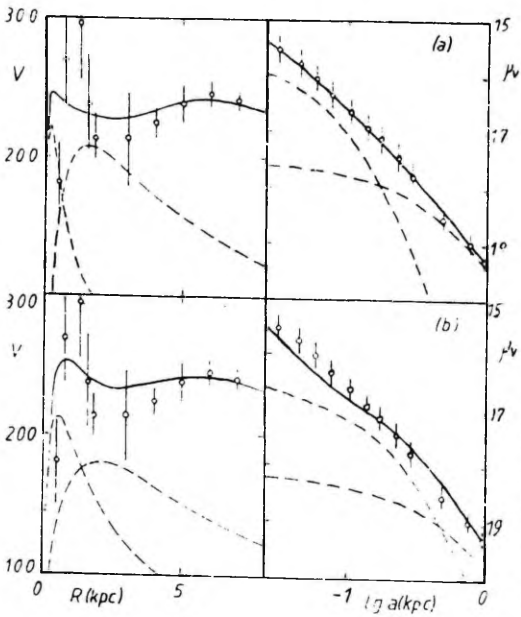

Figure 9 The inner part of the rotation curve and the surface brightness distibution in B (cf. Fig. 1) for three different models. The core radii are (a): 0.15, (b): 0.4 kpc.

In principle, discrimination between the disk and the corona is a complicated problem. On the bases of the rotation curve only it is not possible to determine the parameters of the corona even in case of galaxies with most extended rotation curves. In order to determine the dark matter distribution more distant probes of the gravitational field is needed. For M81 we can use the distribution and kinematics of the satellite galaxies (Sect. 4). In Fig. 4 the rotation curves for three different masses of the corona are given. Model 1 corresponds to $M = 3.2 \cdot 10^{12} M_{\odot}$, model 2 to $M = 1.4 \cdot 10^{12} M_{\odot}$ and model 3 is the model without the corona. As it is seen all three models give a satisfactory fit with the observed rotation velocities. However, while taking into account also the satellite kinematics the model 1 must be strongly preferred.

6 Results and discussion

The seven component model fits all photometric profiles with a mean relative error 0.7% , and the rotational curve with the error 1.8% . Within our model there are no contradictions between the photometrical and kinematical data. The model is in good agreement with both sets of data. This set (the axial ratio, ϵ, the harmonic mean radius, a_o, the total mass of the population, M, the structural parameter, κ and N, and the dimensionless normalizing constants, h and k) is given in Table 2. The final model is represented by solid lines in Figs. 1–7.

The total luminosity of M81 in B is calculated to be $L_B = 1.8 \cdot 10^{10}\,L_\odot$, the optically visible mass $M_{vis} = 9.8 \cdot 10^{10}\,M_\odot$, the corresponding M/L ratio $5.5\,M_\odot/L_\odot$. The mass-to-light ratio of both disk-like components (disk + flat) together is $M/L_B = 11.\,M_\odot/L_\odot$, of all spheroidal components (nucleus+core+bulge+halo) together $M/L_B = 3.5\,M_\odot/L_\odot$.

Table 2. Model parameters

Population	a_0 (kpc)	M ($10^{10}\,M_\odot$)	ϵ	N	κ	h	k
Nucleus	< 0.03	< 0.15	0.86	1.6	0.	14.0	0.136
Core	0.30	1.4	0.97	3.5	0.	983.	.000635
Bulge	1.4	1.6	0.69	1.5	0.	11.3	.172
Halo	8.0	1.5	0.60	2.	0.	33.3	.050
Disk	3.1	4.8	0.1	.9	0.72	3.28	.603
Flat	6.4	0.63	0.02	0.5	0.78	1.57	1.13
Corona	140.	320.	1.			14.8	0.151

Population	M/L_B ($M_\odot/L_\odot$)	B–V	U–B	V–R
Nucleus	< 36.			
Core	8.5	(1.15)	0.91	0.83
Bulge	3.8	0.93	0.80	0.7
Halo	2.1			
Disk	17.	1.06	0.54	0.79
Flat	4.	0.73	-0.17	0.76

1) Colour indices in parenthesis are uncertain.
2) The parameters a_o, ϵ for the disk and flat subsystems are for positive mass components.

The model constructed in this paper for the galaxy M81 is based on a large body of observational data. Surface photometry along the major and

minor axis in the UBVRI colours, rotation velocities, velocity dispersion data, distributions of neutral and molecular hydrogen have been taken into account for decomposing the galaxy into the subsystems and for the determination of the population parameters.

Rohlfs & Kreitschmann (1980) constructed a two component model for M81. The bulge was modelled by Brandt model and for the disk they used an exponential model with central density depression enabling to represent more adequately the observed rotational velocities for R < 6kpc. The structural parameters of the components were determined by fitting the model calculations with the observed rotation curve. The M/L ratios were derived by comparison with the light distibution in B-colour along the major axis. The masses for the disk and bulge calculated by us nearly coincide with those by Rohlfs & Kreitscmann.

In a two-component model by Kent (1987) the bulge was assumed spherical and the disk infinitly thin. The model bases on the light distribution in r-colour along the minor and major axis and on the rotation velocities from 3 kpc to 22 kpc. The structural parameters of the bulge and the disk were determined from the surface photometry and then the M/L ratios were derived from the kinematics. Also in this model it was derived that on the bases of the rotational curve alone 'it was possible to find acceptable models with any scale radius a [of the dark corona] between 0 and ∞. The total visible M/L ratio was obtained by Kent was $M/L_R = 4.5\ M_\odot/L_\odot$ (corresponding to $M/L_B = 6.6$, if B–R = 1.6). Taking into account the differences in models the coincidence with our result is good. Unfortunately it is not possible to compare the mass-to-light ratios separately for the bulges and the disks, because the mass of the bulge was not determined directly from observations.

All our models of M81, independently on the amount of the dark matter, are essentially the 'maximum disk' models. This results from the specific rotation curve of M81. In this sense the galaxy M81 is different from our neighbouring Andromeda galaxy. For M31 it was obtained that the 'maximum disk' is not the best approximation. It seems rather that every galaxy must be handled individually and the optimum disk must be chosen for every galaxy.

References

Bendinelli, O., Parmeggiani, G., Zavatti, F.: 1986. *Astrophys. J.* **308**, 611

Brouillet, N., Baudry, A., Combes, F.: 1988. *Astron. Astrophys.* **196**, L17

Burstein, D., Heiles, C.: 1984. *Astrophys. J. Suppl.* **54**, 33

Capaccioli, M., de Vaucouleurs, G.: 1983. *Astrophys. J. Suppl.* **52**, 465

Carter, D., Dixon, K.L.: 1978. *Astron. J.* **83**, 574

Cohen, J.G.: 1979. *Astrophys. J.* **228**, 405

Connolly, L.P., Mantarakis, P.Z., Thompson, L.A.: 1972. *Publ. Astron. Soc. Pacific* **84**, 61

Davoust, E., Paturel, G., Vauglin, I.: 1985. *Astron. Astrophys. Suppl.* **61**, 273

de Bruyn, A.G., Crane, P.C., Price, R.M., Carlson, J.B.: 1976. *Astron. Astrophys.* **46**, 243

Delisle, S., Hardy, E.: 1992. *Astron. J.* **103**, 711

de Vaucouleurs, G.: 1968. *Applied Optics* **7**, 1513

Einasto, J., 1972, Tartu Astrofüüs. Obs. Teated Nr. 40, 3 = Einasto, J., 1974 Galactic Models and Stellar Orbits. In: Mavridis, L.N. (ed.) Proc. First European Astr. Meeting, vol 2, Stars and the Milky Way System. Springer, Berlin, Heidelberg, New-York, p. 291

Einasto, J., Tenjes, P., Barabanov, A.V., Zasov, A.V.: 1980a. *Astrophys. Space Sci* **67**, 31

Einasto, J., Tenjes, P., Traat, P.: 1980b. *Astron. Circ.* No. 1089, 1

Elmegreen, D.M., Elmegreen, B.G.: 1984. *Astrophys. J. Suppl.* **54**, 127

Freedman, W.L.: 1988. *Astrophys. J.* **332**, L63

Georgiev, Ts.B., Getov, R.G.: 1991. *Pisma v Astron. Zh.* **17**, 393

Gottesman, S.T., Weliachew, L.: 1975. *Astrophys. J.* **195**, 23

Illingworth, G.: 1976. *Astrophys. J.* **204**, 73

Illingworth, G.: 1980. In: *ESO Workshop on Two Dimensional Photometry.* Eds. Crane, P., Kjär, K. ESO, p. 299

Ivanov, G.R.: 1992. *Monthly Notices Roy. Astron. Soc.* **257**, 119

Jones, W.B., Gallet, R.M., Obitts, D., de Vaucouleurs, G.: 1969. *Publ. Astron. Dept. Univ. Texas* Ser. 2, **1**, No. 8

Karachentsev, I.D.: 1986. Personal communication

Keel, W.C.: 1989. *Astron. J.* **98**, 195

Kent, S.M.: 1987. *Astron. J.* **93**, 816

Kormendy, J.: 1985. *Astrophys. J.* **292**, L9

Roberts, M.S., Rots, A.H.: 1973. *Astron. Astrophys.* **26**, 483

Rohlfs, K., Kreitschmann, J.: 1980. *Astron. Astrophys.* **87**, 175

Rohlfs, K., Kreitschmann, J.: 1988. *Astron. Astrophys.* **201**, 51

Rots, A.H.: 1975 *Astron. Astrophys.* **45**, 43

Rots, A.H., Shane, W.W.: 1975. *Astron. Astrophys.* **45**, 25

Sage, L.J., Westphal, D.J.: 1991. *Astron. Astrophys.* **242**, 371

Sandage, A.R., Becklin, E.E., Neugebauer, G.: 1969. *Astrophys. J.* **157**, 55

Schweizer, F.: 1976. *Astrophys. J. Suppl.* **31**, 313

Vennik, J.: 1986. *Astron. Nachr.* **307**, 157

Whitmore, B.C., McElroy, D.B., Tonry, J.L.: 1985. *Astrophys. J. Suppl.* **59**, 1

CHAPTER 6 REVIEW OF CONSTRUCTED MODELS*

1 Introduction

In the present Dissertation the models of 14 galaxies were constructed. The sample was chosen from a list of well-observed galaxies (Tenjes et al. 1982) and it includes galaxies of various morphological types and of different luminosities. The models of the galaxies M31, M87 and M81 were described in detail in previous Chapters. In this Chapter we review the models of remaining 11 galaxies.

In Table 1 the morphological type, absolute luminosity M_B, the distance D (in Mpc), the angle i between the symmetry plane of the galaxy and the line-of-sight, and the references to the surface photometry and kinematical data are given for the galaxies, which were modelled. The references to the observations published before 1982 can be found in Tenjes et al. (1982). The column 'Kinematics' corresponds both to the data on the rotation velocities as well as on the velocity dispersions.

2 Overview of the model components

Photometry of the galaxies made in excellent seeing conditions reveals as a rule the presence of compact and bright *nucleus* in the very center of a galaxy. Kinematical data, if available, indicate that the nucleus is dynamically nearly independent component. Although the nuclei contain only a small fraction of the galactic mass, they are prominent structural features.

The spheroidal part of the galaxies is far from physical homogenity and several components may be distinguished there. *The bulge* is dominated by old stars with normal metal content. Its flattening is modest with comparable amounts of rotational and pressure support. The inner part of the bulge is often more metal-rich (the colour index (U–B) may differ by $0.1 - 0.3^m$. For this reason we can separate a metal-rich *core* from the bulge. Under *the halo* we mean an old metal-poor population consisting of the globular clusters and old field stars (like RR-Lyrae variables). The total mass of field stars is by two orders of magnitudes larger than the total mass of globular clusters. The density distribution of the halo need not to be spherical.

---

* This Chapter bases in part on the paper by Tenjes, P., "Subsystems in galaxies and their mass-to-luminosity ratios". In: *The formation and evolution of galaxies and their constituents. I.*, Tallinn: Valgus, 1988, p. 73–97

Table 1. General characteristics of galaxies and the references to the main kinds of observations used.

Name	Type	M_B	D	i	Photometry	Kinematics
Fornax	E0	-12.2	0.16	0.	1	2, 6, 7, 8
Sculptor	E3	-10.8	0.07	0.	5	2, 3, 4
NGC 221	cE2	-15.7	0.7	0.	9, 10, 11, 12 13, 15	14, 15, 16, 17
NGC 3379	E1	-19.6	8.0	0.	18, 19, 20	21, 22, 23
NGC 4486	E0-1	-22.2	20.	0.	q.v. Chapter 4	
NGC 3115	S0	-20.0	10.	2.	24, 25, 26, 27	27, 28, 29
NGC 4594	SA(s)a	-22.3	20.	6.	30, 31, 32, 33 34, 35	33, 36, 37 38, 39
NGC 3031	SA(s)ab	-20.2	3.3	59.	q.v. Chapter 5	
NGC 224	SA(s)b	-20.8	0.7	13.	q.v. Chapter 2	
NGC 4321	SAB(s)bc	-20.7	20.	55.	40, 47, 48, 49	50, 51, 52, 53
NGC 5457	SAB(s)cd	-21.3	7.2	20.	40, 47	
NGC 6503	SA(s)cd	-18.0	6.1	16.	54, 55	54, 55, 56 57, 58
NGC 7793	SA(s)dm	-18.7	3.1	36.	40, 59	60
NGC 2366	IB(s)m	-16.9	3.2	25.	54	54, 55

1 – Eskridge (1988a), 2 – Seitzer & Frogel (1985), 3 – Armandroff & Da Costa (1986), 4 – Aaronson & Olszewski (1987), 5 – Eskridge (1988b), 6 – Aaronson & Olszewski (1986), 7 – Paltoglou (1989), 8 – Mateo et al. (1991), 9 – Sharov & Lyutyi (1983), 10 – Kent (1987), 11 – Michard & Nieto (1991), 12 – Tenjes (1992), 13 – Lugger et al. (1992), 14 – Pellet & Simien (1982), 15 – Tonry (1984), 16 – Dressler & Richstone (1988), 17 – Nolthenius & Ford (1986), 18 – Davis et al. (1985), 19 – Capaccioli et al. (1990), 20 – Peletier et al. (1990), 21 – Davies & Illingworth (1983), 22 – Davies & Birkinshaw (1988), 23 – Franx et al. (1989), 24 – Capaccioli et al. (1987), 25 – Silva et al. (1989), 26 – Surma et al. (1990), 27 – Kormendy & Richstone (1992), 28 – Cappelaro et al. (1990), 29 – Illingworth & Schechter (1982), 30 – Jarvis & Freeman (1985), 31 – Burkhead (1986), 32 – Kent (1988), 33 – Kormendy (1988), 34 – Wainscoat et al. (1990), 35 – Knapen et al. (1991), 36 – Bajaja et al. (1984), 37 – Rubin et al. (1985), 38 – Wagner et al. (1989), 39 – Kormendy & Illingworth (1982), 40 – Elmegreen & Elmegreen (1984), 47 – Whitemore & Kirshner (1982), 48 – Watanabe et al. (1982), 49 – Boroson et al. (1983), 50 – Arsenault et al. (1988), 51 – Guhathakurta et al. (1988), 52 – Distefano et al. (1990), 53 – Schechter (1983), 54 – Wevers (1984), 55 – Bottema (1989), 56 – de Vaucouleurs & Caulet (1982), 57 – van Moorsel & Wells (1985), 58 – Karachentsev & Petit (1990), 59 – Carignan (1985), 60 – Carignan & Puche (1990).

In spiral galaxies there exist two disk-like components. ***The disk*** consists of stars of normal metal content but with quite different ages (the mean age is about 7 Gyr). From observations it results that the disk has nearly exponential density distribution. The youngest stars belong to the spiral-arm population which we call ***the flat subsystem.*** Typical representatives of this component are open clusters, OB-associations, O-B stars etc. The flat subsystem contains also some nonstellar component (in Sdm galaxies it may be even the dominating part) as neutral and molecular hydrogen and dust. Its flattless is the largest. In our models we fix the axial ratio of the flat subsystems on the basis of our galaxy as $\epsilon = 0.02$. For disk-like components we allow a toroidal structure, i.e. the central density minimum.

From very different kind of observations it results that significant amount of dark matter may be associated with galaxies (Chapter 1). Following Einasto et al. (1974) we call this component as *the corona.* To probe the gravitational field of the corona most distant test particles must be used, as for example the dwarf satellite galaxies, surrounding the parent galaxy. From an analyse of galactic groups by Vennik (1986) it results that the distribution of dwarf galaxies in a synthetic group is well described by our density distribution law (Chapter 2, Eq. A2) with the parameter $a^o/a_o = 5.7$. This parameter we fixed for the corona.

3 Description of the modelling

The structure of the galaxies is studied by determining numerical values of parameters of their main populations. The galaxies were assumed to be in a steady state. All components represent physical subsystems composed of stars with similar age, chemical composition, and velocity distribution, i.e. they are physically homogeneous. Equidensity surfaces of the galactic populations are approximated by similar concentric ellipsoids or as sums of such ellipsoids.

The details of the modelling procedure were described in Chapters 2, 4 and 5. The relations connecting main observations with model parameters are given in Chapter 2, Appendix A.

The set of initial data contains besides the surface protometry and kinematical data also the spatial distribution of globular clusters (for the galaxies NGC 3379 (Pritchet & van den Bergh 1985), NGC 3115 (Hanes & Harris 1986), NGC 4594 (Harris et al. 1984, Bridges & Hanes 1992)), the distribution of extreme flat population objects for the galaxies NGC 4321 (Schweizer 1976, Hodge & Kennicutt 1983), NGC 5457 (Schweizer 1976, Bosma et al. 1981), NGC 6503 (Wevers 1984), NGC 7793 (Carignan & Puche 1990, Davoust & de Vaucouleurs 1980), NGC 2366 (Wevers 1984), and the kinematics of planetary nebulae (NGC 221: Nolthenius & Ford 1986) as well as satellite galaxies

(NGC 3379, NGC 5457: Vennik 1986).

The number of combined observational data points for each galaxy was 200–400. The photometrical profiles were taken with equal weights, and the rotation curve had the same weight as the surface photometry. The velocity dispersions and satellite kinematics were used only for mass determination. Globular clusters were taken as test particles of the halo subsystem. Young stars, OB-associations, open clusters and gas were used as representatives of the flat subsystem.

The initial number of the degrees of freedom in the fitting process was 35–60 depending on the number of components in a model. As a rule, this number was reduced because some parameters were kept fixed in the fitting process (q.v. Chapter 2.4 for details). In all models the parameter κ, indicating the depth of the central density depression, was fixed as zero for all components except the disk and the flat component. Next, the corona was assumed to be spherical. Also the outer radius were fixed for the coronae. They were determined from the kinematics of dwarf satellite galaxies of the parent galaxy. In galaxies where the halo and/or the flat subsystem were identified, the radius, the mass and the structural parameters of these components were also fixed on the basis of the distribution of corresponding test particles. As a result the final number of free parameters was 20–40.

The least squares algorithm presumes that the number of subsystems for a particular galaxy is fixed (although during the calculations the radius/mass/-luminosity of a particular component may be reduced to zero). All components of the model represent really existing subsystems with different physical properties. We do not add artifical components to improve the fit with observations.

As a galaxy is supposed to be a superposition of subsystems, in principle all parameters are mutually related. However, quite frequently such dependence may be weak. The connection between the parameters is illustrated in the case of the most well-observed galaxies M31 (Chapter 2) and M81 (Chapter 5).

4 Results

In Table 2 the final set of best-approximation parameters (the axis ratio ϵ, the mass M, the harmonic mean radius a_o, the structure parameter N, the mass-to-light ratio in B-colour M/L_B, and the colour indices (B–V), (U–B)) is given for our sample of galaxies.

The final models fit all the photometric profiles with relative errors 0.2–0.8 percent. The rotation curves were fitted with errors 1–1.8 percent. The distribution of globular clusters were fitted by the halo models with relative errors 1.2–1.6 percent.

Table 2. Calculated best-fit parameters

Subsystem	ϵ	M ($10^{10}\,M_\odot$)	a_o (kpc)	N	M/L_B ($M_\odot/L_\odot$)	(B–V)	(U–B)
Fornax							
halo	0.65	0.003	0.45	1.1	3.9	0.63	0.08
Sculptor							
halo	0.75	0.0021	0.28	0.96	4.8	0.70	
NGC 221							
nucleus	0.83	0.0094	0.008	1.4	4.7		
bulge	0.84	0.0781	0.094	4.0	2.3	0.90	0.33
NGC 3379							
nucleus	0.97	< 1.42	< 0.1	2.2	$< 23.$		
bulge	0.89	1.76	0.95	1.9	4.2	0.94	(0.50)
halo	0.8	0.70	4.7	3.	2.4	0.73	(0.30)
corona	1.	290.	110.				
NGC 3115							
bulge	0.8	0.74	0.086	1.7	4.9	1.01	
halo	0.65	2.0	6.4	4.	2.6	0.75	0.55
disk(+)	0.25	9.2	2.1	1.7	6.7	0.93	0.64
disk(−)	0.44	−2.97	1.2	1.7	6.7	0.93	0.64
corona	1.	300.	60.				
NGC 4594							
nucleus	0.79	< 1.6	< 0.15	3.0	< 3.7		
bulge	0.59	12.	2.21	2.0	2.9	1.01	0.76
disk(+)	0.1	22.7	8.14	.54	5.0	1.00	0.80
disk(−)	0.2	−5.68	4.07	.54	5.0	1.00	0.80
halo	0.73	29.7	18.4	4.0	1.7	0.80	(0.75)
corona	1.	800.	90.				
NGC 4321							
bulge	0.83	1.3	0.79	.54	1.7	0.59	
disk	0.1	15.6	8.71	1.	4.2	0.79	0.26
flat(+)	0.02	2.6	10.1	.5	1.31	0.63	−0.28
flat(−)	0.053	−0.35	3.79	.5	1.31	0.63	−0.28

Table 2. continued ...

Subsystem	ϵ	M (10^{10} $M_\odot$)	a_o (kpc)	N	M/L_B ($M_\odot/L_\odot$)	(B–V)	(U–B)
NGC 5457							
bulge	0.9	0.58	0.53	1.1	3.4	0.78	
disk	0.1	7.6	6.0	1.	4.1	0.70	0.21
flat	0.02	3.1	10.3	.56	2.2	0.51	–0.34
corona	1.	500.	110.				
NGC 6503							
bulge	0.8	0.04	0.26	2.4	1.8	0.57	(0.1)
disk(+)	0.1	0.45	1.58	.69	2.1	0.82	0.15
disk(–)	0.28	–0.055	0.55	.69	2.1	0.82	0.15
flat	0.02	0.31	3.94	1.1	1.81	0.60	–0.15
corona	1.	50.	40.				
NGC 7793							
bulge	0.7	0.004	0.047	1.6	2.	0.62	
disk	0.1	0.3	1.23	0.89	2.4	0.65	(0.0)
flat(+)	0.02	0.60	2.15	0.77	2.6	0.4	–0.2
flat(–)	0.03	–0.27	1.44	0.77	2.6	0.4	–0.2
corona	1.	80.	50.				
NGC 2366							
disk	0.1	0.14	2.7	.33	3.5	0.05	–0.32
flat(+)	0.02	0.104	1.43	.24	6.0	–0.04	–0.90
flat(–)	0.04	–0.026	0.67	.24	6.0	–0.04	–0.90

In Table 2 we identified the stellar population of the dwarf spheroidal galaxies Fornax and Sculptor as the halo. This results from the analysis of their global characteristics (dimensions, masses, colour indices). However, deep CCD photometry showed a brighter than expected main-sequence turnoff magnitude, indicating that some star formation has continued until a few Gyrs ago (Hodge 1989) and that some amount of intermediate-age population must exist in these galaxies. At present we are not able to derive separately the parameters for these two populations and they are united as the halo. Perhaps this is also the reason of somewhat higher mass-to-light ratios for the Fornax and Sculptor we may expect for the pure halo subsystem.

The mass-to-light ratio of the flat subsystems varies largely from galaxy to galaxy, from 1.3 to 6.0 $M_\odot/L_\odot$. This results because the flat subsystems has also a nonstellar part (interstellar gas), which in Sd–Sm galaxies may be even dominating in mass over the stellar part. As a result, the mass-to-light ratio

of the flat subsystem in these galaxies may be quite large.

The parameters for the core, the bulge and disk-like subsystems will be analysed in Chapter 7.

References

Aaronson, M., Olszewski, E.W.: 1986. *Astron. J.* **92**, 580

Aaronson, M., Olszewski, E.W.: 1987. *Astron. J.* **94**, 657

Armandroff, T.E., Da Costa, G.S.: 1986. *Astron. J.* **92**, 777

Arsenault, R., Boulesteix, J., Georgelin, Y., Roy, J-R.: 1988. *Astron. Astrophys.* **200**, 29

Bajaja, E., van den Bergh, G., Faber, S.M., Gallagher, J.S., Knapp, G.R., Shane, W.W.: 1984. *Astron. Astrophys.* **141**, 309

Boroson, T.A., Strom, K.M., Strom, S.E.: 1983. *Astrophys. J.* **274**, 39

Bosma, A., Goss, W.M., Allen, R.J.: 1981. *Astron. Astrophys.* **93**, 106

Bottema, R.: 1989. *Astron. Astrophys.* **211**, 236

Bridges, T.J., Hanes, D.A.: 1992. *Astron. J.* **103**, 800

Burkhead, M.S.: 1986. *Astron. J.* **91**, 777

Capaccioli, M., Held, E.V., Nieto, J-L.: 1987. *Astron. J.* **94**, 1519

Capaccioli, M., Held, E.V., Lorentz, H., Vietri, M.: 1990. *Astron. J.* **99**, 1813

Cappellaro, E., Capaccioli, M., Held, E.V.: 1990. In *Bulges of galaxies*, ESO Workshop, Chile, p. 227

Carignan, C.: 1985. *Astrophys. J. Suppl.* **58**, 107

Carignan, C., Puche, D.: 1990. *Astron. J.* **100**, 394

Davies, R.L., Birkinshaw, M.: 1988. *Astrophys. J. Suppl.* **68**, 409

Davies, R.L., Illingworth, G.: 1983. *Astrophys. J.* **266**, 516

Davis, L.E., Cawson, M., Davies, R.L., Illingworth, G.: 1985. *Astron. J.* **90**, 169

Davoust, E., de Vaucouleurs, G.: 1980. *Astrophys. J.* **242**, 30

de Vaucouleurs, G., Caulet, A.: 1982. *Astrophys. J. Suppl.* **49**, 515

Distefano, A., Rampazzo, R., Chincarini, G., de Souza, R.: 1990. *Astron. Astrophys. Suppl.* **86**, 7

Dressler, A., Richstone, D.O.: 1988. *Astrophys. J.* **324**, 701

Einasto, J., Kaasik, A., Saar, E.: 1974. *Nature* **250**, 309

Elmegreen, D.M., Elmegreen, B.G.: 1984. *Astrophys. J. Suppl.* **54**, 127

Eskridge, P.B.: 1988a. *Astron. J.* **96**, 1352

Eskridge, P.B.: 1988b. *Astron. J.* **95**, 1706

Franx, M., Illingworth, G., Heckman, T.: 1989. *Astrophys. J.* **344**, 613

Guhathakurta, P., van Gorkom, J.H., Kotanyi, C.G., Balkowski, C.: 1988. *Astron. J.* **96**, 851

Hanes, D.A., Harris, W.E.: 1986. *Astrophys. J.* **304**, 599

Harris, W.E., Harris, H.C., Harris, G.L.H.: 1984. *Astron. J.* **89**, 216

Hodge, P.: 1989. *Annual Review Astron. Astrophys.* **27**, 139

Hodge, P., Kennicutt Jr., R.C.: 1983. *Astron. J.* **88**, 296

Illingworth, G., Schechter, P.L.: 1982. *Astrophys. J.* **256**, 481

Jarvis, B.J., Freeman, K.C.: 1985. *Astrophys. J.* **295**, 324

Karachentsev, I., Petit, M.: 1990. *Astron. Astrophys. Suppl* **86**, 1

Kent, S.M.: 1987. *Astron. J.* **94**, 306

Kent, S.M.: 1988. *Astron. J.* **96**, 514

Knapen, J.H., Hes, R., Beckman, J.E., Peletier, R.F.: 1991. *Astron. Astrophys.* **241**, 42

Kormendy, J.: 1988. *Astrophys. J.* **335**, 40

Kormendy, J., Illingworth, G.: 1982. *Astrophys. J.* **256**, 460

Kormendy, J., Richstone, D.: 1992. *Astrophys. J.* **393**, 559

Lugger, P.M., Cohn, H.N., Cederbloom, S.E., Lauer, T.R., McLure, R.D.: 1992. *Astron. J.* **104**, 83

Mateo, M., Olszewski, E., Welch, D.L., Fischer, P.: 1991. *Astron. J.* **102**, 914

Michard, R., Nieto, J-L.: 1991. *Astron. Astrophys.* **243**, L17

Nolthenius, R., Ford, H.: 1986. *Astrophys. J.* **305**, 600

Paltoglou, G.: 1989. *Bull. Am. Astron. Soc.* **21**, 1130

Peletier, R.F., Valentijn, E.A., Jameson, R.F.: 1990. *Astron. Astrophys.* **233**, 62

Pellet, A., Simien, F.: 1982. ***Astron. Astrophys.*** **106**, 214

Pritchet, C.J., van den Bergh, S.: 1985. ***Astron. J.*** **90**, 2027

Rubin, V.C., Burstein, D., Ford Jr., W.K., Thonnard, N.: 1985. ***Astrophys. J.*** **289**, 81

Schechter, P.L.: 1983. ***Astrophys. J. Suppl.*** **52**, 425

Schweizer, F.: 1976. ***Astrophys. J. Suppl.*** **31**, 313

Seitzel, P., Frogel, J.A.: 1985. ***Astron. J.*** **90**, 1797

Sharov, A.S., Lyutyi, V.M.: 1983. ***Astron. Zh.*** **60**, 1

Silva, D.R., Boroson, T.A., Thompson, I.B., Jedrzejewski, R.I.: 1989. ***Astron. J.*** **98**, 131

Surma, P., Seifert, W , Bender, R.: 1990. ***Astron. Astrophys.*** **238**, 67

Tenjes, P.: 1992. in preparison

Tenjes, P., Kalamees, P., Einasto, J., Jõeveer, M., Brosche, P., Lentes, F.-Th.: 1982. *The List of Elite-Galaxies.* Tartu Astr. Obs. Teated Nr. 68., Valgus, Tallinn

Tonry, J.L.: 1984. ***Astrophys. J.*** **283**, L27

van Moorsel, G.A., Wells, D.C.: 1985. ***Astron. J.*** **90**, 1038

Vennik, J.: 1986. *Astron. Nachrich.* **307**, 157

Wagner, S.J., Dettmar, R-J., Bender, R.: 1989. ***Astron. Astrophys.*** **215**, 243

Wainscoat, R.J., Hyland, A.R., Freeman, K.C.: 1990. ***Astrophys. J.*** **348**, 85

Watanabe, M., Kodaira, K., Okamura, S.: 1982. ***Astrophys. J. Suppl.*** **50**, 1

Wevers, B.M.H.R: 1984. *A study of spiral galaxies, using HI synthesis observations and photographic surface photometry*, Groningen, Ph. D. Dissertation

Whitemore, B.C., Kirshner, R.P.: 1982. ***Astron. J.*** **87**, 500

CHAPTER 7 PHYSICAL PROPERTIES OF GALACTIC POPULATIONS

1 Introduction

The physical evolution of stellar systems depends on several parameters, which are usually only poorly known. While studying the structure of stellar populations in galaxies it is possible to obtain quantitative information which help to understand the formation and evolution processes (Sandage 1986). In present Chapter on the basis of the models constructed earlier we analyse the most important parameter of galactic subsystems – the mass-to-luminosity ratio. The M/L ratio of a stellar ensemble depends on the balance between the amount of large- and low-mass stars. This in turn depends mainly on the age and initial metallicity of the ensemble. Here we look what we are able to conclude about these quantities.

2 The mass-to-light ratios for spheroidal and disk subsystems

Sandage et al. (1970) suggested that the relative size of the spheroidal component in galaxies is determined by the relative amount of low angular momentum matter in a protogalaxy, and that this matter fragments into stars during the rapid collapse phase while the high mean angular momentum matter subsequently settles to the disk in the gaseous form. Therefore, the spheroids and the disks should experience different star formation histories and these two components should be analysed separately.

In our models the masses for spheroidal subsystems were determined from the tensor virial theorem (Chapter 2, Appendix A). For disks the masses were calculated on the basis of the rotation law. In Fig. 1 the dependence of the calculated mass-to-light ratios on colour indices for spheroidal subsystems – the core and the bulge – is given.

It is seen that spheroidal components lie in two quite separate regions. Points on the left-hand side (with colour indices 0.55–0.80) belong to late-type Sc – Sdm galaxies while those on the right-hand side to early-type and elliptical galaxies.

The distinct structure of the bulges of early- and late-type spiral galaxies is supported by an analysis of their UV-colours. It was found by Frogel (1985) that the bulges of late-type spirals have the energy distributions that are significantly bluer than those of early type spirals and E galaxies. Their blue energy distribution arises from a population of young stars mixed with the old population. In fact, it may be misleading to speak of an "old" and "young" population in Sc–Sm galaxies since star formation has probably never

really stopped in many of them. This is further supported by the fact that in the central regions of late-type spirals modelled by us there is no or little gas depression. This is obviously not the case for early-type spirals (M31, M81, M104) where the disk-like components must have toroidal structure (Einasto et al. 1980).

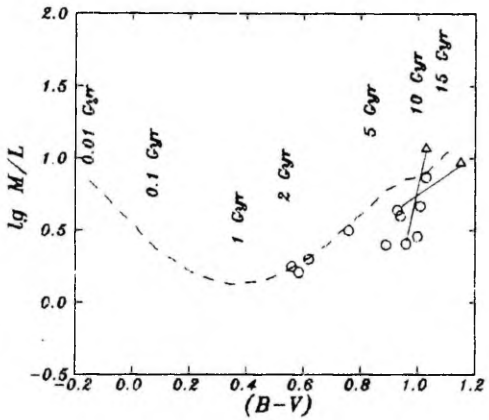

Figure 1. The mass-to-light ratios in B-colour M/L_B for spheroidal galactic subsystems v.s. colour index (B–V). Triangles – the core, open circles – the bulge. The dashed curve with corresponding ages in units of 10^9 yrs is from the chemical evolution model by Traat (1990).

Therefore, it is reasonable to conclude that both old and young stars are present in the bulges of late-type spiral galaxies. When comparing our models with the evolution models by Traat (1990) it results that their effective age is 1.5–4 Gyr.

The points corresponding to early-type bulges and ellipticals do not lie in the evolutionary curve. It is not possible to explain their position also with different star-formation rates or with gas accretion events. Probably the differences in their mass-to-light ratios must be ascribed to different initial chemical composition, from $Z = 0.01$ to $Z = 0.003$. However, we like to stress that the conversion of the M/L – (B–V) relation into initial value of Z depends also from other stellar evolution parameters (the rate of star formation, accretion processes, the form of IMF etc.).

Similar relation was constructed also for disk models (Fig. 2). For a given (B–V) larger scatter of mass-to-light ratios exists. Probably this is the result of infall or capture events unrelated to the bulk of the galaxy-formation process.

3 The mean mass-to-light ratio of visible matter

One of the crucial problems in extragalactic astronomy is the decomposition of a galaxy into ordinary and dark matter populations and a study of their relationship. It is difficult directly to calculate the masses of visible and dark matter because dynamical information concerns the sum of the two kinds of matter and, as a rule, we do not know the mass distribution of optically visible galactic populations. For this reason, some simplifying assumptions are often made, such as the 'maximum disk' or 'maximum bulge' hypothesis etc. However, in order to increase the accuracy of our final results it is desirable to determine all parameters of galactic populations directly from observations. To do so, we have to use all available data on populations. Modelling methodics is described in Chapter 2.4, final parameters of the models are listed in Chapter 6.

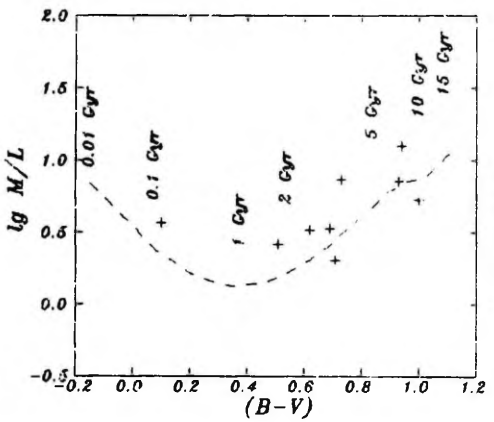

Figure 2. Dependence of mass-to-light ratios M/L_B for disk models on their colour index (B–V).

In Table 3 calculated mass-to-light ratios of the visible matter are given for our sample of galaxies.

Knowing the luminosity function (LF) of galaxies the mean mass-to-light ratio of the visible matter can be calculated. The galaxies in our sample cover the range in absolute luminosities from 10^7 to $10^{11}\,L_{\odot}$. However, as it was emphasized by Binggeli et al. (1988) there is not an universal LF for all galaxy types. Moreover, the mass-to-light ratios of the galaxies seem to depend rather from the morphological types than from their luminosities. (For elliptical galaxies Bacon et al. (1985) did not detected any clear correlation between the M/L ratio and absolute luminosity of a galaxy.) Because the most complete dataset still is available for the 'standard' Virgo cluster we used the

LFs by Sandage et al. (1985) to calculate the weights to the relative luminosity contribution of E, S0, Sa+Sb, Sc, Sd+Sm and dE morphological types. Our data from Table 3 together with the calculated weights give the mean luminosity weighed mass-to-light ratio of the visible matter $M/L_B = 4.1 \pm 1.4$ $M_\odot/L_\odot$. While using the weights resulting from the LFs of a sample of field galaxies by Kraan-Korteweg & Tammann (1979) and Tammann et al. (1979) the mean luminosity weighted mass-to-light ratio is $M/L_B = 3.7 \pm 1.3$ $M_\odot/L_\odot$.

The number of the galaxies used is the minimum one needed for any statistics. But at present it is difficult to increase the sample considerably, as we must limit ourselves only to well-observed galaxies. It also results from our models that there is not a universal rule to use or not to use the 'maximum disk' model. Rather it seems that every galaxy must be handled individually and some kind of optimum disk must be chosen for every particular case.

Table 3. The M/L ratios of the visible matter

Name	Type	Magnitude	Distance (Mpc)	M/L_B ($M_\odot/L_\odot$)
Fornax	E0	-12.2	0.16	4.1
Sculptor	E3	-10.8	0.07	9.7
NGC 221	cE2	-15.7	0.7	2.1
NGC 3379	E1	-19.6	8.0	5.0
NGC 4486	E0-1	-22.2	20.	4.9
NGC 3115	S0	-20.0	10.	4.8
NGC 4594	SA(s)a	-22.3	20.	2.4
NGC 3031	SA(s)ab	-20.2	3.3	5.5
NGC 224	SA(s)b	-20.8	0.7	4.8
NGC 4321	SAB(s)bc	-20.7	20.	2.9
NGC 5457	SAB(s)cd	-21.3	7.2	3.3
NGC 6503	SA(s)cd	-18.0	6.1	2.0
NGC 7793	SA(s)dm	-18.7	3.1	2.4
NGC 2366	IB(s)m	-16 9	3.2	4.1

Comparing the empirical relation between the mass-to-light ratios M/L_B and the (B–V) colours for spiral galaxies with the theoretical one predicted by Larson & Tinsley (1978) photometrical evolution model, Tinsley (1981) found a discrepancy between them. The observed increase of M/L_B with (B–V) is much shallower than that predicted theoretically. Tinsley (1981) concluded that later type spirals must have relatively more dark matter than early ones. This hypothesis has been reanalysed by Arimoto & Jablonka (1991) and Jablonka & Arimoto (1992) by using more sophisticated models and a better dataset. Comparing theoretical M/L versus colour relations of their model with those

derived from Sa–Sc galaxies observed by Rubin et al. (1982, 1985) and Burstein et al. (1982) they concluded that the ratio of dark-to-luminous mass is uniform among spiral galaxies.

In principle, the physical conditions in the collapsing interstellar matter may vary largely from galaxy to galaxy. This must result very different values for their M/L ratios. As it is seen from Table 3 the M/L ratio of visible matter varies surprisingly little from galaxy to galaxy, indicating **rather similar overall properties of collapsing interstellar matter as well as star formation process.** Taking into account the result of Jablonka & Arimoto we can conclude also that **the amount of the dark matter surrounding a galaxy is proportional to the luminosity of the galaxy.**

References

Arimoto, N., Jablonka, P.: 1991. *Astron. Astrophys.* **249**, 374

Bacon, R., Monnet, G., Simien, F.: 1985. *Astron. Astrophys.* **152**, 315

Bingelli, B., Sandage, A., Tammann, G.A.: 1988. *Annual Review Astron. Astrophys.* **26**, 509

Burstein, D., Rubin, V.C., Thonnard, N., Ford, W.K.Jr.: 1982. *Astrophys. J.* **253**, 70

Einasto, J., Tenjes, P., Barabanov, A.V., Zasov, A.V.: 1980. *Astrophys. Space Sci.* **67**, 31

Frogel, J.A.: 1985. *Astrophys. J.* **298**, 528

Jablonka, J., Arimoto, N.: 1992. *Astron. Astrophys.* **255**, 63

Kraan-Korteweg, R.C., Tammann, G.A.: 1979. *Astron. Nachr.* **300**, 181

Larson, R.B., Tinsley, B.M.: 1978. *Astrophys. J.* **219**, 46

Rubin, V.C., Ford Jr., W.K., Thonnard, N., Burstein, D.: 1982. *Astrophys. J.* **261**, 439

Rubin, V.C., Burstein, D., Ford Jr., W.K., Thonnard, N.: 1985. *Astrophys. J.* **289**, 81

Sandage, A.: 1986. *Annual Review Astron. Astrophys.* **24**, 421

Sandage, A., Freeman, K.C., Stokes, N.R.: 1970. *Astrophys. J.* **160**, 831

Sandage, A., Binggeli, B., Tammann, G.A.: 1985. *Astron. J.* **90**, 1759

Tammann, G.A., Yahil, A., Sandage, A.: 1979. *Astrophys. J.* **234**, 775

Tinsley, B.M.: 1981. *Monthly Notices Roy. Astron. Soc.* **194**, 63

Traat, P.: 1990. In: *Chemical and dynamical evolution of galaxies*, ed F.Ferrini, J.Franco, F.Matteucci (eds.), Pisa: ETS Editrice, p. 650

CHAPTER 8 INTRINSIC SHAPE OF ELLIPTICAL GALAXIES*

1 Introduction

The discovery that most E-type galaxies rotate much too slowly to account for their observed flattening (Bertola & Capaccioli 1975, Illingworth 1977) lead to an idea that elliptical galaxies lack rotational symmetry. Subsequent explanation in terms of anisotropic velocity dispersion tensors (Binney 1976, 1978) enabled to conclude that elliptical galaxies could be (but not necessarily are) triaxial in shape. Although the structure of stellar orbits in triaxial galaxies was investigated as far back as in early 70–ies (Kuzmin 1973) the renaissance of studies on the structure of elliptical galaxies started when Schwarzchild (1979, 1982) demonstrated by numerical models that triaxial equilibrium models can exist.

If triaxiality is taken into account, modelling of the intrinsic structure of an elliptical galaxy becomes highly degenerate (Contopulos 1956, Stark 1977, Rybicki 1987) and cannot be solved on the basis of photometry alone. Moreover, the direction of the angular momentum in a triaxial galaxy can be oriented in any direction on the plane defined by the shortest and the longest axis, depending on the balance between the momenta of the short and long tube orbits (de Zeeuw & Franx 1991). This introduces an additional free parameter – the kinematic misalignment.

In order to shed light on the structure of triaxial galaxies two approaches are still used. Nonuniqeness of deprojection process can be reduced by using a large sample of galaxies and assuming that the viewing angles are randomly distributed in space. Such approach was introduced by Binney (1985) who explored two extrema cases with the angular momenta parallel to either the shortest or to the longest axis. The analysis was extended by Franx et al. (1991) who used a more sophisticated model and a better dataset. Another possibility is to concentrate on detailed modelling of individual galaxies as it was done recently by Bertola et al. (1991) in the case of NGC 5077. The model

---

* This Chapter bases on the papers by Tenjes, P., Busarello, G., Longo, G. "Triaxial elliptical galaxies with dust lanes: an atlas of velocity fields", Napoli: Liguori Editore, 1992, and Tenjes, P., Busarello, G., Longo, G., Zaggia, S., "On the intrinsic shape of elliptical galaxies," *Astronomy and Astrophysics* submitted (1992).

used by Bertola et al. were based largely on the modelling of gas velocity fields.

However, for several ellipticals, even with gas/dust disks, only stellar kinematics is available. For this reason it would be useful to limit ourselves to stellar velocity fields only. We present here the first results of a work aimed to determining the intrinsic shape of individual elliptical galaxies by means of their observed photometric and kinematical properties. We try to study the structure of three elliptical galaxies with gas/dust disks and to see what constraints can be obtained to their intrinsic shape.

2 Method

We adopt a conventional coordinate system, with the shortest axis of a triaxial galaxy oriented along the z axis, the longest axis along the x axis and the intermediate one along the y axis. The direction to the observer is determined by its polar coordinates θ and ϕ (Fig. 1).

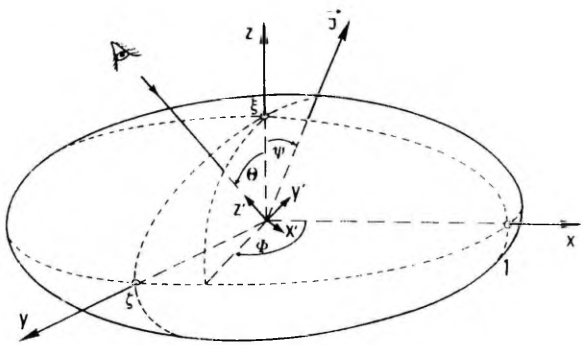

Figure 1. Coordinate system used for the projection. z'-axis is directed to the observer and is determined by polar coordinates ϕ and θ.

We assume that the luminosity density distribution is given by the modified Hubble profile (Binney and Tremaine 1987)

$$l = L_o(a_v^2 + r_o^2)^{3/2}, \tag{1}$$

with ellipsoidal isophotes

$$a_v^2 = x^2 + \frac{y^2}{\zeta^2} + \frac{z^2}{\xi^2}, \tag{2}$$

where ζ and ξ are the axial ratios ($1 \geq \zeta \geq \xi$), and L_o and r_o are the scale parameters. The coordinates (x', y', z') are defined in such a way that z' is oriented to the observer and x', y' lie on the plane of the sky. The direction of the line-of-sight with respect to the principal axis of density distribution is determided by the polar coordinates (ϕ, θ). Coordinates (x, y, z) and (x', y', z') are related by the rotation matrix

$$\begin{pmatrix} x \\ y \\ z \end{pmatrix} = \begin{pmatrix} -\sin\phi & -\cos\phi\cos\theta & \cos\phi\cos\theta \\ \cos\phi & -\sin\phi\cos\theta & \sin\phi\sin\theta \\ 0 & \sin\theta & \cos\theta \end{pmatrix} \begin{pmatrix} x' \\ y' \\ z' \end{pmatrix}.$$

Then the projected along line-of-sight surface density is (Stark 1977, Binney 1985)

$$\Sigma(x', y') = \int_{-\infty}^{\infty} l(a_v^2) dz' = \frac{2}{\sqrt{f}} \int_0^{\infty} l(z''^2 + a_s^2) dz'', \tag{3}$$

where

$$z'' = \sqrt{f}\left(z' + \frac{g}{2f}\right) \qquad a_s^2 = h - \frac{g^2}{4f} \tag{4}$$

$$\begin{aligned} f &= \sin^2\theta\left(\cos^2\phi + \frac{\sin^2\phi}{\zeta^2}\right) + \frac{\cos^2\theta}{\xi^2} \\ g &= \sin\theta\sin 2\phi\left(\frac{1}{\zeta^2} - 1\right)x' + \sin 2\theta\left(\frac{1}{\xi^2} - \cos^2\phi - \frac{\sin^2\phi}{\zeta^2}\right)y' \\ h &= \left(\sin^2\phi + \frac{\cos^2\phi}{\zeta^2}\right)x'^2 + \sin 2\phi\cos\theta\left(1 - \frac{1}{\zeta^2}\right)x'y' + \\ &\quad + \left[\cos^2\theta\left(\cos^2\phi + \frac{\sin^2\phi}{\zeta^2}\right) + \frac{\sin^2\theta}{\xi^2}\right]y'^2 \end{aligned} \tag{5}$$

The light distribution (1) turns out to be:

$$\Sigma(x', y') = \frac{2L_o}{\sqrt{f}} \int_o^{\infty} (z''^2 + a_s^2 + r_o^2)^{-3/2} dz'' =$$

$$= \frac{2L_o}{\sqrt{f}(a_o^2 + r_o^2)} = \frac{2L_o}{\sqrt{f}\left(h - \frac{g^2}{4f} + r_o^2\right)}, \tag{6}$$

where f, h, g are given by Eq. (5).

We assume also that no figure rotation is present. In order to calculate the projected velocity field we need to introduce an additional parameter, i.e. the angle ψ between the intrinsic angular momentum and the z-axis. Then the intrinsic velocity field can be written in the form (cf. de Zeeuw & Lynden-Bell (1988) for p =1)

$$\vec{u}(\vec{r}) = \frac{-2v_o}{(a_v^2 + r_o^2)^{1/2}} \left(\frac{y}{\zeta^2} \cos\psi; \frac{z}{\xi^2} \sin\psi - x \cos\psi; -\frac{y}{\zeta^2} \sin\psi \right). \tag{7}$$

The line-of-sight component of the rotational velocity at a point (x', y') on the plane of the sky is given by

$$v(x', y') = \frac{1}{\Sigma} \int_{-\infty}^{\infty} l\vec{u} \cdot \hat{z}' dz', \tag{8}$$

where the unit vector $\hat{z}'$ is given by Fig. 1 or by the rotation matrix

$$\hat{z}' = \begin{pmatrix} \cos\phi \sin\theta \\ \sin\phi \sin\theta \\ \cos\theta \end{pmatrix}. \tag{9}$$

At first we have to calculate $(\vec{u} \cdot \hat{z}')$ in Eq. (8), where $\vec{u}$ is given by (7) and $\hat{z}'$ by (9).

$$\vec{u} \cdot \hat{z}' \sim \left(\frac{y}{\zeta^2} \cos\psi; \frac{z}{\xi^2} \sin\psi - x \cos\psi; -\frac{y}{\zeta^2} \sin\psi \right) \cdot \begin{pmatrix} \cos\phi \sin\theta \\ \sin\phi \sin\theta \\ \cos\theta \end{pmatrix} =$$

(x, y, z must first be converted to x', y', z' according to the rotation matrix)

$$= \cos\phi \sin\theta \frac{\cos\psi}{\zeta^2} (x' \cos\phi - y' \sin\phi \cos\theta + z' \sin\phi \sin\theta) +$$

$$+ \sin\phi \sin\theta [\frac{\sin\psi}{\xi^2} (y' \sin\theta + z' \cos\theta) - \cos\psi(-x' \sin\phi - y' \cos\phi \cos\theta +$$

$$+ z' \cos\phi \sin\theta)] - \cos\theta \frac{\sin\psi}{\zeta^2} (x' \cos\phi - y' \sin\phi \cos\theta + z' \sin\phi \cos\theta) =$$

$$= \cos\phi \sin\theta \frac{\cos\psi}{\zeta^2}(x' \cos\phi - y' \sin\phi \cos\theta) - \cos\theta \frac{\sin\psi}{\zeta^2}(x' \cos\phi -$$

$$-y' \sin\phi \cos\theta) + \sin\phi \sin\theta (\frac{\sin\psi}{\xi^2} y' \sin\theta + x' \sin\phi \cos\psi + y' \cos\psi \cos\phi \cos\theta) +$$

$$+\frac{1}{2}(\sin 2\phi \sin^2\theta \frac{\cos\psi}{\zeta^2} + \sin 2\theta \sin\phi \frac{\sin\psi}{\xi^2} - \sin 2\phi \sin^2\theta \cos\psi -$$

$$-\sin 2\theta \sin\phi \frac{\sin\psi}{\zeta^2})z'.$$

Therefore,

$$\vec{u} \cdot \hat{z}' \sim P(x', y') + Qz', \tag{10}$$

where

$$P(x', y') = x' \left[\sin\theta \cos\psi \left(\frac{\cos^2\phi}{\zeta^2} + \sin^2\phi\right) - \cos\theta \sin\psi \frac{\cos\phi}{\zeta^2}\right] +$$

$$+ y' \left[\frac{1}{4} \sin 2\phi \sin 2\theta \cos\psi \left(1 - \frac{1}{\zeta^2}\right) + \sin\phi \sin\psi \left(\frac{\sin^2\theta}{\xi^2} + \frac{\cos^2\theta}{\zeta^2}\right)\right]$$

$$Q = \frac{1}{2} \sin 2\phi \sin^2\theta \cos\psi \left(\frac{1}{\zeta^2} - 1\right) + \frac{1}{2} \sin 2\theta \sin\phi \sin\psi \left(\frac{1}{\xi^2} - \frac{1}{\zeta^2}\right).$$

Taking into account Eq. (7) and (10), the line-of-sight velocity (8) can be written in the form:

$$v(x', y') = \frac{-2L_o v_o}{\Sigma} \int_{-\infty}^{\infty} \frac{P(x', y') + Qz'}{(a_v^2 + r_o^2)^2} dz'.$$

This integral can be processed in the same way shown in Binney (1985). It is however important to stress that our $P(x', y')$ and Q are different from those of Binney. The result is

$$v(x', y') = \frac{-L_o v_o \pi}{\Sigma \sqrt{f}} \frac{\left(P - \frac{Qq}{2f}\right)}{(a_o^2 + r_o^2)^{3/2}}.$$

And, by using Eq. (6) we obtain

$$v(x', y') = \frac{-v_o \pi}{2} \frac{\left(P - \frac{Qq}{2f}\right)}{(a_o^2 + r_o^2)^{1/2}}, \tag{12}$$

where P and Q are given by Eq. (11) and a_*, g, f by Eqs. (4–5).

Hence, once the intrinsic shape (ζ and ξ) of the galaxy and the kinematic misalignment (ψ) are chosen, the model can be projected on the sky for different orientations of the line of sight, determined by its polar coordinates θ and ϕ.

For each set of parameters it is possible to calculate a stellar velocity field (Eq. 12) and an isophotal contour map (Eq. 6), which can be directly compared with the observed galaxy. The comparison of the model with the observations allows us to put (in some cases strict) constraints on the intrinsic shape of the galaxy.

In the cases when also a gas/dust ring is present, one more constraint comes from the inclination of the gas ring with respect to the line of sight. Several surveys have identified about half a hundred of such galaxies (Hawarden et al. 1981, Sparks et al. 1985, Bertola 1987), roughly 60–70% of which have obscuring lanes along the minor axis. The morphology and kinematics of cold gas in a triaxial Stäckel-type potential was studied by de Zeeuw & Franx (1989). It was derived that the isophotes of the gas disk are roughly ellipses elongated along the intermediate or the shortest axis. The morphology of the gas depends on the density distribution of the galaxy and on the intrinsic density distribution of the gas/dust layer. Unfortunately the latter is largely unknown.

For many ellipticals the gas/dust disk extends up to the outer edge or even outside of the visible stellar body of the galaxy In these cases also the dark mass may contribute to the total potential of the galaxy but little is known about the shape of the dark matter corona. Due to these uncertainties the assumption of intrinsically circular isophotes in the outer parts of the gas disk can be useful. However, we must be careful in applying this simplification in every individual case.

To help the observers to choose between various models, an Atlas of Velocity Fields was prepared (Tenjes et al. 1992) where the projected stellar velocity fields together with the apparent light and dust lane morphology are calculated and presented in form of figures. For each set of initial data two figures are given. The upper one is the velocity field and the configuration of the galaxy, while the lower one gives the minor and major axis rotation curves. Ellipsoids drawn by continuous line mark the apparent stellar isophote contour of the galaxy (as stated before, in our models equidensity surfaces are similar ellipsoids). Ellipses marked by open squares give the shape of the projected gas (and/or dust) disk. In the case of nearly minor axis dust lanes the gas (dust) disks must lay always on the yz-plane, i.e. perpendicular to the longest axis of the triaxial figure (although we made the calculations also for disks perpendicular to the shortest axis). The velocity field is drawn with equal velocity step for all figures. The smaller number of isovelocity contours

in a figure means therefore, that the maximum rotation velocity is smaller. To help understanding the radial scale in the figures, we expressed them in units of $\zeta r_o = 5''$. This corresponds to the typical light profile of a bright galaxy ($M_B \sim -20$) at the redshift $V_o \sim 1500$km/s. This unit can however be transformed in dimensionless units by substituting $10'' = 2$.

In the lower figures (rotation curves) filled triangles give the expected velocities along the apparent major axis, while open triangles correspond to the minor axis. Figures are plotted with a cutoff at $v/v_o = 1.5$ (notice that v_o is not a maximum rotation velocity, but simply a normalization parameter).

In order to minimize the number of figures in the Atlas we adopted reasonably large steps in both the intrinsic axial ratios ξ and ζ and in the kinematic misalignment ψ. In most cases plots are presented for $\psi = 0°, 8°, 15°, 45°$, and $90°$. The intrinsic shape of the galaxies was assumed to be maximally triaxial, i.e. the lenght of the intermediate axis y is the exact average of the shortest and the longest axis in accordance with the statistics made by Binney (1985). Such configurations lay also in the region of most probable triaxialities given by Franx et al. (1991). The smallest axial ratio ξ changes with the step 0.1 from 0.4 to 0.9 (as in fact there are no ellipticals with Hubble type later than E6).

The galaxies are ordered in the Atlas according to their apparent flattening, and, inside each class of ellipticity, they are ordered according to their orientation and kinematic misalignment. This allows the reader to put limits on the intrinsic shape and orientation of the galaxy by directly comparing the photometric and kinematical data to those found in the Atlas.

In the case of triaxial galaxies, the projected stellar velocity fields in general have several specific properties:

1. the direction of the maximum velocity gradient does not generally coincide with the apparent major axis;
2. the zero velocity gradient is generally not oriented along the apparent minor axis;
3. the angle between the directions of the maximum and zero velocity gradients is not generally 90°;
4. the velocity field is not symmetrical with respect to the direction of the maximum velocity gradient.

All these features depend on the intrinsic configuration of a galaxy and on the viewing angles. For this reason the comparison with observations is more interesting in the cases where more information on the velocity fields are available, i.e. for instance galaxies which have rotation velocities measured at different

position angles and/or at positions of the spectrograph slit offcentered.

3 Results

In the present work we apply the models to three elliptical galaxies, which were selected for the following reasons:

i) They belong to different Hubble classes: E0 (NGC 5898), E1 (NGC 1947), and E3 (NGC 1052).

ii) They do not show isophote twisting and have no, or little, variation of ellipticity with radius (our model assumes that projected isophotes are concentric and coaxial ellipsoids).

iii) They have rotation curves observed at several position angles.

NGC 5898

A detailed photometry of NGC 5898 in B and R colors was done by Jedrzejewski (1987), who derived a mean apparent isophotal axial ratio $\epsilon = 0.95 \pm 0.03$. Together with the presence of an absorbing dust lane this makes the determination of isophote twisting extremely uncertain. However, as the color index B–R is constant in the galaxy, indicating homogeneous stellar content, we can approximate the isodensity contours of the galaxy by similar coaxial ellipsoids.

From the analysis of the B–I color map Sparks et al. (1985) report the presence in NGC 5898 of an inner disk and outer arc of dust with the same axial ratio about 0.65 ± 0.10 (the error was estimated by eye from their figure).

A triaxial galaxy projects onto the plane of the sky as an E0 galaxy only when it is observed under the specific viewing angles given by

$$\phi = 0,$$

$$\sin^2 \theta = \frac{1 - \zeta^2}{1 - \xi^2}. \tag{13}$$

As the apparent axis ratio of the dust disk/arc is the same at two different distances from the centre we can conclude that the disk is intrinsically nearly circular. In this case we can derive the viewing angle $\theta_1 = 50^\circ$, if the gas lies perpendicular to the shortest axis, or $\theta_2 = 40^\circ$, if the gas lies perpendicular to the longest axis. The uncertainty ± 0.1 in the axial ratio of the dust ring corresponds to the error in θ of $\Delta\theta = 8^\circ$. Therefore, within the errors we can

take $\theta = 45° \pm 8$. In Fig. 2 the intrinsic axial ratios resulting from Eq. (13) are given by a long-dashed line. The region limited by short-dashed lines corresponds to the uncertainties in θ.

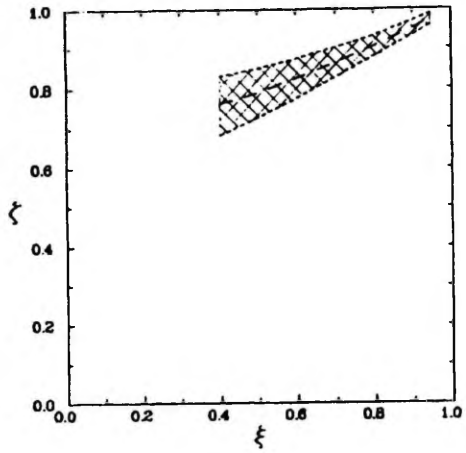

Figure 2 The region of possible axial ratios of NGC 5898. The exact solution is designated by the long-dashed line. The hatched region corresponds to the uncertainty in θ.

NGC 1052

The surface photometry of NGC 1052 by Peletier et al. (1990) gives us the axial ratio of isophotes $\epsilon = 0.71 \pm 0.04$. The position angle of the major axis was derived to be 118°. From (B–I) colour map Sparks et al. (1985) identified the outer dust lane with the axial ratio of 0.5 ± 0.05. In (B–R) and Hα the disk is mapped by Kim (1989). HI observations of the disk were made by van Gorkom et al. (1986). Up to the distances $\leq 50''$ the apparent isophotes of the gas in $H\alpha$ and 21 cm lines are nearly elliptical with the axial ratios similar to the dust lane (outside the Holmberg radius two outer HI lobes are seen and a tidal tail). Being the member of the group (the mean velocity dispersion of the group member galaxies is 104 km/s) it is very likely that a significant amount of dark matter may be related with the galaxy.

The gas morphology enables us to constrain the axial ratios and the viewing angles (Figs. 3 and 4).

It is clear that these two Figures are not independent. Not all combinations of ξ, ζ, ϕ, and θ from hatched regions of Figs. 3 and 4 can be accepted but

for a certain pair of ξ, ζ corresponds only a subregion of ϕ, θ. The true figure must be 4-dimensional! In order to compensate for this insufficiency we refer to Table 1.

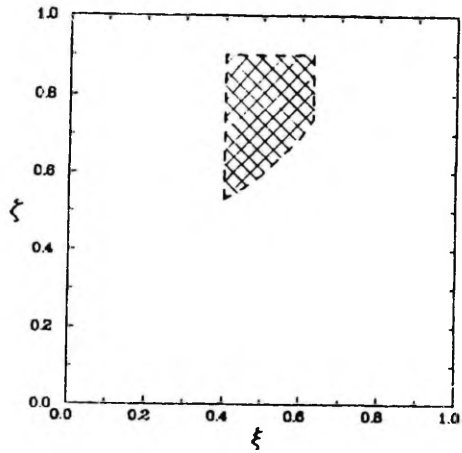

Figure 3 Permitted axial ratios of the galaxy NGC 1052

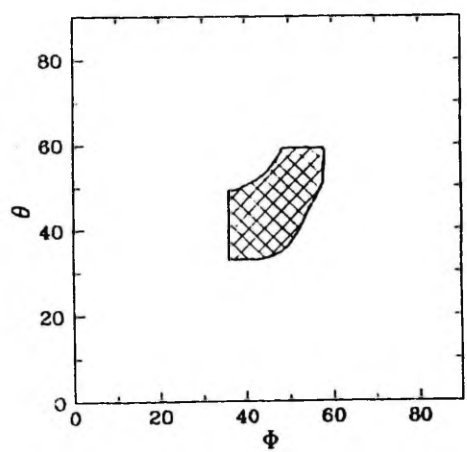

Figure 4 Permitted viewing angles of the galaxy NGC 1052.

Stellar rotation along nearly major axis has been measured by Whitmore et al. (1987) and Bertola et al. (1984). Binney et al. (1990) have obtained spectra along position angles of 28°, 73°, 117°, 164°, and also offcentered by 13" parallel and 15" perpendicular to the major axis. On basis of these rotational velocities the smoothed velocity field can be drawn (Fig. 5). The main feature is that the galaxy is a nearly perfect major axis rotator.

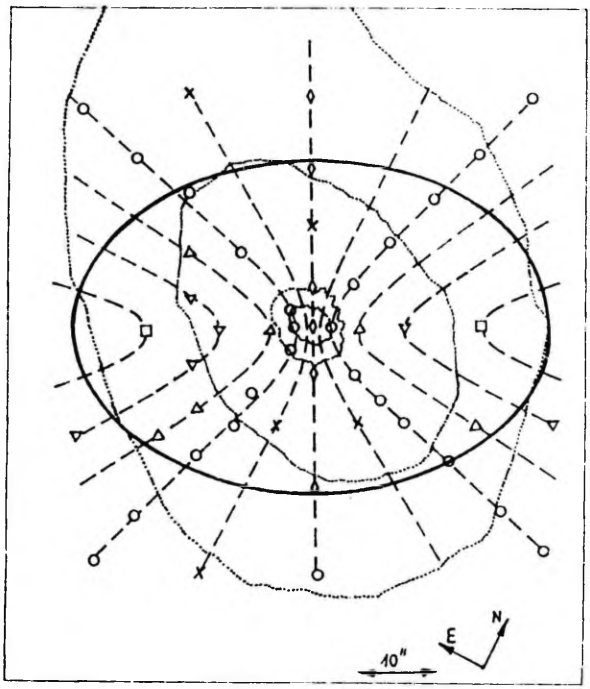

Figure 5 The observed velocity field of NGC 1052. Velocities are plotted with an interval of 20 km/s (◇–0, ×–20, ○–40, △–60, ▽–80, ⊔–100 km/s). Extrapolated isovelocity contours are drawn by dashed lines. The 20^m per square arcsecond R-colour isophote of the galaxy is given by a thick line ellipse. The Hα and innermost HI surface density contours are given by dotted lines.

Binney et al. (1990) successfully fitted the rotational velocities of NGC 1052 with an oblate model. However, as it was noted also by authors, their model is only an approximation since actually NGC 1052 is triaxial because of orientation of the gas rotation axis.

To estimate kinematic misalignment we chose three representative points from the hatched region of Fig. 3: I: $\xi = 0.4$, $\zeta = 0.7$; II: $\xi = 0.5$, $\zeta = 0.75$; III: $\xi = 0.6$, $\zeta = 0.8$. Corresponding viewing angles are given in Table 1. From the Atlas of Velocity Fields we can check the velocity fields corresponding to E3 galaxies with the dust lane axial ratio 0.5. The following models have the maximum velocity gradient along the major axis (Fig. 6 and Table 1):

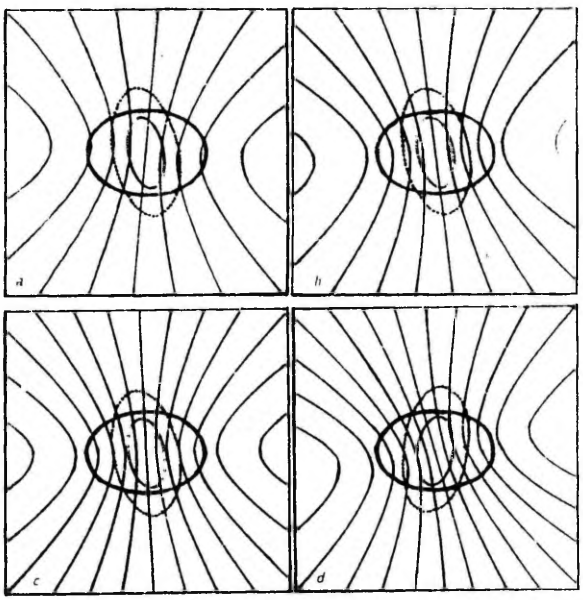

Figure 6 The model velocity fields of NGC 1052 as taken from Tenjes et al. (1992). Ellipsoids drawn with continuous line mark the apparent stellar isophote contour of the galaxy. Ellipses marked by dashed lines give the shape of the projected gas/dust disk. Other curves represent the velocity field. (a): model I, (b): model II, (c): model IIIa, (d): model IIIb.

Table 1 The intrinsic parameters of three representative models of NGC 1052

I $\xi = 0.4, \zeta = 0.7, \phi = 40 \pm 4, \theta = 40 \pm 5, \psi = 15 \pm 3;$
II $\xi = 0.5, \zeta = 0.75, \phi = 47 \pm 5, \theta = 48 \pm 6, \psi = 13 \pm 4;$
IIIa $\xi = 0.6, \zeta = 0.8, \phi = 55 \pm 4, \theta = 61 \pm 8, \psi = 8 \pm 5;$
IIIb $\xi = 0.6, \zeta = 0.8, \phi = 125 \pm 4, \theta = 61 \pm 8, \psi = 0 \pm 5.$

The errors in the viewing angles result from the uncertainties of the axial ratios of the brightness isophotes and of the dust lane. The errors in kinematic misalignment arise from those of the ratios of major and minor axis rotation velocities.

More observations are needed, especially from several offset positions to discriminate between the models listed above. At present we can only give larger weight to model III, as the maximum rotation velocities in models I and II seem to be too small.

NGC 1947

According to the photometry by Bertola et al. (1992) the galaxy NGC 1947 has the mean isophote axial ratio 0.92 ± 0.03. The major axis has the position angle 30° and shows only little twisting. The dust lane is seen up to the visible edge of the galaxy. The apparent axial ratio of the dust ring is 0.26 ± 0.05 (Möllenhoff 1982, Bertola et al. 1992) and the position angle 120°. These data set limits to the true axial ratios of the galaxy $0.7 > \xi, \zeta > 0.9$. The range for the axial ratios ξ and ζ is quite narrow and we can take as a reliable solution

$$\xi = 0.8,$$

$$\zeta = 0.9.$$

The region of permitted viewing angles is given in Fig.7.

Stellar rotation velocities were observed by Bertola et al. (1992) along the position angles 30°, 75°, 120°, 165° and by Longo et al. (1992) at position angles 0° and 90°. The rotation velocities are noisy and a velocity field in a way as it was done for NGC 1052 is not possible to construct. It is possible only to conclude about the maximum rotational velocity gradient along the apparent major axis.

The kinematic misalignment was estimated from the Atlas for viewing angles $\phi = 47°$, $\theta = 25°$. The configuration corresponding to the minor axis rotation (Fig. 8) has the parameter $\psi = 12° \pm 8$.

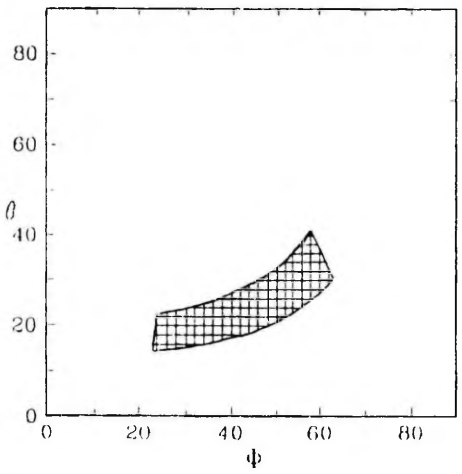

Figure 7 The region of permitted viewing angles for NGC 1947

4 Conclusions

In the present work we have shown how the observed light distribution and radial velocity field can be used to set constraints on the configuration parameters and on the viewing angles of triaxial elliptical galaxies. The method has been applied to three properly chosen elliptical galaxies. Even though the sample is limited, we would like conclude that in two of our models the kinematical misalignment is small or absent. This can be subjected to further investigation.

Statler (1987, 1991) calculated a family of self-consistent models for "perfect ellipsoids". The distribution functions were calculated numerically with Schwarzchild's (1979) method. In the inner parts of several models double-peaked velocity fields were obtained similar to those observed by Franx & Illingworth (1988) and Bender (1990). Such models are very useful in order to clarify the structure of elliptical galaxies and, particularly, the nature of counter-rotating cores. However, it is difficult to compare the results of Statler with ours, because we have no information on the behaviour of the kinematic misalignment in Statler's models.

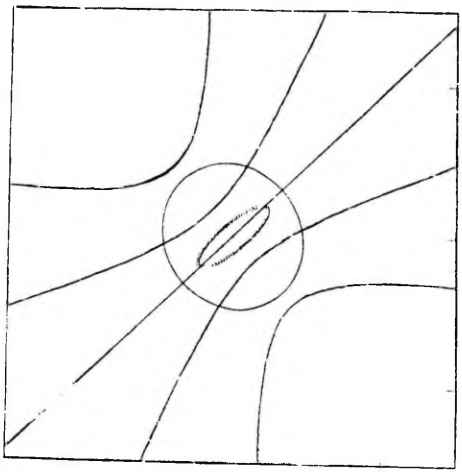

Figure 8 The model velocity field of NGC 1947 corresponding to the axial ratios $\xi = 0.8$, $\zeta = 0.9$, the viewing angles $\phi = 47°$, $\theta = 25°$ and kinematical misalignment $\psi = 12°$. The symbols are the same as in Fig. 6.

For further work we need to have a much larger sample of galaxies. More detailed velocity fields are also urgently needed. This would help to clarify the problem of the intrinsic shapes of elliptical galaxies and to find their distribution.

References

Bender, R.: 1990. In: *Dynamics and interactions of galaxies*, R.Wielen (ed.), Berlin/Heidelberg: Springer-Verlag, p. 232

Bertola, F.: 1987. In: *Structure and dynamics of elliptical galaxies, IAU Symp. No. 127*, P.T. de Zeeuw (ed.), Dordrecht: Reidel, p. 135

Bertola, F., Capaccioli, M.: 1975. *Astrophys. J.* **200**, 439

Bertola, F., Bettoni, D., Rusconi, L., Sedmak, G.: 1984. *Astron. J.* **89**, 356

Bertola, F., Bettoni, D., Danziger, J., Sadler, E., Sparke, L., de Zeeuw, T.: 1991. *Astrophys. J.* **373**, 369

Bertola, F., Galletta, G., Zeilinger, W.W.: 1992. *Astron. Astrophys.* **254**, 89

Binney, J.: 1976. *Monthly Notices Roy Astron. Soc.* **177**, 19

Binney, J.: 1978. *Monthly Notices Roy. Astron. Soc.* **183**, 501

Binney, J.: 1985. *Monthly Notices Roy. Astron. Soc.* **212**, 767

Binney, J., Tremaine, S.: 1987. *Galactic dynamics*, Princeton: Princeton University Press

Binney, J.J., Davies, R.L., Illingworth, G.D.: 1990. *Astrophys. J.* **361**, 78

Contopoulos, G.: 1956. *Zeitschr. für Astrophys.* **39**, 126

de Zeeuw, P.T., Franx, M.: 1989. *Astrophys. J.* **343**, 617

de Zeeuw, P.T., Franx, M.: 1991. *Annual Review Astron. Astrophys.* **29**, 239

de Zeeuw, P.T., Lynden-Bell, D.: 1988. *Monthly Notices Roy. Astron. Soc.* **232**, 419

Franx, M., Illingworth, G.: 1988. *Astrophys. J.* **327**, L55

Franx, M., Illingworth, G., de Zeeuw, T.: 1991. *Astrophys. J.* **383**, 112

Hawarden, T.G., Elson, R.A.W., Longmore, A.J., Tritton, S.B., Corwin, H.G.: 1981. *Monthly Notices Roy. Astron. Soc.* **196**, 747

Illingworth, G.: 1977. *Astrophys. J.* **218**, L43

Jedrzejewski, R.I.: 1987. *Monthly Notices Roy. Astron. Soc.* **226**, 747

Kim, D.-W.: 1989. *Astrophys. J.* **346**, 653

Kuzmin, G.G.: 1973. In: *Dynamics of galaxies and clusters*, T.B. Omarov (ed.), Alma-Ata: Akad. Nauk Kaz. SSR, p. 71 [Transl. in: *Structure and dynamics of elliptical galaxies, IAU Symp. No. 127*, P.T. de Zeeuw (ed.), Dordrecht: Reidel, p. 553]

Longo, G., Busarello, G., Tenjes, P., Zaggia, S.: 1992. in preparation

Möllenhoff, C.: 1982. *Astron. Astrophys.* **108**, 130

Peletier, R.F., Davies, R.L., Illingworth, G.D., Davis, L.E., Cawson, M.: 1990. *Astron. J.* **100**, 1091

Rybicki, G.B.: 1987. In: *Structure and dynamics of elliptical galaxies, IAU Symp. No. 127*, P.T. de Zeeuw (ed.), Dordrecht: Reidel, p. 397

Schwarzschild, M.: 1979. *Astrophys. J.* **232**, 236

Schwarzschild, M.: 1982. *Astrophys. J.* **263**, 599

Sparks, W.B., Wall, J.V., Thorne, D.J., Jorden, P.R., van Breda, I.G., Rudd, P.J., Jorgensen, H.E.: 1985. *Monthly Notices Roy. Astron. Soc.* **217**, 87

Stark, A.A.: 1977. *Astrophys. J.* **213**, 368

Statler, T.S.: 1987. *Astrophys. J.* **321**, 113

Statler, T.S.: 1991. *Astron. J.* **102**, 882

Tenjes, P., Busarello, G., Longo, G.: 1992. *Triaxial elliptical galaxies with dust lanes: an atlas of velocity fields*, Memorie dell'Accademia di Scienze Fisiche e Matematiche. Napoli: Liguori editore

van Gorkom, J.H., Knapp, G.R., Raimond, E., Faber, S.M., Gallagher, J.S.: 1986. *Astron. J.* **91**, 791

Whitmore, B.C., McElroy, D.B., Schweizer, F.: 1987. *Astrophys. J.* **314**, 439

SUMMARY (IN ESTONIAN)

Regulaarsete galaktikate mudelid

Üks kaasaegse astronoomia olulisemaid probleeme on massijaotuse uurimine galaktikates, nn. tavalise ja nähtamatu aine komponentide eraldamine ning nende omavahelise jaotuse uurimine. Galaktikate nähtava osa struktuuri analüüs võib aidata valida erinevate galaktikate tekke stsenaariumide vahel ning selgitada ka nähtamatu aine olemust. Vaid tähesüsteemide radiaalsel heleduse jaotusel baseeruvad lihtsad mudelid ei ole seni võimaldanud olulisel määral otsustada erinevate galaktikate tekke teooriate vahel, kuna mitmed teooriad ühilduvad võrdselt hästi vaatlustega. Paremaid tulemusi on võimalik saada mitmekomponendiliste mudelitega, kus modelleeritakse ka galaktikates esinevaid populatsioone.

Galaktika morfoloogia kujuneb välja protogalaktika kollapsi ajal. Sealjuures sõltub tekkiva galaktika kuju kollapseeruva aine dünaamilistest omadustest ja tähetekke protsessist. Tähetekke tulemid eri aegadel erinevad üksteisest füüsikaliselt, omades erinevat ruumjaotust, keemilist koostist ja erinevat kinemaatikat, mis püüab säilitada ruumjaotusi. Seega, uurides galaktikates tähepopulatsioonide struktuuri, on võimalik saada kvantitatiivset informatsiooni galaktikate tekke- ja evolutsiooniprotsesside mõistmiseks. Efektiivseim meetod tähesüsteemide ehituse analüüsimiseks on mudelite konstrueerimine. Sobilik empiiriline mudel peab kajastama ka erinevate koostisosade (kerasparvede, gaasi jm.) jaotust, kinemaatikat, keemilise koostise muutuseid jm. Sealjuures pakuvad evolutsiooni seisukohalt erilist huvi galaktikates vaadeldud metallilisuse muutused. Erinevad evolutsioonilised stsenaariumid ennustavad seoseid keemilise koostise jaotuse ja aine tiheduse jaotuse vahel. Seega, metallilisuse analüüs võimaldab siduda galaktikate keemilist ja dünaamilist evolutsiooni ning analüüsida keemilise evolutsiooni protsesse.

Neutraalse vesiniku vaatlused osutasid 1970-ndatel, et spiraalsete galaktikate välisosades on gaasi pöörlemiskiirused enam-vähem konstantsed. Sarnaseid tulemusi saadi hiljem veel ligi 60 galaktikate jaoks gaasi optiliste emisioonijoonte põhjal. See oli ootamatu tulemus, kuna tol ajal vaadeldi tähti põhiliste massi kandjatena ning galaktikate heledusjaotuste järgi pidi ringkiirus välisosades kahanema. Vastuolu vaadeldud ja ennustatud pöörlemiskiiruste vahel võib iseloomustada lokaalsete mass-heledus suhete abil, mis galaktikate keskosades on $\sim 5-10$ ning välisosades $> 100-500$. See osutab, et väljaspool optilist raadiust peab olema lisamassi. Teiste sõnadega, galaktikad peavad olema ümbritsetud massiivsetest kroonidest. Käesolevaks ajaks on väga erinevat

liiki vaatlustest saadud, et galaktikate massid on suuremad, kui tuleneks lihtsast konstantse mass-heledus suhte oletusest (kuuma gaasi soojuskiirgus, mida on vaadeldud röntgen-lainepikkustel; galaktikaparvedes leitud gravitatsioonilise "läätse" poolt tekitatud kujutised). Kõik see osutab, et galaktikatega on seotud oluline kogus nähtamatut ainet.

Nähtamatu aine ruumjaotuse kohta on vähe teada. Nähtamatu aine ilmutab ennast ainult gravitatsiooni potentsiaali kaudu. Potentsiaali annavad panuse aga nii nähtav kui ka nähtamatu komponent. Kuna nähtava aine jaotuse mastaapi ja struktuuriparameeterit on võimalik saada pindfotomeetriast, siis jääb alles üks vaba parameeter – nähtava aine mass-heledus suhe või nähtamatu ja nähtava aine masside suhe. Et saada nähtamatu aine hulka ja jaotust, oletatakse tihti nähtamatu ja nähtava aine suhe olevat minimaalne (maksimaalse ketta hüpotees) või oletatakse nähtavale ainele mingi mass-heledus suhe. Siiski on need vaid oletused, soovitatav oleks aga määrata kõik galaktikate populatsioonide parameetrid vaatlustest.

Vaatluste põhjal galaktika jaotamine alisüsteemideks on keeruline protseduur. Suure arvu vabade parameetrite tõttu ei pruugi probleemile olla ühest lahendit. Kuid kui võrrelda parameetrite väärtusi modelleerimise käigus ka teiste galaktikate struktuuriga, samuti keemilise evolutsiooni mudelitega, on võimalik töö käigus elimineerida ilmselt mittefüüsikalisi lahendeid.

Et aidata astronoome orienteeruda vaatlustes, organiseeriti IAU galaktikate fotomeetria ja kinemaatika töögrupi juurde allrühm, mis soovitas koostada põhiliste galaktikate nimekirja koos viidetega olulisematele vaatlustele. See ülesanne täideti (Tenjes jt. 1982) ning sellest nimekirjast eraldasime detailseks modelleerimiseks sobilike galaktikate valimi. Valim sisaldas erinevate morfoloogiliste tüüpidega ja erinevate heledustega galaktikaid. Kõigi valimi galaktikate jaoks kasutasime sama modelleerimise metoodikat. Loodame, et sel teel saame adekvaatsema pildi galaktikate nähtavast struktuurist ning nähtamatu aine jaotusest.

Käesoleva dissertatsiooni eesmärk on uurida lähemate galaktikate struktuuri ning määrata nende komponentide parameetrid. Kõik komponendid lähendavad füüsikalisi allsüsteeme, mis koosnevad sarnase vanuse, keemilise koostise ja kiiruste jaotusega tähtedest, st. nad on füüsikaliselt homogeensed. Galaktika populatsioonide samatihedus pinnad lähendatati sarnaste kontsentriliste ellipsoididega või nende ellipsoidide summaga.

Massijaotuse probleemi välisgalaktikates formuleerisid esmakordselt Öpik (1922) ning Babcock (1938, 1939). Hiljem mudeleid täiustati, tuues sisse ruumtiheduse sõltuvuse galaktotsentrilisest kaugusest (Kuzmin (1943, 1952), Schmidt (1957)). Eelpool toodud mudelid baseerusid aga pöörlemiskõveratel ning ei võtnud arvesse teisi vaatlusliike galaktikate ehituse kohta. Uus lähenemine arendati välja Sizikovi (1969) ja Einasto (1969, 1972) poolt. Nendes töödes

arvestati nii kinemaatilisi kui fotomeetrilisi vaatlustulemusi ning näidati, et taoline lähenemine võimaldab kirjeldada galaktikaid allsüsteemide summana.

Meie naabri, Andromeda galaktika M31 ehitust uuritakse 2. peatükis. Kogutud vaatlusandmeid pindfotomeetria kohta seitsmes värvis (U kuni K), pöörlemiskõvera, tähtede kiiruste dispersioonide, kerasparvede jaotuse, aga ka noore tähelise komponendi ja gaasi jaotuse kohta võimaldavad galaktika jaotada tsentraalseks tuumaks, metallirikkaks südamikuks ja bulgeks, metallivaeseks haloks, vanaks täheliseks kettaks, nooreks gaasilis-täheliseks kettaks ning nähtamatuks massiivseks krooniks. Analüüsiti populatsioonide parameetrite tundlikkust erinevatele vaatlusandmetele. Arvutati nende populatsioonide tiheduse jaotuse parameetrid, värvusindeksid ja mass-heledus suhted. Galaktika optiliselt nähtava osa keskmiseks mass-heledus suhteks saadi $M/L_B = 4.8 \pm 1.5\,M_\odot/L_\odot$, ning kogumassi ja nähtava massi suhteks $M_T/M_{vis} = 43$. Lokaalne M/L suhe galaktika optilisel piiril tuli parima lähenduse mudelis 2500.

3. peatükis vaatlesime galaktika M31 noore tähelise komponendi struktuuri. Arvestades täheassotsiatsioonide, hajusparvede ja teiste noorte tähtede jaotust, saadi selle komponendi keskmistatud pindtiheduse jaotus. Saadud jaotust võrreldi neutraalse ($HI + H_2$) vesiniku jaotusega. Leiti, et noore tähelise komponendi tihedus on võrdeline gaasi pindtihedusega astmes 1.30 ± 0.22, ehk ruumtihedusega astmes 1.17 ± 0.25. Tähetekke karakteristlik aeg on $t_* = 4.6 \pm 1.5 \times 10^9$a., praegune tähetekke kiirus $\dot{M} = 0.81 \pm 0.36\,M_\odot$/a.

Elliptiliste galaktikate ehitusele oli kuni 80-ndate aastateni pühendatud palju vähem tähelepanu. Esimesed mudelid baseerusid siin galaktika heledusjaotusel, mida lähendati mingi lihtsa analüütilise valemiga. Elliptilised galaktikad oletati omavat pöördellipsoidaalset sümmeetriat, mille lapikus on tingitud pöörlemisest. Siiski, juba 50-ndatel aastatel näitas Kuzmin (1953), et kolmanda liikumisintegraali olemasolu avaldab mõju tähesüsteemi pöörlemiskiirustele. Einasto (1972) töötas välja algoritmi sferoidaalse süsteemi massijaotuse arvutamiseks, kus galaktika kuju määravad kiiruste dispersioonid, st. kus täheorbiidid ei ole ringikujulised ning pöörlemiskiirused on palju väiksemad ringkiirustest. Elliptiliste galaktikate pöörlemiskiiruste mõõtmised 1970-ndate teisel poolel stimuleerisid galaktikate dünaamika alaseid teoreetilisi uuringuid. Mitmete galaktikate puhul saadud pöörlemiskiiruste keeruline struktuur osutab, et elliptiliste galaktikate ehitus võib olla küllalt komplitseeritud.

Hiidelliptilise galaktika M87 ehitust käsitletakse 4. peatükis. Koguti kõik vaatlusandmed pindfotomeetria kohta UBVRI värvustes, tähtede kiiruste dispersioonide, kerasparvede jaotuse ja kiiruste dispersioonide, aga ka röntgenkiirguse jaotuse kohta. Neid andmeid kasutades jaotati galaktika tsentraalseks tuumaks, metallirikkaks bulgeks, metallivaeseks haloks ja massiivseks nähtamatuks krooniks. Arvutati populatsioonide struktuuriparameetrid, värvusindeksid ja mass-heledus suhted, samuti ka gravitatsiooni potent-

siaali käik ja massijaotus funktsioonid. Galaktika optiliselt nähtava osa mass-heledus suhe on $M/L_B = 4.9 \pm 2.0\,M_\odot/L_\odot$, kogumassi ja nähtava massi suhe $M_T/M_{vis} = 130$.

Spiraalgalaktika M81 ehitust analüüsitakse 5. peatükis. Vaatlustest lähtuvalt kirjeldati galaktikat tuuma, metallirikka südamiku, bulge, metallivaese halo, noore allsüsteemi, ketta ja massiivse krooni summana. Krooni parameetrid arvutati satelliitgalaktikate kinemaatikast. Galaktika nähtava osa mass-heledus suhe on $M/L_B = 5.5 \pm 1.9\ M_\odot/L_\odot$.

6. peatükis toome ära parima lähenduse parameetrid valimi ülejäänud 11 galaktika jaoks. Kirjeldatakse modelleerimiseks vajalikke vaatlusandmeid. Modelleerimise metoodika on analoogne eelnevates peatükkides kasutatuga. Saadud tulemusi kasutatakse galaktikate allsüsteemide füüsikaliste parameetrite analüüsil.

7. peatükis analüüsitakse galaktikate populatsioonide füüsikalisi omadusi. Kuna galaktikate sferoidid ja kettad omavad erinevat tähetekke ajalugu, analüüsime neid eraldi. Konstrueerisime vanade allsüsteemide jaoks sõltuvuse nende mass-heledus suhete ja värvusindeksi vahel. Sellest nähtub, et hilist tüüpi (Sc – Sdm) galaktikate bulgedes esineb nii vanu kui ka noori tähti. Nende efektiivne vanus on $1.5-4\ 10^9$ *a*. Varajast tüüpi (S0 – Sb) spiraalgalaktikate bulgede ja elliptiliste galaktikate M/L suhte erinevused on tõenäoliselt tingitud nende erinevast algsest keemilise koostisest. Sarnane sõltuvus konstrueeriti ka ketaste mudelitele. Antud värvusindeksi (B–V) jaoks on siin täheldatav suurem hajuvus mass-heledus suhetes. Tõenäoliselt on see põhjustatud aine täiendavast langemisest galaktikasse, mis ei ole seotud ülejäänud tähetekkega.

Meie galaktikate valim sisaldab kõikide olulisemate morfoloogiliste tüüpide esindajaid. Seetõttu saame arvutada nähtava aine keskmise mass-heledus suhte meie lokaalses ümbruses. Kasutades Virgo parve heledusfunktsiooni, saime keskmiseks nähtava aine heleduse järgi kaalutud mass-heledus suhteks $4.1 \pm 1.4\ M_\odot/L_\odot$.

Peatükis 8 pakume välja meetodi, kuidas kasutada vaatlusandmeid, et saada hinnata elliptiliste galaktikate tõelisi telgede suheteid, vaatenurki, mille all me galaktikat näeme ning kinemaatilist nihet (nurk impulssmomendi ja ellipsoidi lühima telje vahel). Meetodi kasutamiseks on vaja teada tähelise komponendi morfoloogiat ja kinemaatikat ning soovitatavalt ka gaasilise komponendi morfoloogiat. Rakendades seda kolmele elliptilisele galaktikale, leiame, et neist kahel juhul on kinemaatiline nihe väike või null.

List of Publications

1. Tenjes, P.: 1977. "Galaktika M31 struktuur." In: *ÜTÜ vabariikliku konverentsi materjale. 1977. I.*, Tartu: TRÜ, pp. 12–16.

2. Einasto, J., Haud, U., Kaasik, A., Tenjes, P., Traat, P.: 1977. "Mass distribution in M31." *Tartu Astrophys. Obs. Prepr.* A-4, pp. 1–8.

3. Tenjes, P., Haud,U.: 1978. "On the mass-to-luminosity ratios of galactic populations." In: *All Union conference of young astrophysisists, devoted to V.A. Ambartsumjan's 70-th birthday*, Yerevan: Acad.Sci. Armenian SSR, pp. 16.

4. Einasto, J., Tenjes, P., Traat, P.: 1979. "A mass distribution model of the Andromeda galaxy." *Astron. Circ.* Nr. 1032, pp. 5–7.

5. Einasto, J., Tenjes, P., Traat, P.: 1980. "Galactic models with massive corona: M81." *Astron. Circ.* Nr. 1089, 1–3.

6. Einasto, J., Tenjes, P., Barabanov, A.V., Zasov, A.V.: 1980. "Central holes in disks of spiral galaxies." *Astrophys. Space. Sci.* **67**, pp. 31–44.

7. Einasto, J., Tenjes, P., Traat, P.: 1980. "Two-component model of the elliptical galaxy M32." *Astron. Circ.* Nr. 1132, pp. 5–6.

8. Einasto, J., Tenjes, P., Traat, P.: 1981. "Dependence of local mass-to-luminosity ratio on radius in galaxies M31 and M81." *Astron. Circ.* Nr. 1179, pp. 1–2.

9. Einasto, J., Tenjes, P.: 1981. "Relation between the mass-to-luminosity ratio and colours for old subsystems of galaxies." *Astron. Circ.* Nr. 1179, pp. 2–4.

10. Tenjes, P., Kalamees, P., Einasto, J., Jõeveer, M., Brosche, P., Lentes, F.-Th.: 1982. "A list of elite-galaxies." *Tartu Astrofüüs. Obs. Teated*, Nr. 68, pp. i–viii, 1–56.

11. Kuzmin, G.G., Veltmann, U.-I.K., Tenjes, P.L.: 1986. "Quasi-isothermal models of spherical stellar systems. Application to the galaxies M87 and M105." *Tartu Astrophys. Obs. Publ.* **51**, pp. 232–242.

12. Tenjes, P.: 1988. "Subsystems in galaxies and their mass-to-luminosity ratios." In: *The formation and evolution of galaxies and their constituents. I.*, M.Jõeveer (ed.). Tallinn: Valgus, pp. 74–97.

13. Tenjes, P., Einasto, J., Haud, U.: 1991. "Galactic models with massive coronae. III. Giant elliptical galaxy M 87." *Astron. & Astrophys.* **248**, pp. 395–403.

14. Tenjes, P., Haud, U.: 1991. "The Schmidt star formation law in the Andromeda galaxy." *Astron. & Astrophys.* **251**, 11–14.

15. Tenjes, P.: 1991. "The mass-to-light ratio of visible matter." In: *Galaxy Environments and the Large Scale Structure of the Universe, Proc. Intern. Workshop at Trieste, Oct. 22–25, 1991.* SISSA-ISAS. pp. 335–340.

16. Tenjes, P.: 1992. "The surface photometry of galaxies. I. The galaxies NGC 3379 and M 81." *Baltic Astronomy* **1**, 7–16.

17. Tenjes, P., Busarello, G., Longo, G.: 1992. "Triaxial elliptical galaxies with dust lanes: an atlas of velocity fields." *Memorie dell'Accademia di Scienze Fisiche e Matematiche.* Napoli: Liguori Editori, pp. i–xi, 1–89.

18. Tenjes, P., Haud, U., Einasto, J.: 1992. "Galactic models with massive coronae. IV. The Andromeda galaxy M 31." *Astron. & Atrophys.* (submitted).

19. Tenjes, P., Busarello, G., Longo, G., Zaggia, S.: 1992. "On the intrinsic shape of elliptical galaxies." *Astron. & Astrophys.* (submitted).

TA rotaprint.